FACULDADE DE ENGENHARIA DA UNIVERSIDADE DO PORTO

Impact of Carbon Neutrality Roadmap on Electricity Prices

Margarida Silva de Matos



Mestrado em Engenharia Eletrotécnica e de Computadores

Supervisor: Prof. Dr. José Nuno Fidalgo

October 12, 2026

© Margarida Matos, 2026

Resumo

A transição para a neutralidade carbónica está a transformar os sistemas elétricos europeus, com implicações profundas para os preços grossistas de eletricidade. Esta dissertação analisa o impacto do Roteiro para a Neutralidade Carbónica 2050 (RNC2050) nos preços do mercado diário do Mercado Ibérico de Eletricidade (MIBEL), com foco em dois drivers estruturais: o crescimento da procura associado à eletrificação e o aumento da penetração de energias renováveis.

Para estimar a evolução dos preços da eletricidade, são desenvolvidos dois modelos complementares: uma rede neuronal artificial (RNA) e uma regressão linear bayesiana (RLB), estimados com dados horários do período 2023–2025. Os modelos são aplicados a cenários alinhados com o RNC2050 para os horizontes 2030, 2040 e 2050, sob duas famílias de cenários: o Cenário A, que incorpora trajetórias projetadas para os preços do gás natural (TTF) e do carbono (EU ETS), e o Cenário B, que mantém estes preços constantes nos níveis históricos, isolando assim o efeito estrutural da transformação do mix de geração.

Os resultados demonstram que, sob preços de combustível constantes (Cenário B), o crescimento da procura domina o efeito da *ordem de mérito* da expansão renovável, conduzindo a preços superiores à *baseline* em todos os horizontes (até $+10\%$ em 2040). O efeito das renováveis manifesta-se na redistribuição temporal dos preços: os perfis intradiários evoluem para um padrão *duck-curve*, com o vale de preços ao início da tarde a aprofundar-se e o pico noturno a persistir, alargando a amplitude diária de 47 para 55 EUR/MWh em 2050. A hora de preço mínimo desloca-se da hora 15 para a hora 16, um resultado consistente com a interação Solar×Hora, que permite ao modelo representar uma depressão mais acentuada dos preços durante o período da tarde à medida que a penetração fotovoltaica aumenta. Sob o Cenário A, o declínio projetado do preço do gás e a subida do preço do carbono exercem efeitos parcialmente compensatórios, resultando em variações líquidas modestas (-4 a $+7\%$). A comparação entre modelos mostra que, apesar do melhor ajustamento à amostra histórica ($R^2 = 0{,}883$ *versus* 0,593), a RNA desenvolvida neste estudo apresenta projeções economicamente implausíveis no Cenário A para 2040 e 2050, quando os preços do gás e do carbono se afastam substancialmente do domínio de estimação. Este resultado evidencia os riscos da utilização de modelos não condicionados em exercícios de extrapolação de longo prazo. A RLB, com priors informativos fundamentados na teoria económica, produz projeções mais estáveis e interpretáveis, com intervalos probabilísticos condicionais às hipóteses de cada cenário.

A dissertação conclui que o percurso de descarbonização do RNC2050 não conduz necessariamente, por si só, a uma redução dos preços grossistas de eletricidade, e que a trajetória dos preços dos combustíveis fósseis é o fator determinante na distinção entre cenários de preço. Estes resultados têm implicações para o desenho de políticas energéticas, a gestão de mercados de eletricidade e a avaliação da viabilidade económica da transição energética.

Abstract

The transition to carbon neutrality is reshaping European electricity systems, with profound implications for wholesale electricity prices. This dissertation analyses the impact of Portugal's Carbon Neutrality Roadmap 2050 (RNC2050) on day-ahead electricity prices in the Iberian Electricity Market (MIBEL), focusing on two key structural drivers: electrification-driven demand growth and increasing renewable energy penetration.

To estimate the evolution of electricity prices, two complementary models are developed: an Artificial Neural Network (ANN) and a Bayesian Linear Regression (BLR), both estimated using hourly data from the 2023–2025 period. The models are applied to RNC2050-aligned scenarios for the 2030, 2040, and 2050 horizons under two scenario families: Scenario A incorporates projected trajectories for natural gas (TTF) and carbon (EU ETS) prices, and Scenario B, which holds these prices constant at historical levels, thereby isolating the structural effect of the generation-mix transformation.

The results show that, under constant fuel prices (Scenario B), demand growth outweighs the merit-order effect of renewable expansion, leading to wholesale electricity prices above the baseline across all projection horizons (up to +10% in 2040). The effect of renewables manifests in the temporal redistribution of prices: intraday profiles evolve towards a duck-curve pattern, with the early-afternoon price trough deepening and the evening peak persisting, widening the daily price range from 47 to 55 EUR/MWh by 2050. The hour of minimum price shifts from hour 15 to hour 16, a result consistent with the Solar$\times$Hour interaction, which enables the model to represent a stronger afternoon price depression as photovoltaic penetration increases. Under Scenario A, the projected decline in natural gas prices and the increase in carbon prices exert partially offsetting effects, resulting in relatively modest net price changes (between -4% and $+7\%$). Model comparison shows that, despite achieving a higher in-sample fit ($R^2 = 0.883$ versus 0.593), the ANN developed in this study produces economically implausible projections under Scenario A for the 2040 and 2050 horizons, when gas and carbon prices deviate substantially from the estimation domain. This result highlights the risks of using unconditioned models in long-term extrapolation exercises. The BLR, supported by informative priors grounded in economic theory, produces more stable and interpretable projections, with probabilistic intervals conditional on the assumptions of each scenario.

The dissertation concludes that the decarbonisation pathway envisaged by the RNC2050 does not necessarily, by itself, lead to lower wholesale electricity prices, and that the future trajectory of fossil fuel prices is the primary determinant distinguishing alternative price scenarios. These findings have important implications for energy policy design, electricity market operation, and the assessment of the economic viability of the energy transition.

Sustainable Development Goals

This dissertation contributes primarily to the following United Nations Sustainable Development Goals (SDGs):

SDG 7 — Affordable and Clean Energy. The dissertation analyses how the large-scale deployment of renewable energy sources under Portugal's Carbon Neutrality Roadmap affects wholesale electricity prices in the Iberian market. By quantifying the conditions under which the expansion of clean generation lowers or raises prices, and by identifying the role of demand growth in moderating or amplifying those effects, the work provides evidence that can support the design of electricity markets capable of maintaining affordability during the transition to clean energy. The analysis of price volatility and of the changing intraday price patterns further informs the design of market mechanisms that support affordable electricity in high-renewable systems.

SDG 13 — Climate Action. The entire analytical framework of the dissertation is built around the RNC2050, Portugal's long-term climate strategy. By translating the roadmap's decarbonisation targets into projected wholesale electricity prices, the work contributes to the understanding of the economic implications of climate action in the electricity sector. The scenario-based approach, which separates the effects of generation-mix transformation from those of fuel and carbon prices, provides a structured framework for assessing how different climate-consistent pathways affect market outcomes.

Acknowledgements

I would like to express my deepest gratitude to all those who supported me throughout this journey.

To my supervisor, Professor José Nuno Fidalgo, for his unwavering dedication to this work. His weekly meetings, calm guidance, and thoughtful advice were essential at every stage of this dissertation. Beyond the technical rigour, his patience and encouragement gave me the confidence to navigate the most challenging phases of the research. I could not have asked for a better mentor.

To my parents and my brother, for everything. For the sacrifices I did not always see, for the love I never had to question, and for the quiet certainty that I would always have a place to come home to. You gave me the foundation on which everything else was built. Thank you for believing in me before I believed in myself, for holding me together in the most challenging moments, and for celebrating every step as if it were the greatest achievement in the world. These five years were mine, but this degree is ours.

To my grandfather, for the everyday calls and for being one of my greatest sources of strength. Your pride in my achievements has been a constant motivation, and your belief in my future has carried me further than you know.

To the rest of my family, for always being there and for never letting me feel alone in this journey.

To my boyfriend, for his love, patience, and unwavering belief in me. Thank you for standing beside me through every challenge, for lifting me up when the weight felt too heavy, and for reminding me of what I am capable of when I needed it most. Your love made even the most exhausting days feel lighter, and your presence gave me the strength to keep going. I am deeply grateful for you.

To my best friends and my safe place: Di, Inês, Bia, and Laura. Thank you for every late-night conversation that put the world back into perspective, for knowing exactly when I needed to laugh and when I needed to be heard, and for a love that distance and busy lives have never diminished. You have seen me at my best and at my worst, and you have stayed through all of it. I carry a piece of each of you in everything I do.

To my university friends, and especially to Rita, for the beautiful memories that made these years unforgettable. For sharing both the happiest and the hardest moments, for the group projects, the study sessions, the late nights, and the laughter that made it all worthwhile. This degree would not have been the same without you.

To my friends from Viana, for being a constant presence and a safe harbour, no matter the distance. Your support has meant more than I can express.

To all of you, thank you.

Contents

List of Acronyms and Symbols xvii

1 Introduction 1
- 1.1 Background and Motivation . . . 1
- 1.2 Problem Statement and Objectives . . . 3
- 1.3 Research Questions . . . 4
- 1.4 Scope and Delimitations . . . 5
- 1.5 Dissertation Structure . . . 6

2 Electricity Markets and the Energy Transition 9
- 2.1 Carbon Neutrality and the Transformation of the Electricity System . . . 9
  - 2.1.1 The European and Portuguese Decarbonisation Framework . . . 9
  - 2.1.2 Structural Transformation of Demand and Supply . . . 10
- 2.2 Liberalised Electricity Markets and the Day-Ahead Market . . . 12
  - 2.2.1 Market Architecture and Trading Horizons . . . 12
  - 2.2.2 The Day-ahead Market as the Core Price-formation Mechanism . . . 13
- 2.3 Price Formation and the Merit-Order Mechanism . . . 14
  - 2.3.1 Short-run Marginal Costs and the Supply Curve . . . 14
  - 2.3.2 Uniform Pricing, Merit-order Dispatch and Inframarginal Rents . . . 16
- 2.4 The Iberian Electricity Market (MIBEL) . . . 16
  - 2.4.1 Structure, Governance and Cross-border Integration . . . 16
  - 2.4.2 Historical Price Dynamics . . . 17

3 Electricity Price Drivers and the State of the Art 21
- 3.1 Price Drivers in the Energy Transition . . . 21
- 3.2 Modelling Approaches in the Literature . . . 23
- 3.3 Research Gap and Contribution . . . 25

4 Methodology 27
- 4.1 Methodological Framework and Research Design . . . 27
  - 4.1.1 Overall Analytical Strategy . . . 27
  - 4.1.2 Rationale for a Multi-Model Approach . . . 28
  - 4.1.3 Research Workflow . . . 29
- 4.2 Data and Pre-Processing . . . 30
  - 4.2.1 Data Sources . . . 30
  - 4.2.2 Variable Selection and Justification . . . 31
  - 4.2.3 Data Cleaning and Normalisation . . . 33
- 4.3 Evaluation Framework . . . 34

4.3.1 Performance Metrics . . . 34
4.3.2 Bayesian-Specific Metrics . . . 35
4.4 Neural Network Model . . . 36
4.4.1 Architecture and Input Selection . . . 36
4.4.2 Training Process . . . 37
4.4.3 Sensitivity Analysis . . . 38
4.5 Bayesian Linear Regression . . . 38
4.5.1 Model Formulation . . . 38
4.5.2 Variable Selection and Prior Specification . . . 39
4.5.3 Interaction Terms: Solar × Hour . . . 42
4.5.4 Hourly vs. Daily Model . . . 43
4.5.5 MCMC Estimation and Convergence Diagnostics . . . 44
4.6 RNC2050 Scenario Construction . . . 44
4.6.1 Methodological Assumptions . . . 45
4.6.2 Scenario Inputs: Scaling Factors and Price Assumptions . . . 46
4.6.3 Conceptual Dispatch Logic . . . 49
4.6.4 Operational Constraints . . . 50

5 Results and Discussion **53**
5.1 Descriptive Analysis of Historical Prices . . . 53
5.1.1 Price Distribution . . . 53
5.1.2 Generation Shares and System Composition . . . 54
5.1.3 Intraday Renewable Generation Profiles . . . 55
5.1.4 Solar Generation: Hour-by-Month Structure . . . 56
5.1.5 Wind Generation: Seasonal Profile . . . 57
5.1.6 Empirical Validation of Operational Constraints . . . 58
5.2 Artificial Neural Network . . . 58
5.2.1 In-Sample Performance . . . 58
5.2.2 Scenario Projections . . . 60
5.2.3 Intraday Price Profiles . . . 61
5.2.4 Assessment . . . 63
5.3 Bayesian Linear Regression: Estimation . . . 64
5.3.1 Development Stages . . . 64
5.3.2 Posterior Coefficients . . . 64
5.3.3 Baseline Profiles . . . 67
5.4 BLR Scenario Projections . . . 70
5.4.1 Constraint Diagnostics and Stage Comparison . . . 70
5.4.2 Effect of BLR Specification Stages on Scenario Projections . . . 71
5.4.3 Projected Price Levels . . . 73
5.4.4 Intraday Price Profiles Under Scenarios . . . 74
5.4.5 Rightward Shift of the Price Minimum . . . 76
5.4.6 Seasonal Price Profiles . . . 79
5.4.7 Projected Volatility and Frequency of Negative Prices . . . 80
5.4.8 Hourly Versus Daily Model Divergence . . . 82
5.5 Sensitivity to the GAS_MIN Constraint . . . 83
5.5.1 Effect on Price Levels . . . 83
5.5.2 Effect on Profiles . . . 84
5.6 Model Comparison and Suitability . . . 86

6 Conclusions **89**
6.1 Answers to Research Questions 89
6.2 Interpretation in Light of the Literature 91
6.3 Recommendations 92
6.4 Limitations of the Analysis 93
6.5 Future Work 94

References **97**

List of Figures

2.1 Evolution of the installed capacity of the power generation sector and of the carbon intensity of electricity generation in Portugal under the RNC2050. Source: RNC2050 [4]. 12
2.2 Aggregated supply and demand curves for one hour of the MIBEL day-ahead market, with the matched segments highlighted. Source: OMIE, MIBEL day-ahead market [15]. 15
2.3 Average annual day-ahead price in the Portuguese zone of MIBEL (EUR/MWh), 2015–2025, with the crisis years 2021–2022 highlighted. Source: author's elaboration based on OMIE data [15]. 18

4.1 Methodological workflow adopted in this dissertation. 29
4.2 Posterior inclusion probabilities from the spike-and-slab variable selection, MIBEL day-ahead price, 2023–2025. The dashed line marks the median-probability inclusion threshold (PIP = 0.5). 40

5.1 Distribution of hourly day-ahead prices in the Portuguese zone of MIBEL, 2023–2025. Vertical lines: mean (72.6 EUR/MWh) and median (78.9 EUR/MWh). . . 54
5.2 Combined VRE share (% of load) by hour of day, 2023–2025. Shaded bands: P75 and P95 envelopes. 56
5.3 Mean solar generation share (% of load) by hour and month, 2023–2025. The colour scale ranges from 0% (night-time) to approximately 39% (summer midday). 56
5.4 Wind generation share (% of load) by month, 2023–2025. Bars: mean; error bars: P75 and P95. 57
5.5 ANN predicted versus observed prices (3 000 randomly sampled observations). The diagonal represents perfect prediction. 59
5.6 ANN intraday price profiles under Scenario B (constant fuel prices): baseline versus 2030, 2040, and 2050. 62
5.7 ANN intraday price profiles under Scenario A (projected fuel prices): baseline versus 2030, 2040, and 2050. 63
5.8 Prior-to-posterior updating: prior mean (open circle) and posterior median with 95% HDI (solid circle and bar) for each economically motivated variable. The Solar×Hour interaction terms are omitted from this figure. 66
5.9 BLR hourly baseline intraday price profile: posterior predictive median (solid line) with 90% credible interval (shaded band), 2023–2025. 68
5.10 BLR hourly baseline monthly price profile: posterior predictive median with 90% credible interval, 2023–2025. 69
5.11 BLR hourly: median projected prices under Scenarios A and B by development stage. 72

5.12 Projected intraday price profiles under Stage 1 (flat priors, without Solar×Hour interaction) for baseline, 2030, 2040, and 2050 under Scenarios A (left) and B (right). 72
5.13 Intraday price profiles under Scenarios A (left) and B (right): posterior predictive median by hour for baseline, 2030, 2040, and 2050 (BLR hourly, Stage 2). 75
5.14 Solar share, net load and price profiles: historical baseline versus 2050 Scenario B (BLR hourly, Stage 2). 77
5.15 Decomposition of the intraday price profile by factor group: baseline versus Scenario B 2050 (BLR hourly, Stage 2). 78
5.16 Monthly price profiles under Scenarios A (left) and B (right): posterior predictive median by month for baseline, 2030, 2040, and 2050 (BLR hourly, Stage 2). . . . 79
5.17 Intraday price profiles under Scenarios A (left) and B (right): posterior predictive median by hour for baseline, 2030, 2040, and 2050 (BLR hourly, Stage 3). 84
5.18 Monthly price profiles under Scenarios A (left) and B (right): posterior predictive median by month for baseline, 2030, 2040, and 2050 (BLR hourly, Stage 3). . . . 85

List of Tables

2.1 Final energy by carrier and year under the RNC2050 (PJ). Source: RNC2050 [4] 11

3.1 Price drivers in the energy transition and their role in the dissertation. 23

4.1 Summary of the estimated models and their analytical capabilities 28
4.2 Input variables, definition, and economic rationale 32
4.3 Sequential comparison of candidate input specifications 36
4.4 Comparison of alternative hidden-layer architectures 37
4.5 Perturbation-based sensitivity analysis – ANN Model F, 60 neurons 38
4.6 Prior distributions adopted for the Bayesian model 41
4.7 Differences between the hourly and daily BLR specifications 43
4.8 RNC2050 capacity and demand targets used for scenario construction 47
4.9 Effective scaling factors after saturation 48
4.10 Fuel and carbon-price assumptions by scenario 49
4.11 Operational constraints, values by model and horizon 50

5.1 Descriptive statistics of generation shares (% of load) and system aggregates, 2023–2025 ($N = 26\,304$). 54
5.2 Empirical validation of the operational constraints: historical statistics versus scenario limits. 58
5.3 ANN prediction error by price regime, 2023–2025. 60
5.4 ANN prediction error by season and by period of the day. 60
5.5 ANN scenario projections (EUR/MWh). 60
5.6 ANN suitability by scenario and horizon. 63
5.7 Posterior coefficients of the final hourly BLR (EUR/MWh per standard deviation of input). HDI: 95% highest-density interval. 64
5.8 Prior-to-posterior updating for the economically motivated variables (EUR/MWh per standard deviation of input). 66
5.9 BLR hourly: baseline intraday price profile (posterior predictive distribution, EUR/MWh). 67
5.10 BLR hourly: baseline monthly price profile (posterior predictive distribution, EUR/MWh). 69
5.11 Frequency with which each operational constraint binds (% of 26 304 scenario hours). These diagnostics apply to both the ANN and BLR Stage 2 (seven-constraint configuration, without GAS_MIN). 70
5.12 BLR hourly: median projected prices (EUR/MWh) under Scenarios A and B by development stage. 71
5.13 Scenario projections: median prices (EUR/MWh) and percentage change versus baseline. BLR intervals are 90% posterior predictive [P5–P95]. 73

5.14 Difference A−B in median projected prices (EUR/MWh). Negative values indicate that the Scenario A fuel and carbon trajectories reduce prices relative to constant-fuel Scenario B. 74
5.15 Monthly price profiles for BLR Hourly Stage 2. 79
5.16 Projected price volatility and frequency of negative prices by scenario and horizon (BLR hourly, Stage 2). Brackets denote the [P5–P95] interval of each statistic computed across the 8 000 MCMC posterior draws, reflecting the posterior uncertainty about that statistic. 81
5.17 Divergence between hourly and daily BLR median projections (EUR/MWh): hourly minus daily (Stage 2). 82
5.18 BLR scenario projections with GAS_MIN (Stage 3). Median prices (EUR/MWh) and percentage change versus baseline. Intervals are 90% posterior predictive [P5–P95]. 83
5.19 Effect of the GAS_MIN constraint on median projected prices (EUR/MWh): Stage 3 minus Stage 2. 83
5.20 Monthly median projected prices (EUR/MWh) under Scenarios A and B, BLR hourly Stage 3. 85
5.21 Comparative assessment of the three model configurations. 86

List of Acronyms and Symbols

List of Acronyms

ANN	Artificial Neural Network
BLR	Bayesian Linear Regression
CCGT	Combined Cycle Gas Turbine
DGEG	Direção-Geral de Energia e Geologia (Portuguese Directorate-General for Energy and Geology)
ENTSOG	European Network of Transmission System Operators for Gas
ERSE	Entidade Reguladora dos Serviços Energéticos (Portuguese Energy Services Regulatory Authority)
ESS	Effective Sample Size
EU	European Union
EU ETS	European Union Emissions Trading System
HDI	Highest Density Interval
HMC	Hamiltonian Monte Carlo
IEA	International Energy Agency
IPCC	Intergovernmental Panel on Climate Change
IRENA	International Renewable Energy Agency
LCOE	Levelised Cost of Electricity
MAE	Mean Absolute Error
MAPE	Mean Absolute Percentage Error
MCMC	Markov Chain Monte Carlo
MIBEL	Mercado Ibérico de Eletricidade (Iberian Electricity Market)
NUTS	No-U-Turn Sampler
OMIE	Operador del Mercado Ibérico de Energía (Iberian Market Operator — spot markets)
OMIP	Operador do Mercado Ibérico de Energia, Polo Português (Iberian Energy Derivatives Exchange)
PIP	Posterior Inclusion Probability
PNEC	Plano Nacional Energia e Clima (National Energy and Climate Plan)
PV	Photovoltaic
REN	Redes Energéticas Nacionais (Portuguese Transmission System Operator)
RMSE	Root Mean Squared Error
RNC2050	Roteiro para a Neutralidade Carbónica 2050 (Carbon Neutrality Roadmap 2050)
SDAC	Single Day-Ahead Coupling
SDG	Sustainable Development Goal
SRMC	Short-Run Marginal Cost

TIMES	The Integrated MARKAL-EFOM System
TTF	Title Transfer Facility (Dutch natural-gas trading hub)
VRE	Variable Renewable Energy

List of Symbols

α	Intercept of the BLR model (EUR/MWh)
β_j	Regression coefficient for variable j (EUR/MWh per σ)
c	Saturation parameter in the tanh function ($c = 6$)
ε_t	Model error term at observation t
f_{demand}	Demand scaling factor relative to 2020 baseline
$f_{\text{effective}}$	Effective generation-share scaling factor
$f_{\text{effective}}^{\text{sat}}$	Saturated scaling factor (after tanh)
N	Number of observations
$\hat{R}$	Potential scale reduction factor (convergence diagnostic)
R^2	Coefficient of determination
S_j	Perturbation-based sensitivity index (EUR/MWh per $\sigma/10$)
$\bar{y}$	Sample mean of observed prices (EUR/MWh)
$\hat{y}$	Model-predicted price (EUR/MWh)
y_t	Observed price at hour t (EUR/MWh)
z	Standardised (z-score) value of an input variable
δ_j	Perturbation magnitude for variable j
μ_x	Sample mean of input variable x
σ	Standard deviation of the model residuals (EUR/MWh)
σ_x	Sample standard deviation of input variable x
P5, P95	5th and 95th percentiles of the posterior predictive distribution

Chapter 1

Introduction

1.1 Background and Motivation

Climate change is among the defining challenges of the twenty-first century, and the mitigation of greenhouse gas emissions has become a structuring objective of European and national policy. The European Union has committed to climate neutrality by 2050, with binding intermediate milestones, and these commitments have been translated by Member States into long-term decarbonisation strategies that cut across every sector of the economy [1, 2, 3]. Portugal has articulated its own trajectory in the Roadmap for Carbon Neutrality 2050 (RNC2050), which sets out the national path towards net-zero emissions in a sustained manner, establishing the main guidelines and identifying cost-effective options to achieve it across different socio-economic development scenarios [4, 5]. For the nearer 2030 horizon, the RNC2050 is complemented by the National Energy and Climate Plan 2030 (PNEC 2030), which translates its long-term vision into intermediate targets and policy measures [6].

Within this transformation, the electricity sector occupies a position of singular importance, because it is simultaneously a sector to be decarbonised and the principal instrument through which other sectors are decarbonised. On the supply side, electricity generation is among the first activities to approach full decarbonisation, as low marginal cost wind and solar generation displaces fossil-based production. On the demand side, electrification of transport, heating and industry replaces the direct combustion of fossil fuels with electricity, so that an increasing share of final energy is delivered as electricity. The combination is deliberate: decarbonisation strategies foresee a generation mix that becomes progressively cleaner at the same time as the volume of electricity it must serve expands substantially. The electricity system is therefore the central transmission channel of climate policy, and the conditions under which it operates are being reshaped at an unusually rapid pace.

These movements are not merely prospective, in the Portuguese case they are already well advanced. Portugal has closed its last coal-fired power plant, renewable sources supplied more than 70% of national electricity consumption in 2024, and the share of natural gas in generation has fallen to historically low levels [7]. Looking forward, the RNC2050 envisages the near-complete

decarbonisation of electricity generation by mid-century, a continued and large expansion of installed renewable capacity, and renewable shares of final energy of the order of 86–88% [4]. Portugal is thus among the European systems in which the structural transformation analysed in this dissertation is most clearly observable, which makes it a particularly informative setting in which to study the economic consequences of decarbonisation.

While the environmental rationale for this transition is well established, its economic implications, and in particular its consequences for wholesale electricity prices, remain considerably less well characterised. In liberalised electricity systems, the wholesale price is far more than an accounting figure: it determines a large part of the cost borne by households and industry, conditions the competitiveness of energy-intensive sectors, and provides the central signal that guides investment in new generation and flexibility. Because the price paid to all dispatched units is the marginal cost of the most expensive unit required to meet demand, the wholesale price also governs the distribution of revenue across technologies and the recovery of the fixed costs of capital-intensive assets, including renewables themselves. Understanding how decarbonisation reshapes this price is therefore inseparable from any serious assessment of the economic sustainability of the energy transition.

The difficulty is that the transition exerts two opposing influences on price formation, and their net effect is not obvious in advance. On one side, the expansion of wind and solar generation, whose short-run marginal cost is close to zero, displaces higher-cost thermal generation from the margin and exerts downward pressure on average prices: this is the merit-order effect [8, 9]. On the other side, electrification-driven demand growth raises system load and increases the frequency with which higher-cost dispatchable units are required to meet demand, exerting upward pressure, particularly in hours of low renewable availability. Superimposed on these level effects is a change in the shape of prices: as variable renewable shares rise, prices become more volatile [10], low and even negative prices become more frequent during periods of renewable surplus [11, 12], and the value that renewables capture in the market tends to decline as their output is increasingly self-correlated [13, 14]. Whether the average wholesale price rises or falls under a given decarbonisation pathway depends on the relative pace of these forces, on the temporal alignment between demand and renewable supply, and on conditioning factors such as fuel and carbon prices.

The recent electricity market price record illustrates how consequential this interaction is, and how far it is from monotone. The Iberian market experienced extreme volatility between 2020 and 2022, with prices falling to historical lows during the pandemic before surging to unprecedented levels during the European energy crisis as fuel and carbon costs soared, and then easing as markets stabilised and renewable output grew [15]. The episode demonstrated that, even in a system with a high and rising renewable share, wholesale prices remain strongly conditioned by fuel and carbon markets, and that the price outcome of the transition cannot be inferred from the renewable share alone. It is precisely this conditional, non-monotone character that motivates a careful, scenario-based analysis rather than a simple extrapolation.

The Iberian context is a particularly compelling setting in which to conduct such an analysis. The Iberian Electricity Market (MIBEL) [16, 17] jointly organises the wholesale markets of Portugal and Spain, already operates with some of the highest variable-renewable shares in continental Europe, and is comparatively weakly interconnected with the rest of the European system. This relative isolation means that Iberian prices are governed to an unusual degree by internal supply and demand conditions, so that the price signatures of the transition, the deepening midday price troughs associated with solar generation, the persistence of high evening prices, episodes of market splitting between the Portuguese and Spanish zones, and the appearance of very low and occasionally negative prices, are already observable in practice rather than hypothetical. The severity of these dynamics during the 2022 crisis prompted unprecedented regulatory interventions in both Portugal and Spain [18], underscoring the importance of understanding how the marginal-pricing mechanism transmits fuel costs into wholesale prices. Anchoring the analysis in RNC2050 trajectories and in observed MIBEL outcomes therefore transforms a generic question about decarbonisation and prices into a concrete, empirically grounded and policy-relevant case study, which is the central purpose of this dissertation.

1.2 Problem Statement and Objectives

Despite the evident importance of price dynamics for both policymakers and market participants, the relationship between carbon neutrality strategies and wholesale electricity price formation remains insufficiently explored, and the existing literature is divided between two traditions that rarely meet. Long-term energy-system planning models, of the bottom-up techno-economic optimisation type that informs national roadmaps [19], determine least-cost technology deployment and emissions trajectories under policy constraints. Within these models, electricity prices appear only indirectly, as shadow values of constraints or as marginal values defined over coarse time slices, and the hourly market mechanisms through which day-ahead prices are actually formed are largely abstracted away. Market-oriented analyses, by contrast, reproduce marginal pricing and operational detail at high temporal resolution [20, 21], but they frequently rely on stylised inputs and short horizons that are not transparently anchored in the policy-defined pathways of national decarbonisation roadmaps. The result is a persistent disconnect: the trajectories that policy actually prescribes are seldom translated into the wholesale price outcomes that markets actually produce.

The central problem addressed in this dissertation lies in this gap. It concerns the economic implications of carbon neutrality pathways for wholesale electricity prices in a market-based system, and specifically how the structural changes prescribed by the RNC2050 translate into day-ahead price dynamics in MIBEL. Addressing this problem requires an approach that is simultaneously consistent with national policy trajectories, resolved at the hourly level at which the relevant price features emerge, faithful to the marginal-pricing logic of the market, and capable of attributing the resulting price changes to their underlying causes.

The RNC2050 prescribes a set of ambitious targets, among which two are decisive for the evolution of electricity prices: the electrification of society, which aims to replace fossil fuels with electricity across most sectors of the economy, and the development of a generation park progressively based on endogenous, renewable sources of energy. These two targets act on wholesale prices in opposite directions. As a consequence of the first, electricity consumption is expected to increase, which tends to push prices in MIBEL upward. The growth in the renewable market share anticipated by the second has the opposite effect, since prices are typically lower when renewable production is high. The way the price trend ultimately evolves therefore depends on the joint trajectory of these two drivers, and assessing this dependence is the central purpose of the dissertation. Other influences on prices, most notably fuel and carbon prices, are retained in the analysis but treated as conditioning factors rather than as structural drivers of the transition.

Accordingly, the main objective of this dissertation is to estimate the impact of the RNC2050 on electricity market prices in MIBEL, considering the effects of the two drivers, consumption growth and renewable growth, and how the price trend depends on their evolution. A complementary objective is to derive, from the outcomes of the study, a set of recommendations for policymakers, regulatory bodies and electricity-market participants. In pursuing these aims, the work also examines the mechanisms through which each driver acts and the way their interaction shapes price outcomes under decarbonisation-consistent scenarios. The main objective is pursued through the following specific objectives:

1. to synthesise the RNC2050 targets and trajectories relevant to electricity prices, and to translate them into internally consistent scenarios for the evolution of electricity demand and the generation mix up to 2050;

2. to develop and assess data-driven models relating MIBEL day-ahead prices to their fundamental drivers, and to adopt the approach best suited to projecting prices under decarbonisation scenarios;

3. to estimate the impact of the RNC2050 trajectories on these prices under the scenarios, isolating the effect of the two structural drivers, consumption and renewable growth, from that of fuel and carbon prices through the scenario design; and

4. to identify the critical scenarios and the conditions under which prices change most or under which the projections are least reliable.

1.3 Research Questions

The problem and objectives above are articulated through three interrelated research questions, which together address the individual and combined effects of the two structural drivers on wholesale price formation.

The first question concerns the demand side. **RQ1: How does electrification-driven electricity demand growth influence price formation in the day-ahead wholesale market, and**

in particular how does rising demand affect the frequency with which higher-cost marginal technologies are required to meet load? This question targets the mechanism by which additional load moves the system up its supply curve, increasing reliance on dispatchable thermal generation in specific hours and thereby raising both the level and the variability of prices.

The second question concerns the supply side. **RQ2: To what extent does increasing renewable penetration alter wholesale price levels and their temporal distribution through the displacement of higher-cost generation?** This question addresses the merit-order effect and its distributional implications, recognising that renewable expansion acts less by uniformly lowering prices than by reshaping their temporal structure, concentrating low-price hours in periods of high renewable availability.

The third question concerns the interaction of the two drivers. **RQ3: How does the interaction between demand growth and renewable deployment jointly shape wholesale price outcomes under carbon neutrality scenarios in MIBEL, including the level, the intraday profile, and the volatility of prices?** Because the two drivers act in opposite directions and evolve at different rates across the planning horizon, their combined effect cannot be obtained by adding their individual effects, and characterising this net interaction is the central empirical contribution of the dissertation.

1.4 Scope and Delimitations

Electricity prices are influenced by a wide range of factors, including fuel and carbon prices, interconnection capacity, system flexibility, market design and regulation. While acknowledging the importance of all of these, this dissertation adopts a deliberately bounded scope in order to preserve coherence with its objectives and to keep the analysis tractable and interpretable. The boundaries of the study are set along four dimensions: the market segment and geography considered, the variables that are varied as opposed to held as context, the modelling methodology adopted, and the questions that are explicitly placed outside the analysis.

In terms of market segment and geography, the analysis concentrates on the wholesale day-ahead market, which constitutes the core price-formation mechanism in MIBEL and the reference against which intraday and balancing prices are formed. The geographical focus is the Iberian context, with particular attention to Portugal within the MIBEL framework, and the temporal scope follows the horizons of national planning, extending to 2050. The models are estimated on the period 2023–2025, selected because it represents the most recent interval with complete and consistent data, captures the rapid expansion of solar generation in Portugal, and postdates the Iberian exception mechanism discussed in Section 2.4.2. Electricity demand and the generation mix evolve across the projection horizons (2030, 2040, 2050) according to RNC2050 trajectories, while fuel and carbon prices are varied across the two scenario families to separate their effect from that of the structural transformation.

Fuel and carbon prices occupy a deliberately intermediate position in this scope, and the way they are handled is one of the methodological choices of the dissertation. They are not treated as

structural drivers of the transition, but neither are they ignored: because the historical record shows that they remain decisive for price levels whenever thermal generation is marginal, omitting them would compromise the realism of the analysis and confound the attribution of price changes. They are therefore retained as conditioning regressors in the empirical models, so that the price response is reproduced faithfully, and they are varied only through the design of two scenario families: a projection-consistent family, in which gas and carbon prices follow trajectories informed by published projections and by author-defined modelling assumptions, and a constant-fuel family, in which they are held at present levels so that the isolated effect of the two structural drivers can be observed. This design separates the structural-driver effect from the confounding influence of commodity markets while preserving a realistic representation of price formation.

With respect to methodology, the dissertation adopts a data-driven, market-oriented approach rather than a full bottom-up dispatch or investment-optimisation model. Two models are developed: an artificial neural network and a Bayesian linear regression. The suitability of each for the scenario projections is assessed empirically, with the Bayesian model offering interpretable coefficients and explicit uncertainty quantification and the neural network capturing non-linear price-formation patterns. The methodological rationale for these choices is developed in subsequent chapters.

Finally, several questions are explicitly placed outside the scope of this work, and stating them clearly is important both for honesty and for the correct interpretation of the results. The dissertation does not perform full power-system, unit-commitment or generation-investment optimisation, and it does not model the intraday adjustment sessions or the balancing market, restricting attention to day-ahead price formation. Network constraints within bidding zones are not represented in detail, prices are treated at the zonal level. Demand-side flexibility, storage beyond pumped hydro, and prospective back-up technologies such as large-scale batteries, hydrogen or reinforced interconnection are not modelled explicitly. As a consequence, the low-renewable hours of the most decarbonised horizons constitute the region of greatest projection uncertainty, a limitation that is made explicit when the results are interpreted. For the same reason, the scenario results are intended as directional and relative assessments of price effects under alternative decarbonisation-consistent conditions, rather than as precise point forecasts of future prices.

1.5 Dissertation Structure

The remainder of the dissertation is organised into five further chapters. Chapter 2 establishes the conceptual and empirical foundations: it describes the decarbonisation framework and the structural transformations it imposes on the electricity system, sets out the organisation of liberalised markets and the merit-order mechanism, and characterises MIBEL, including its governance, cross-border integration and observed price dynamics. Chapter 3 develops the state of the art: it analyses the price drivers acting during the transition, reviews the modelling literature, and states the research gap and the contribution of the dissertation. Chapter 4 presents the methodology, including the data sources, the artificial neural network and Bayesian regression models,

the evaluation framework, and the RNC2050 scenario construction. Chapter 5 presents and discusses the results, comparing the two models and analysing the scenario projections. Chapter 6 answers the research questions, derives recommendations for policymakers, regulators and market participants, discusses the limitations of the study, and outlines directions for future research.

Chapter 2

Electricity Markets and the Energy Transition

The RNC2050 prescribes two structural transformations whose effects on wholesale prices act in opposite directions: electrification raises demand, while the expansion of renewable generation with near-zero marginal cost tends to lower prices. This chapter establishes the foundations needed to analyse that tension.

2.1 Carbon Neutrality and the Transformation of the Electricity System

2.1.1 The European and Portuguese Decarbonisation Framework

The transformation of the electricity system is driven, before anything else, by a policy framework that has made the reduction of greenhouse gas emissions a binding objective. At the European level, the European Green Deal commits the Union to climate neutrality by 2050 and frames decarbonisation as a cross-cutting economic strategy rather than a purely environmental goal [1]. This long-term objective is supported by intermediate targets and by an architecture of instruments, of which the EU Emissions Trading System is central to the electricity sector, since it places a price on carbon emissions [22] and thereby raises the variable cost of fossil-based generation. The scientific and economic rationale for the trajectory is set out in the assessments of the Intergovernmental Panel on Climate Change and in the decarbonisation scenarios of the International Energy Agency, both of which identify the power sector as the cornerstone of any credible path to net zero [2, 3].

Portugal has translated these commitments into a coherent national strategy articulated across two complementary instruments. The Roadmap for Carbon Neutrality 2050 (RNC2050) defines the long-term vision, establishing the goal of net-zero emissions by mid-century and outlining sectoral trajectories for energy production and consumption [4]. Its central premise is the progressive substitution of fossil fuels by low-carbon energy carriers, and above all by electricity, in transport,

buildings and industry. The National Energy and Climate Plan 2030 (PNEC 2030) complements this vision with binding intermediate targets and policy measures for the nearer horizon. In its original form it set a target of at least 80% renewable electricity by 2030, subsequently raised in its 2024 revision, alongside targets for the share of renewables in gross final energy consumption and for greenhouse-gas reductions relative to 2005 [6]. The two instruments are mutually consistent: the PNEC operationalises, for 2030, the deeper transformation that the RNC2050 projects to 2050.

The practical effect of this framework is already visible in the Portuguese system, which makes the country an unusually advanced case of the transition under study. The last coal-fired power plant in Portugal closed in November 2021, removing the most carbon-intensive technology from the generation mix. In 2024, renewable sources supplied approximately 71% of national electricity consumption, an all-time record, with hydropower and wind each contributing close to 28% of supply, solar approaching 10% and biomass around 6%. Over the same period, natural gas fell to roughly 10% of generation, its lowest share since 1979, while net electricity imports covered about 20% of consumption [7]. These figures illustrate that the structural changes prescribed by the decarbonisation framework are not distant projections but an ongoing reconfiguration of the system, and they establish the empirical baseline against which the future scenarios of this dissertation are constructed.

2.1.2 Structural Transformation of Demand and Supply

The decarbonisation framework reshapes the electricity system simultaneously from the demand side and from the supply side, and it is the combination of the two that defines the conditions under which future prices will be formed. On the demand side, the defining feature of carbon neutrality pathways is the electrification of end-use sectors that have traditionally relied on the direct combustion of fossil fuels. In the Portuguese context this includes the large-scale adoption of electric vehicles in transport, the diffusion of heat pumps and other electric heating technologies in buildings, and the electrification of selected industrial processes [4, 3]. The consequence is a structural increase in electricity demand: national planning projects that electricity evolves from a secondary energy carrier into the dominant vector of final energy consumption by mid-century.

The magnitude of this shift is documented in Table 2.1, which reports the projected evolution of final energy by carrier under the RNC2050. Final electricity consumption rises markedly across the horizon, while petroleum products decline steeply and natural gas, after a transitional role, falls in the later decades. The overall share of renewables in final energy is projected to reach the order of 86–88% by 2050. Crucially, this transformation is not only quantitative. Electrification also alters the temporal structure of demand, because new electrified loads exhibit consumption patterns that differ from traditional demand: transport charging introduces profiles linked to mobility behaviour, while electrified industrial processes may raise baseload demand. Many of these new uses are, under current infrastructure assumptions, relatively rigid or time-constrained, which can limit short-term demand flexibility and concentrate additional load in particular hours, especially

where electrified consumption is poorly aligned with periods of high renewable availability [3]. Here it suffices to establish that both the level and the shape of demand are being reshaped.

Table 2.1: Final energy by carrier and year under the RNC2050 (PJ). Source: RNC2050 [4]

Final energy (PJ)	**2015**	**2020**	**2030**	**2040**	**2050**
Total	632.7	651.1	598–602	507–519	460–478
Electricity	165.1	173–174	193–199	265–270	308–317
Petroleum products	288.7	285–294	178–180	51–63	17–25
Natural gas	67.8	80	94–100	56–62	30–34
Biomass and waste	56.4	53	65–68	49–51	18–26
Renewables (share)	28%	29%	46–47%	71–72%	86–88%

On the supply side, the framework drives a rapid expansion of installed renewable capacity, dominated by onshore wind and solar photovoltaic, accompanied by a sustained decline in the carbon intensity of electricity generation. These technologies are commonly referred to as variable renewable energy (VRE), because their output depends directly on meteorological conditions, principally wind speed and solar irradiance, and cannot be dispatched on demand. Figure 2.1 documents this projected evolution under the RNC2050, in which variable renewable capacity grows substantially while fossil-based capacity is progressively withdrawn. The sharp reduction in carbon intensity already observed in the early 2020s reflects both the accelerated deployment of renewables and the retirement of fossil generation, of which the closure of the last coal plant is the clearest example. The expansion is reinforced by a continuing decline in the cost of renewable technologies: over the past decade, technological learning, economies of scale and supply-chain optimisation have substantially reduced the levelised cost of utility-scale solar and onshore wind, so that an increasing share of new capacity is competitive with, or cheaper than, fossil alternatives [23].

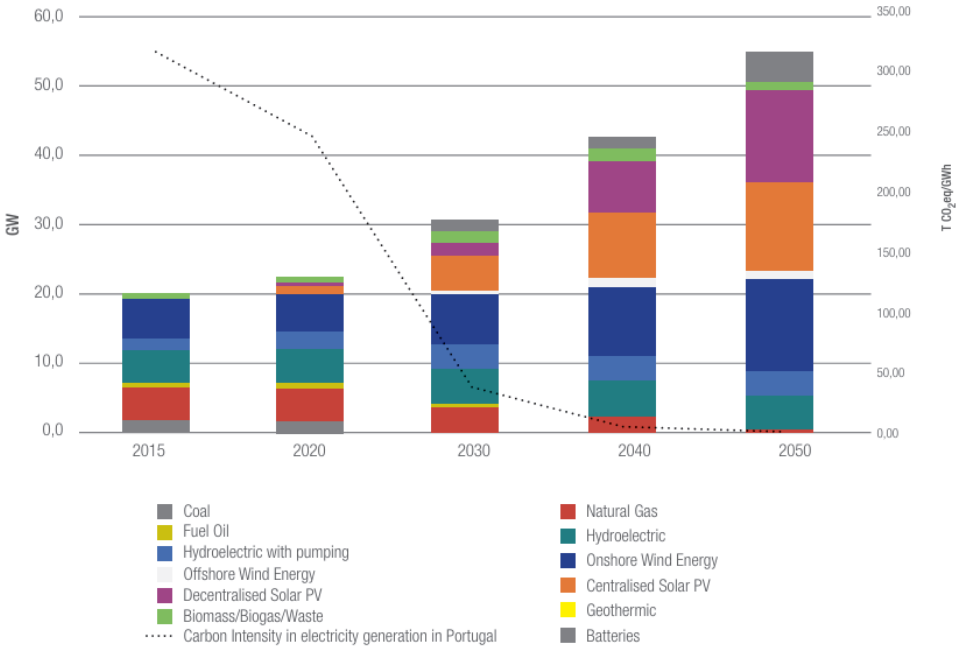


Figure 2.1: Evolution of the installed capacity of the power generation sector and of the carbon intensity of electricity generation in Portugal under the RNC2050. Source: RNC2050 [4].

The economic significance of this supply-side transformation follows from a cost characteristic that distinguishes wind and solar from conventional generation: once installed, their short-run marginal cost is close to zero, because they require no fuel and incur negligible variable operating costs. As their share of capacity grows, an increasing fraction of demand can be met by generation with near-zero marginal cost, which fundamentally alters the conditions of price formation described later in this chapter. At the same time, because wind and solar output is variable and weather-dependent, the supply available at near-zero cost fluctuates considerably from hour to hour and from season to season. The system therefore moves towards a configuration in which average production costs fall but the temporal variability of supply rises, so that the conditions under which prices are formed alternate between periods of abundant low-cost generation and periods in which dispatchable generation must cover residual demand. The price consequences of this configuration, and the interaction between rising demand and rising renewable supply, are analysed in Section 2.3.

2.2 Liberalised Electricity Markets and the Day-Ahead Market

2.2.1 Market Architecture and Trading Horizons

Liberalised electricity systems are organised not as a single trading venue but as a sequence of interconnected markets operating over different time horizons. This architecture is a direct consequence of the physical characteristics of electricity, most importantly the fact that it cannot be economically stored at scale with conventional technologies, that supply and demand must

be balanced continuously and in real time, and that the transmission network imposes physical constraints on where electricity can flow [24]. Because production and consumption must be matched at every instant, the market must progressively translate long-term expectations into firm operational decisions, and it does so through a sequential structure organised around the principle of progressive information revelation: as delivery approaches, each successive market stage incorporates increasingly accurate information on demand, renewable availability and network conditions [24, 25].

The longest horizon is occupied by the forward and futures markets, in which electricity is traded for delivery months or years ahead. Their primary function is risk management: producers, retailers and large consumers use them to hedge against price uncertainty and to stabilise revenues or costs, and the price signals they provide support investment in capital-intensive generation by reducing revenue risk [26]. In the Iberian context these derivatives are traded on OMIP, the Iberian Energy Derivatives Exchange, based in Portugal. The instruments traded there are financial contracts that reference future electricity prices but do not by themselves determine physical dispatch [27]. Closer to delivery, short-term trading is organised through the day-ahead, intraday and balancing markets, which coordinate supply and demand near real time and which, in MIBEL, are operated by the Iberian Market Operator (OMIE) [15]. The day-ahead market establishes, for each hour of the following day, a reference schedule of generation and consumption. The intraday markets then allow participants to adjust their positions as updated information becomes available, most importantly to correct forecast errors in demand and in variable renewable output. Finally, the balancing mechanisms operate after market closure to resolve the residual deviations between scheduled and actual generation or consumption, ensuring the instantaneous security of the system. Although balancing prices reflect genuine real-time scarcity, their influence on overall wholesale price dynamics is secondary relative to the day-ahead market, which remains the reference against which the other stages are formed.

2.2.2 The Day-ahead Market as the Core Price-formation Mechanism

Among these stages, the day-ahead market occupies the central position in price formation and is therefore the focus of this dissertation. It is the principal venue through which supply and demand are coordinated on a daily basis, and it establishes the hourly prices for delivery on the following day that serve as the main reference for the entire system [15, 24]. Its centrality derives from the way it links operational coordination with economic price formation: by fixing the reference dispatch schedule, it provides the baseline from which intraday adjustments and real-time balancing actions depart, so that the prices it produces closely reflect the expected system conditions at the time of delivery.

The operation of the market follows a transparent auction logic. For each hour of the following day, generators submit supply offers and consumers or retailers submit demand bids, based on their forecasts of demand, renewable availability, fuel prices and network conditions. These offers and bids are cleared simultaneously through a centralised auction, which produces a single market-clearing price for each hour in each bidding zone. The defining feature of this process is the

uniform pricing rule: every accepted generation unit receives the same clearing price for a given hour, irrespective of the price at which it offered, and that clearing price equals the marginal cost of the most expensive unit that must be dispatched to meet demand [25]. This rule has two important consequences that are developed in the next section. First, it makes the wholesale price a direct expression of the cost structure of the generation mix, so that changes in either demand or the available mix translate immediately into price changes. Second, it ensures short-run allocative efficiency, because units are dispatched in order of increasing cost, while at the same time shaping how revenue is distributed across technologies. It is precisely because the day-ahead market translates the physical configuration of the system into an observable price in this transparent way that it provides a suitable lens through which to study the price effects of the structural transformation.

2.3 Price Formation and the Merit-Order Mechanism

2.3.1 Short-run Marginal Costs and the Supply Curve

The price that emerges from the day-ahead auction is determined by the interaction between demand and the cost structure of the available generation, formalised through the construction of a supply curve. The relevant cost concept is the short-run marginal cost (SRMC) of each unit, that is, the additional cost of producing one more unit of electricity. The SRMC typically comprises fuel costs, variable operation and maintenance costs, and, where applicable, the cost of carbon emissions. Fixed costs such as capital investment do not enter the marginal cost and therefore do not directly influence short-term dispatch decisions [25, 24].

Generation technologies differ markedly in their marginal cost structure, and this heterogeneity is the foundation of price formation. Fossil-based plants, such as gas-fired combined-cycle units, have marginal costs that are largely determined by fuel and carbon prices, both of which are volatile. Their marginal costs are consequently relatively high and variable, which makes them the technologies most likely to set the price during periods of high demand or low renewable availability. Nuclear and reservoir hydropower occupy intermediate positions, the latter with an opportunity-cost component reflecting the value of stored water. Wind and solar photovoltaic, by contrast, have marginal costs close to zero, since they require no fuel. When generators' offers are aggregated by the market operator, they form an upward-sloping supply curve, the merit order, in which technologies are ranked by increasing marginal cost, with near-zero-cost renewables at the base and fuel-dependent thermal units towards the top [28].

Figure 2.2 shows the aggregated supply and demand curves for a single hour of the MIBEL day-ahead market, as published by OMIE, and makes this construction concrete with real market data.

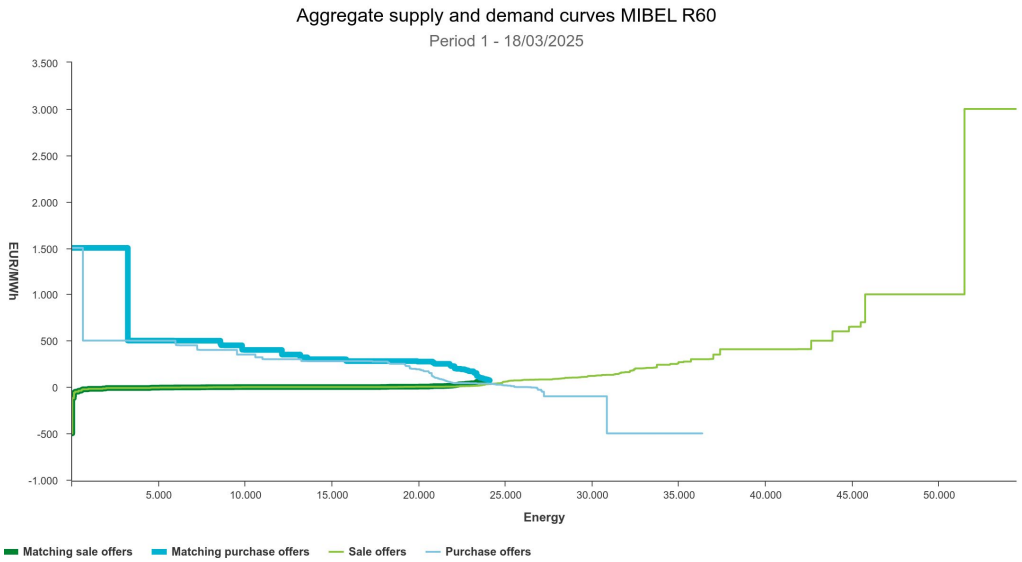


Figure 2.2: Aggregated supply and demand curves for one hour of the MIBEL day-ahead market, with the matched segments highlighted. Source: OMIE, MIBEL day-ahead market [15].

The supply curve (*sale offers*) is the empirical merit order: a block of capacity at the far left is offered at, or close to, the price floor of -500 EUR/MWh, principally zero-marginal-cost renewables and must-run units that bid at the floor to guarantee dispatch and are therefore effectively price-takers. The curve then runs nearly flat and close to zero across a wide central range, before climbing steeply towards the highest offers, of the order of 3 000 EUR/MWh, corresponding to expensive thermal and peaking units. The demand curve (*purchase offers*), by contrast, is high and steep: a large share of demand is bid at prices of several hundred up to about 1 500 EUR/MWh and declines only gradually over the matched range, reflecting the fact that electricity demand must, for the most part, be served regardless of price, before falling to the floor at the right. The market clears where the matched offers (*matching sale offers* and *matching purchase offers*) intersect, fixing the uniform clearing price and the traded volume for that hour. In the illustrated hour the matched curves meet at around 24 000 MWh and a price of the order of a few tens of EUR/MWh.

This empirical picture makes explicit the central property of the market: because the demand curve is nearly vertical, the clearing price is governed mainly by the point of the supply curve at which it is intersected. When residual demand is low, for example during hours of abundant renewable output, the intersection falls in the low-priced segment of the supply curve and the price is very low or even negative. When residual demand is high, for example on a winter evening with little wind or solar, the intersection moves into the steep, fuel-dependent segment and a gas-fired unit sets a substantially higher price. The same supply curve can therefore produce widely different prices within a single day, depending only on the level of demand net of renewable generation. This sensitivity, and its amplification as the variable renewable share grows, is the mechanism through which the structural transformation of the system propagates into prices.

2.3.2 Uniform Pricing, Merit-order Dispatch and Inframarginal Rents

The combination of the supply curve with the uniform pricing rule defines the merit-order dispatch mechanism that governs European wholesale markets. Units are dispatched in ascending order of marginal cost until demand is met, and the marginal cost of the last unit required, the marginal unit, sets the clearing price paid to all dispatched units. This design guarantees that, in the short run, the least-cost combination of available units is used to meet demand, which is the source of its allocative efficiency [25, 24].

A direct and structurally important consequence of uniform pricing is the emergence of inframarginal rents. Every unit whose marginal cost lies below the clearing price receives, for each unit of electricity produced, the difference between the clearing price and its own marginal cost. These rents are not a market distortion but an intrinsic feature of marginal pricing [28]: together with the revenues earned during higher-priced hours, they are the mechanism through which capital-intensive technologies, including renewables, recover the fixed costs that do not enter the marginal cost. This observation matters for the economics of the transition, because technologies with near-zero marginal cost, such as wind and solar, earn essentially all of their revenue as inframarginal rents, and the value of those rents depends on the level of prices in the hours in which they generate.

The merit-order mechanism also explains why the price effects of structural change are not confined to shifts in the average price level. Because the clearing price is set by whichever technology is marginal, and because the marginal technology can change from one hour to the next as demand and renewable output vary, prices become highly sensitive to system conditions. A relatively modest change in residual demand can move the margin from a near-zero-cost renewable unit to a fuel-dependent thermal unit, producing a large jump in price. Systems with high shares of variable renewable energy therefore tend to combine lower average prices with greater short-term volatility, and the price distribution, the relative frequency of low-price and high-price hours, becomes as important an object of analysis as the mean. These mechanisms provide the economic rationale for the variable selection adopted in the price models developed in Section 4.2.2, in which technology-specific generation shares, the TTF natural-gas price and the EU ETS carbon price appear as explanatory variables.

2.4 The Iberian Electricity Market (MIBEL)

2.4.1 Structure, Governance and Cross-border Integration

The Iberian Electricity Market jointly organises the wholesale electricity markets of Portugal and Spain within a single integrated framework. The day-ahead and intraday markets are operated by OMIE, while electricity derivatives are traded on OMIP, and the governance of the market is shared among the Portuguese and Spanish energy and securities regulators [25, 15, 17]. MIBEL operates under the marginal-pricing and uniform-clearing rules described above, applied to each bidding zone, and it forms part of the wider European internal electricity market.

Integration with that wider market occurs through market coupling. Under the Single Day-Ahead Coupling (SDAC), the day-ahead markets of the participating European zones are cleared simultaneously by a common algorithm, which allocates cross-zonal transmission capacity implicitly so that electricity flows from lower-priced to higher-priced zones whenever capacity permits. The framework and the harmonised price limits are defined in European regulation [29]. These harmonised limits set a price floor of -500 EUR/MWh, which means that negative prices are structurally possible, and a maximum clearing price that was raised from 3 000 to 4 000 EUR/MWh in May 2022 in response to the exceptional prices reached during the energy crisis. Within this framework, the coupling between Portugal and Spain enables coordinated price formation across the Iberian Peninsula. When the interconnection capacity between the two countries is sufficient, their prices converge to a single Iberian price reflecting a common marginal technology. When the interconnection becomes congested, market splitting occurs and the two zones clear at distinct prices that reflect their local supply and demand conditions [16]. A defining structural characteristic of MIBEL is that it is comparatively weakly interconnected with the rest of continental Europe, with the cross-Pyrenees capacity between Spain and France remaining limited relative to the size of the Iberian system. As a result, Iberian prices are governed to an unusual degree by internal conditions, which both increases their exposure to domestic structural drivers and makes the Peninsula a relatively self-contained system in which the price effects of the transition can be studied with limited confounding from external markets. The resulting import–export balance is itself a determinant of the Iberian price, since net imports displace higher-cost domestic generation while net exports have the opposite effect. This provides the rationale for including the net cross-border balance among the explanatory variables of the price models.

2.4.2 Historical Price Dynamics

The price behaviour observed in MIBEL over the last decade exhibits, in practice, the dynamics that the merit-order framework predicts in principle, and it provides the empirical anchor against which the scenario results of this dissertation are interpreted. Figure 2.3 shows the evolution of the average annual day-ahead price in the Portuguese zone of MIBEL, based on OMIE annual reports.

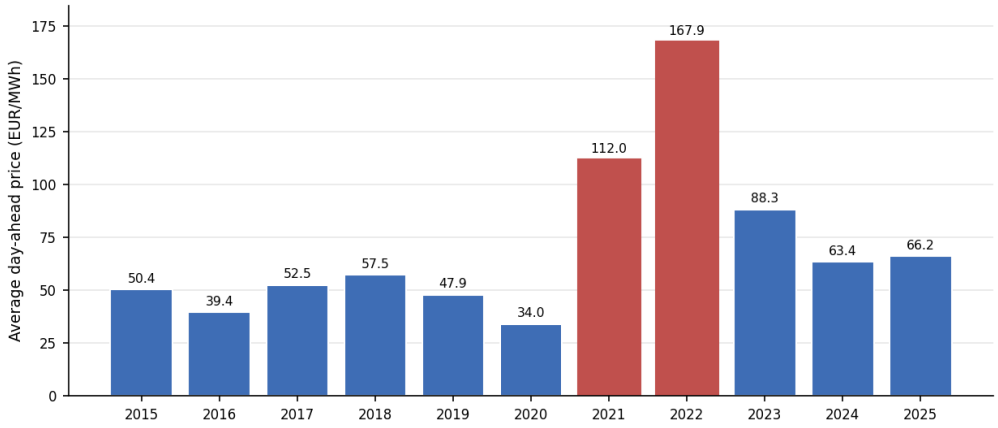


Figure 2.3: Average annual day-ahead price in the Portuguese zone of MIBEL (EUR/MWh), 2015–2025, with the crisis years 2021–2022 highlighted. Source: author's elaboration based on OMIE data [15].

After several years in a moderate range (between roughly 39 and 57 EUR/MWh from 2015 to 2019), the price fell to a historically low level of about 34 EUR/MWh in 2020, driven by depressed demand during the pandemic and low fuel prices. It then surged to around 112 EUR/MWh in 2021 and to an unprecedented 167.9 EUR/MWh in 2022 during the European energy crisis, as natural-gas and carbon prices reached exceptional values, before easing to roughly 88 EUR/MWh in 2023 and 63 EUR/MWh in 2024 as fuel markets stabilised and renewable output expanded, and remaining close to 66 EUR/MWh in 2025 [15]. This record demonstrates that, even in a system with a high and rising renewable share, the level of wholesale prices remains strongly conditioned by fuel and carbon markets whenever thermal generation is marginal, a pattern that persists even under scenarios in which the RNC2050 projects gas generation shares as low as 0.6% of demand, and which motivates the retention of fuel and carbon prices as conditioning variables in the models developed in Chapter 4.

The severity of the 2022 crisis prompted an exceptional policy response that is itself instructive for understanding Iberian price formation. In June 2022, Portugal and Spain introduced a temporary mechanism, widely known as the "Iberian exception", which capped the price of natural gas used by thermal generation and compensated gas plants for the difference relative to the market gas price, with the cost borne by consumers exposed to the wholesale market. In Portugal, it was enacted by Decree-Law No. 33/2022 and it remained in force, after extension, until the end of 2023 [30]. By lowering the effective fuel cost of the marginal gas unit, the mechanism reduced the day-ahead clearing price. A study using synthetic-control methods estimates an average reduction of approximately 65 EUR/MWh, roughly 40%, over the first twelve months of operation in both Spain and Portugal [18]. The episode is relevant here for two reasons: it confirms, through a deliberate intervention, that the day-ahead price in MIBEL is set by the marginal cost of gas-fired generation whenever such generation is on the margin, and it illustrates how strongly the gas-to-power cost linkage propagates through the marginal-pricing mechanism. The mechanism also carries an implication for the estimation of the price models used in this dissertation: since

the first year of the estimation period (2023) partially overlaps with the mechanism, the observed gas-to-electricity price relationship in that year may be attenuated relative to a period of fully market-determined gas costs. This overlap is limited, however, as the mechanism expired before two thirds of the estimation sample (2024–2025).

Beyond the annual averages, the rising share of renewable generation has reshaped the intraday and distributional features of Iberian prices in ways that are directly relevant to this study. The growth of solar generation has produced a pronounced intraday price profile, in which prices fall sharply during the midday and early-afternoon hours of high solar output and rise to a peak in the evening, when demand is high and solar generation has fallen to zero. As solar capacity increases, the midday price trough deepens and broadens while the evening peak persists, widening the daily price range. These intraday effects are taken into account in the modelling framework developed in the methodology chapter. At the same time, hours of very low and occasionally negative prices, which the SDAC price floor permits, have become more frequent during periods of high renewable surplus and weak demand, and episodes of market splitting between the Portuguese and Spanish zones continue to occur when the interconnection binds. These observed features, the deepening intraday trough, the widening price distribution, and the appearance of negative prices, are the empirical signatures of a system with a high and growing share of variable renewables, and they provide concrete reference points against which the modelled scenarios are validated. The mechanisms that generate them, and the way they evolve as the two structural drivers advance, are the subject of the next chapter.

Chapter 3

Electricity Price Drivers and the State of the Art

3.1 Price Drivers in the Energy Transition

The previous chapter established how wholesale prices are formed through the merit-order mechanism. The energy transition does not change this mechanism, but it transforms the economic environment in which it operates. This section analyses the forces that drive prices during the transition, organised around a distinction that structures the rest of the dissertation: between *structural* drivers, which decarbonisation pathways explicitly prescribe and which directly shift the supply and demand curves, and *contextual* drivers, which condition the price response without being varied as part of the transition pathway. The two structural drivers are renewable deployment, acting predominantly downward, and electrification-driven demand growth, acting predominantly upward. The principal contextual drivers are fuel and carbon prices, separated from the structural effects through the scenario design.

The merit-order effect through which variable renewable energy depresses wholesale prices is among the most robustly documented results in energy economics: Sensfuß, Ragwitz and Genoese quantified it for the German market [8], Würzburg, Labandeira and Linares consolidated the evidence for Germany and Austria [9], Hirth attributed a substantial part of the decline in European wholesale prices during the 2010s to renewable expansion [31], and Figueiredo and Pereira da Silva confirmed that the mechanism operates in MIBEL [32]. A direct outcome is price cannibalization: because renewable generators of the same type produce at the same times, their combined output depresses prices precisely in the hours in which they generate, so that the market value of each unit of renewable energy declines as penetration increases. Hirth formalised this effect [13], and subsequent studies have estimated it explicitly, notably López Prol, Steininger and Zilberman for the Californian market [14], with comparable evidence for Italy [33]. The effect is generally stronger for solar than for wind, because solar output is concentrated around midday and is highly self-correlated, whereas wind is more evenly distributed. Cannibalization is central not only to average price levels but also to the intraday profile, and it provides the conceptual link to the

emergence of negative prices. At very high penetration levels, the relationship between installed solar capacity and effective market value becomes increasingly non-linear, an observation that is particularly relevant for the long-term scenario analysis of this dissertation. Two further downward influences reinforce the merit-order effect: the sustained decline in the levelised cost of solar and wind [23], which acts through investment rather than dispatch by enabling sustained capacity additions [3]; and market integration through cross-border interconnection, which allows demand to be met by lower-cost supply in neighbouring markets [34], although this effect is bounded by transmission capacity [16].

On the upward side, electrification is the primary source of pressure within the scope of this work. Higher demand increases the frequency with which the market clears in the steep, fuel-dependent segment of the supply curve, especially during peak hours or hours of low renewable availability. The magnitude of the effect depends on the flexibility of the new demand [3]. During periods of low renewable output, the system must rely on dispatchable resources with high marginal costs, which means that scarcity-driven price spikes become a structural feature of high-renewable systems [34, 3]. Within this framework, flexibility is a transmission mechanism rather than an independent driver. Fuel and carbon prices condition wholesale prices in every hour in which thermal generation is marginal: the natural-gas price is transmitted almost immediately through the marginal-pricing mechanism, and the carbon price internalises emission costs into the bids of fossil plants [35]. Both act on the electricity price only through gas-fired plants on the margin. When the gas share becomes residual, as in the most decarbonised horizons, this transmission channel narrows.

Systems with high shares of variable renewables also tend to exhibit greater short-term price volatility, because weather-dependent shifts in the supply curve can move the marginal technology and produce large price swings [10, 36]. At the extreme of the distribution lie negative prices, which arise when inflexible or must-run generation prefers to pay to continue producing rather than shut down during periods of high renewable surplus and low demand [11, 12]. Literature specifically documenting negative-price episodes in MIBEL remains scarce, reflecting the relatively recent emergence of the phenomenon, which has become increasingly frequent only since 2023–2024 with the rapid expansion of solar generation. Excluding negative-price observations from the analysis would remove the high-renewable, low-price information that the transition makes most relevant, and so these observations are deliberately retained.

The wholesale price under a decarbonisation pathway is therefore the resultant of downward and upward drivers whose relative strength changes over the horizon: the downward drivers dominate in moderately decarbonised states, the upward drivers gain weight in deeply electrified states, and fuel and carbon prices set the level when gas is marginal but their influence weakens as gas becomes residual. Table 3.1 summarises the drivers, their direction, their transmission channels and their relevance to the dissertation.

Table 3.1: Price drivers in the energy transition and their role in the dissertation.

Driver	Direction	Transmission channel	Relevance to the dissertation
Renewable deployment	Downward	Merit-order effect: zero-cost renewables displace higher-cost thermal generation.	Primary structural driver; shapes the supply curve and the average price level.
Price cannibalization	Downward (on renewable value)	Self-correlated output depresses prices in the hours renewables generate.	Shapes the intraday profile and renewable market value; widens the low-price window.
Renewable cost decline	Downward	Lower LCOE enables sustained capacity additions.	Deflationary baseline over the medium and long term.
Market integration	Downward (smoothing)	Cross-border flows access to cheaper supply; price convergence.	Mitigates extremes; bounded by interconnection capacity (relevant for MIBEL).
Demand growth	Upward	Electrification raises load and the frequency of marginal thermal dispatch.	Primary structural driver; demand-side pressure and peaks.
Scarcity / flexibility	Upward	Low-renewable hours require dispatchable capacity at higher cost.	Transmission mechanism; governs peaks and the uncertainty of the 2050 horizon.
Fuel & carbon prices	Conditioning	Internalised in gas-plant bids; act only via marginal gas.	Contextual; handled through scenario design (Scenario A vs B).

3.2 Modelling Approaches in the Literature

Translating the drivers described above into quantitative price projections requires a model, and the literature offers several traditions with different strengths and limitations. A large share of decarbonisation analysis relies on bottom-up, techno-economic optimisation models such as TIMES_PT [4, 6, 19, 5]. Their strength is internal consistency: they jointly determine demand, investment and emissions under policy constraints. For wholesale price analysis, however, they have well-known limitations: prices emerge as shadow values rather than as market outcomes, temporal resolution is often insufficient to resolve the hourly features that matter in high-renewable systems, and conditioning variables such as fuel prices are treated opaquely, making attribution of price changes to structural drivers difficult.

A parallel literature analyses price formation at hourly resolution, using dispatch models or econometric methods that relate observed prices to fundamentals such as residual demand, renewable infeed, and fuel and carbon prices [8, 9, 13]. For the Iberian market, Pereira da Silva and Horta analysed Iberian price volatility [36], and Ciarreta and Zarraga examined the transmission

of prices and volatility between MIBEL and neighbouring markets [35]. The strength of these approaches is their grounding in realised market data. Their limitation for forward-looking analysis is that the estimated relationships are conditional on the historical regime and must be extrapolated with care to deeply decarbonised futures.

A smaller body of work has attempted forward-looking price analysis under high-renewable scenarios. Ketterer [37] estimated the effect of wind penetration on German spot-price volatility and found that higher wind capacity increases both the frequency of low prices and the overall price variance. Cludius et al. [38] quantified the merit-order effect of renewables in the German market up to 2012 and projected its evolution under the *Energiewende* (Germany's energy transition policy), concluding that the price-depressing effect would intensify but be partially offset by rising carbon prices. Prol et al. [14] analysed the impact of solar cannibalisation on the market value of photovoltaics across several European markets, showing that solar market value declines with penetration, a result consistent with the price-depressing solar coefficients estimated in this dissertation. For the Iberian context, Figueiredo and Pereira da Silva [32] quantified the merit-order effect of wind and solar in the Iberian market using historical data, but without extending the analysis to future capacity-expansion scenarios or incorporating demand growth and probabilistic uncertainty. These studies share two common features: they analyse the merit-order effect under relatively stable demand, and they do not embed their projections in a national decarbonisation roadmap with binding targets. The present dissertation addresses both of these gaps.

Because this dissertation employs an artificial neural network and a Bayesian regression, it is necessary to situate these methods in the literature. Electricity price forecasting is a mature field, and comprehensive reviews document its evolution from statistical to machine-learning approaches [20, 21]. Although this literature addresses short-term forecasting rather than the long-term scenario analysis pursued here, the comparative insights regarding interpolation versus extrapolation, interpretability versus flexibility, and the value of probabilistic outputs are directly transferable to the present context. Artificial neural networks capture non-linear relationships without an explicit functional form. Their strength is flexibility and accuracy, their weakness is limited interpretability and the fact that their behaviour outside the training domain is difficult to control. Bayesian regression provides an interpretable and explicitly probabilistic alternative: economically grounded priors discipline extrapolation, and full posterior distributions quantify uncertainty [39]. Recent applications confirm the viability of Bayesian approaches for electricity-price modelling [40, 41]. A linear Bayesian specification offers the further advantage of additive interpretability, allowing the contribution of each driver to the predicted price to be decomposed and attributed. The comparative literature indicates that no single method dominates across all conditions [20, 39, 21]. Given the recognised difficulty of neural networks outside the training domain, their suitability for long-term scenario analysis cannot be assumed, and this dissertation therefore develops both approaches and assesses their relative suitability empirically.

3.3 Research Gap and Contribution

The review above reveals a persistent disconnect between the policy-defined decarbonisation pathways of national roadmaps and the day-ahead wholesale price outcomes observed in market-based systems. Planning models provide coherent trajectories but lack the temporal and market representation required for hourly price formation. Market-oriented studies capture price formation with greater fidelity but rely on stylised scenarios not anchored in national roadmaps, and they rarely combine interpretability with calibrated uncertainty when extrapolating to deeply decarbonised states. To the best of the author's knowledge, no published study brings together, for the Iberian market, the four elements that this dissertation combines: (i) scenarios consistent with the RNC2050; (ii) MIBEL day-ahead prices modelled at both hourly and daily resolution; (iii) an explicit separation of the effects of the generation mix from those of fuel and carbon prices; and (iv) a probabilistic quantification of the uncertainty of the resulting projections.

This dissertation is designed to fill that gap. It develops a scenario-based, market-oriented framework for MIBEL day-ahead prices, grounded in RNC2050 trajectories and focused on the two structural drivers, demand growth and renewable deployment, while treating fuel and carbon prices as conditioning variables separated through a projection-consistent Scenario A and a constant-fuel Scenario B. It develops both a neural network and a Bayesian regression and assesses empirically which is better suited to the scenario projections. This enables the dissertation not only to quantify how decarbonisation reshapes the level, intraday profile and volatility of Iberian wholesale prices, but also to explain why those changes occur and to state where the projections are least reliable, connecting the national decarbonisation roadmap to the short-term economic signals of the wholesale market and providing a basis for the recommendations that close the dissertation.

Chapter 4

Methodology

4.1 Methodological Framework and Research Design

4.1.1 Overall Analytical Strategy

This dissertation employs an empirical, data-driven framework to assess the impact of Portugal's Carbon Neutrality Roadmap on wholesale electricity prices in the MIBEL market. The analytical strategy rests on three sequential components: (i) the statistical characterisation of historical price-formation patterns using hourly data for the period 2023–2025; (ii) the estimation of two forecasting models, namely an Artificial Neural Network (ANN) and a Bayesian Linear Regression (BLR), using the historical patterns; and (iii) the projection of electricity prices under RNC2050-aligned scenarios by applying the estimated models to counterfactual input configurations reflecting 2030, 2040, and 2050 generation mixes.

The proposed methodology does not constitute a long-term energy-system optimisation exercise of the kind implemented in capacity-expansion and investment-planning frameworks such as TIMES [42]. Such models are primarily designed for investment planning and system optimisation rather than reproducing the statistical properties of observed hourly price formation. By contrast, the present study treats the historical data-generating process as the reference and uses it to infer how prices would evolve if the structural composition of the generation mix changed in accordance with RNC2050 targets. This is a deliberate methodological choice: it preserves the empirically observed statistical relationships between generation shares and prices, rather than imposing a theoretical equilibrium structure that may not reflect actual market dynamics in the MIBEL context.

Three scenarios are considered throughout the analysis:

- **Baseline (2023–2025):** Historical observed data, used for model estimation, in-sample validation, and benchmarking purposes.
- **Scenario A:** RNC2050 generation-mix targets combined with projected trajectories for TTF natural-gas prices and EU Emissions Trading System (EU ETS) allowance prices, informed

by the IEA World Energy Outlook 2025 Net Zero Emissions scenario and Bloomberg/ABN AMRO consensus forecasts.

- **Scenario B:** RNC2050 generation-mix targets applied with TTF and CO_2 prices held constant at their 2023–2025 average levels.

The distinction between Scenarios A and B is methodologically central. It enables the separate assessment of two key drivers of electricity-price evolution: changes in the generation mix and changes in fuel and carbon costs. Scenario B isolates the structural effect of the generation-mix transformation by holding fuel and carbon prices constant, whereas Scenario A captures the combined influence of that transformation and projected fuel- and carbon-price developments.

Table 4.1 summarises the three model configurations estimated in this dissertation and their analytical capabilities. The roles that each model ultimately plays in the analysis, in particular the extent to which each is suitable for the scenario projections, are determined empirically and discussed in Chapter 5.

Table 4.1: Summary of the estimated models and their analytical capabilities

Model	**Methodology**	**Temporal resolution**	**Number of inputs**	**Analytical capabilities**
ANN	Feed-forward Artificial Neural Network	Hourly	15	Point estimates of hourly prices; captures non-linear price-formation dynamics.
BLR Hourly	Bayesian Linear Regression	Hourly	16[a]	Posterior predictive distributions; interpretable coefficients; uncertainty quantification.
BLR Daily	Bayesian Linear Regression	Daily	13	Posterior predictive distributions at daily resolution; robustness assessment.

[a] Includes two Solar×Hour Fourier interaction terms (see Section 4.5.4).

4.1.2 Rationale for a Multi-Model Approach

This study employs two modelling approaches: a feed-forward Artificial Neural Network and a Bayesian Linear Regression. As discussed in the literature review, these two families differ in functional flexibility, interpretability, uncertainty quantification, and extrapolation behaviour. Rather than relying on a single framework, a multi-model approach is adopted for two reasons.

First, if both frameworks produce similar conclusions regarding the impact of the RNC2050 scenarios on electricity prices, confidence in the results is strengthened because the findings become less dependent on the assumptions of any individual model. Conversely, divergences between the models can reveal where the choice of modelling approach matters most, which is itself a useful finding.

Second, the two approaches have, by construction, different extrapolation properties, and the scenario analysis requires applying the models to inputs that differ substantially from the historical data. Whether this theoretical difference translates into materially different projections is an empirical question, and comparing the two models under the same scenarios is the most direct way to assess it.

4.1.3 Research Workflow

Figure 4.1 summarises the methodological workflow adopted in this dissertation. After data collection and pre-processing, the ANN and BLR models are estimated on the common historical dataset (2023–2025). The estimated models are then applied to two scenario families, both derived from the RNC2050 generation-mix targets but differing in the treatment of fuel and carbon prices: Scenario A incorporates projected trajectories for the TTF natural-gas price and the EU ETS allowance price, while Scenario B holds both variables constant at their 2023–2025 average levels. This design allows the structural effect of the generation-mix transformation to be assessed independently of fuel- and carbon-price uncertainty. The resulting projections are compared across models, scenarios, and temporal aggregation levels.

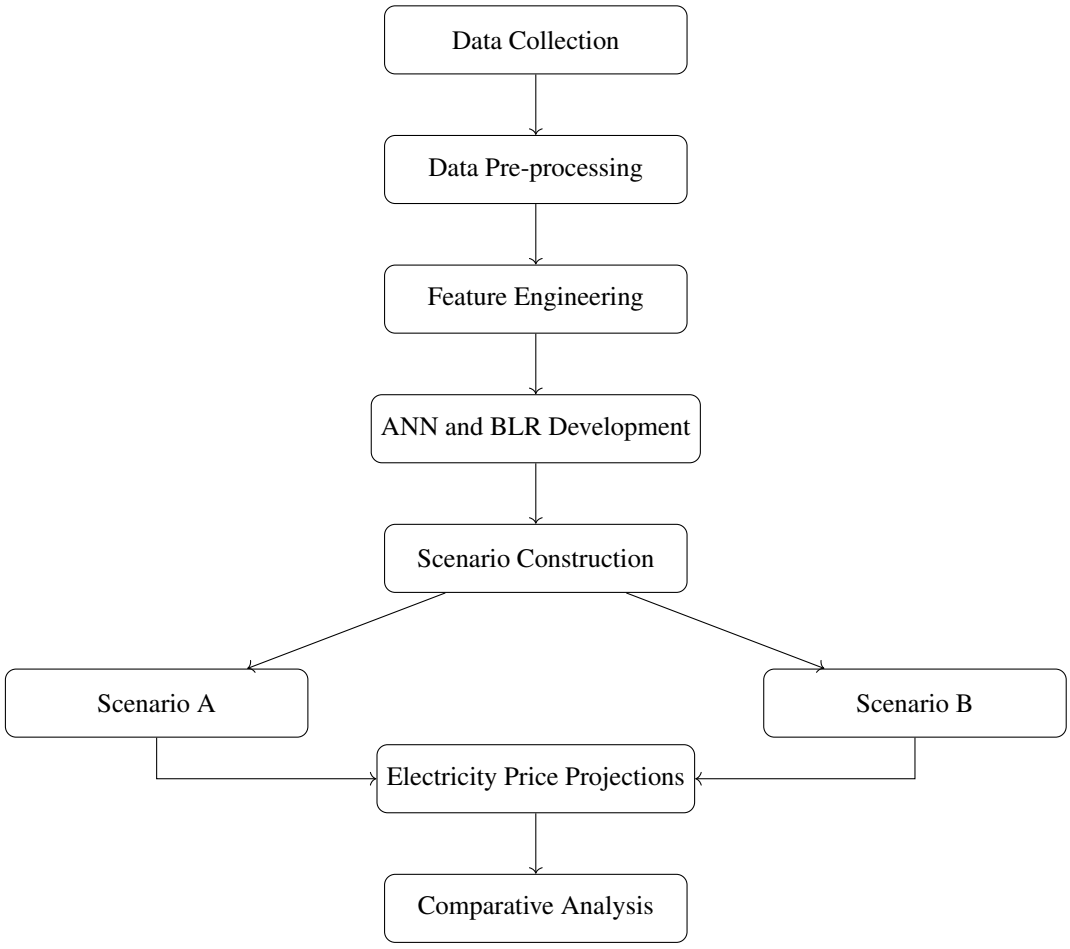


Figure 4.1: Methodological workflow adopted in this dissertation.

4.2 Data and Pre-Processing

4.2.1 Data Sources

The analysis is based exclusively on publicly available data obtained from official institutional sources. Two primary datasets were used: wholesale electricity market data published by OMIE and power-system operation data published by REN.

OMIE (*Operador del Mercado Ibérico de Energía*) provides the hourly day-ahead market prices for the Portuguese bidding zone within the Iberian Electricity Market (MIBEL). The reported price corresponds to the marginal market-clearing price resulting from each hourly auction and is expressed in EUR/MWh. This variable constitutes the dependent variable of the study.

REN (*Redes Energéticas Nacionais*), the Portuguese transmission system operator, provides hourly operational data for the national electricity system. The dataset includes generation by technology, electricity demand, and the net interconnection balance with Spain. Generation is disaggregated into wind, solar photovoltaic, hydroelectric, combined-cycle natural gas, gas cogeneration, pumped-storage hydroelectricity, and other thermal technologies. All variables are reported on an hourly basis in MWh.

The study period extends from 1 January 2023 to 31 December 2025, resulting in a balanced dataset comprising 26,304 hourly observations. This period was selected because it represents the most recent interval for which complete and consistent hourly observations were simultaneously available from both sources. Furthermore, it encompasses a wide range of market conditions, including the elevated wholesale prices observed during 2023 and the more moderate price environment that characterised 2024 and 2025. The selected period also captures a rapid expansion of photovoltaic generation in Portugal: installed solar capacity more than doubled during this interval, growing from approximately 2.7 GW at the start of 2023 to roughly 5.7 GW by the end of 2024, with solar generation reaching about 10% of national electricity consumption in 2024 for the first time. This provides sufficient variation in solar penetration levels for the estimation of solar-related price effects. It should be noted that the first year of the estimation period partially overlaps with the Iberian exception mechanism (Section 2.4.2), which capped the gas price used for electricity price formation until the end of 2023. This may attenuate the estimated TTF coefficient relative to a period of fully market-determined gas costs. The effect is mitigated by the fact that two of the three years of the sample (2024–2025) postdate the mechanism entirely.

In addition to electricity market and system-operation data, fuel and carbon-price variables were incorporated into the analysis. Daily TTF natural-gas prices (EUR/MWh) and EU ETS allowance prices (EUR/tCO_2) were obtained from publicly available market-data providers and matched to the electricity-market dataset by calendar date. Since these variables are published at daily resolution, each observation was assigned to the corresponding 24 hourly records.

4.2.2 Variable Selection and Justification

The explanatory variables were selected on the basis of three considerations: (i) economic theory regarding wholesale electricity-price formation and the merit-order mechanism; (ii) evidence from the literature on European and Iberian electricity markets; and (iii) their relevance to the objectives of the scenario analysis developed in this dissertation.

Generation-related variables are expressed as shares of hourly electricity demand rather than as absolute generation volumes. This representation captures the relative contribution of each technology to meeting system demand and facilitates comparisons across hours with different demand levels. It also provides a natural framework for evaluating future changes in the generation mix under the RNC2050 scenarios.

Electricity demand is represented through two dimensions. First, absolute hourly demand (MWh) captures the direct influence of consumption levels on market-clearing prices. Second, generation shares expressed relative to demand characterise the composition of the generation portfolio required to satisfy that demand. This specification allows demand effects and generation-mix effects to be analysed separately within the modelling framework.

The variables considered in the analysis and their respective economic motivations are summarised in Table 4.2.

Table 4.2: Input variables, definition, and economic rationale

Variable	Definition	Economic rationale
Renewable generation		
sh_eolica	Wind generation share (% of demand)	Merit-order effect: zero-SRMC generation displaces thermal and reduces the clearing price.
sh_solar	Solar PV generation share (% of demand)	As wind; intraday temporal interaction captured separately.
sh_hidrica	Hydroelectric generation share (% of demand)	Zero-SRMC dispatch displaces thermal; reservoir hydro is scheduled flexibly.
Demand		
consumo	Electricity demand (MWh)	Higher demand increases the likelihood of dispatching higher-cost technologies.
Thermal generation		
sh_gas_cc	Combined-cycle gas share (% of demand)	Dominant marginal technology in MIBEL; directly reflects price-setting generation.
sh_gas_cog	Gas cogeneration share (% of demand)	Thermal with positive marginal cost; smaller role than CC.
sh_termica	Other thermal share (% of demand)	Residual thermal (biomass, waste); small and declining.
Storage and exchanges		
sh_bombagem	Pumped storage share (% of demand)	Pumping increases instantaneous demand; operates in high-price conditions.
sh_saldo	Net interconnection balance (% of demand)	Net imports reduce the domestic supply–demand gap and exert downward pressure.
Fuel and carbon prices		
preco_ttf	TTF natural-gas price (EUR/MWh)	Primary pass-through channel from fuel costs to the SRMC of gas-fired generation.
preco_co2	EU ETS allowance price (EUR/tCO_2)	Adds to the SRMC of thermal generation via the ETS; the carbon cost represents a smaller fraction of the SRMC of a gas plant than the fuel cost itself.
Temporal controls		
hora	Hour of day (0–23)	Controls for systematic intraday demand and solar patterns.
mes	Month (1–12)	Controls for seasonal variation in load, hydro inflows, and wind/solar resources.
semana	Week of year (1–53)	Controls for medium-term seasonality and annual trends.
dia_semana	Day of week (1–7)	Controls for weekday/weekend demand patterns (ANN only; excluded from the BLR following spike-and-slab selection, Section 4.5.2.)

A methodological note on the temporal variables is warranted. The hour-of-day, month-of-year, and week-of-year variables are coded as integers and entered linearly after z-score normalisation, rather than transformed into cyclical (sine/cosine) representations. In a linear model such as the BLR, this coding does not enforce the natural adjacency of hour 23 with hour 0, or of December with January. For the hour variable, the cyclical structure is partially recovered by the Solar$\times$Hour interaction terms, which are explicitly parameterised as trigonometric functions with period 24. However, the month and week variables lack an equivalent correction and are treated as monotonic. This is a limitation of the present specification. A sine/cosine encoding of all temporal variables would be a natural refinement and is included among the recommendations for future work (Section 6.5).

Several candidate variables were evaluated but ultimately excluded from the final dataset. Biomass generation was not retained due to its consistently low and stable contribution during the study period, which limited its explanatory value. Installed-capacity variables were also excluded, as generation shares already capture the effective utilisation of available capacity (including both would increase collinearity without adding substantial information).

Some correlation between generation-share variables is expected, as all technologies jointly contribute to meeting demand. More specifically, the generation shares are subject to a structural energy-balance identity (they must sum to approximately 100% of demand), which introduces collinearity that cannot be eliminated by variable selection. This means that the individual regression coefficients should be interpreted with caution: each coefficient estimates the effect of changing one generation share while holding the others constant, but in practice a change in one share necessarily implies offsetting changes in others. The MCMC (Markov Chain Monte Carlo) convergence diagnostics ($\hat{R} < 1.05$, ESS > 1000; see Section 4.5.5) confirm that the posterior is well estimated despite this correlation, but they do not eliminate the structural collinearity itself. Nevertheless, the variables were retained because they represent distinct technologies with different marginal costs and economic roles within the merit-order framework, and because the scenario analysis requires the ability to vary them individually.

4.2.3 Data Cleaning and Normalisation

The OMIE and REN datasets were matched using hourly timestamps covering the period from January 2023 to December 2025. Following the merging process, all 26,304 hourly observations contained valid electricity-price and demand information. Consequently, no missing-value imputation procedures were required.

Negative electricity prices were retained in the dataset. Such observations do not represent data errors but rather legitimate market outcomes that occur under specific operating conditions, particularly during periods of high renewable generation and low demand. Excluding negative-price observations would remove economically meaningful information and could bias the analysis against conditions that are expected to become increasingly relevant under high-renewable systems.

Prior to model estimation, all continuous input variables were standardised using z-score normalisation:

$$x_{\text{norm}} = \frac{x - \mu_x}{\sigma_x} \tag{4.1}$$

where μ_x and σ_x denote the sample mean and standard deviation of the corresponding variable. Z-score standardisation was preferred to min–max scaling because it preserves relative variation in skewed distributions and remains suitable for out-of-sample projections whose values may exceed the historical range. In addition, standardisation places all variables on a common scale, improving numerical stability during ANN training and facilitating prior specification in the Bayesian framework.

4.3 Evaluation Framework

4.3.1 Performance Metrics

Four metrics are used to evaluate model fit, all expressed in the original, non-normalised price scale (EUR/MWh) to ensure direct economic interpretability. For the ANN, all reported metrics are computed across the full dataset of 26,304 observations, reflecting the model's overall fit throughout the historical baseline. This aligns with its application for system characterisation and scenario-based analysis rather than sequential out-of-sample forecasting. The random 70/15/15 partition was used internally only to guide training (early stopping via the validation set) and architecture selection. To confirm that the all-data metrics do not mask overfitting, performance was also computed separately on the three partitions of the final reproducible (fixed-seed) network. The small gap between the training and test R^2 (0.025), together with the near-identical validation and test figures, suggests that the degree of overfitting is limited (see Section 4.4.2), although it should be noted that the random partition does not constitute a genuine out-of-sample test, since adjacent hours may appear in different subsets. For the BLR, the reported metrics reflect the overall in-sample fit, as the Bayesian estimation evaluates goodness-of-fit across the complete posterior distribution. In both cases, the reported R^2 values should be understood as measures of explanatory fit within the estimation sample and should not be compared directly with out-of-sample predictive benchmarks from the electricity-price forecasting literature.

Coefficient of Determination (R^2)

The coefficient of determination measures the proportion of total variance in electricity prices explained by the model:

$$R^2 = 1 - \frac{\sum_{i=1}^{N}(y_i - \hat{y}_i)^2}{\sum_{i=1}^{N}(y_i - \bar{y})^2} \tag{4.2}$$

where y_i denotes the observed price for observation i, $\hat{y}_i$ the model-predicted price, and $\bar{y}$ the sample mean of observed prices.

Values closer to unity indicate a superior fit. As a dimensionless statistic, R^2 is used primarily to compare alternative model architectures and to assess global explanatory power.

Mean Absolute Error (MAE)

$$\text{MAE} = \frac{1}{N}\sum_{i=1}^{N}|y_i - \hat{y}_i| \tag{4.3}$$

Because all deviations contribute linearly, the MAE provides a stable measure of forecasting accuracy in explicit monetary terms and is robust to isolated extreme observations.

Root Mean Squared Error (RMSE)

$$\text{RMSE} = \sqrt{\frac{1}{N}\sum_{i=1}^{N}(y_i - \hat{y}_i)^2} \tag{4.4}$$

By squaring errors before averaging, the RMSE assigns greater weight to large deviations, making it sensitive to extreme price spikes. It is reported alongside the MAE to facilitate benchmarking against the broader electricity-price forecasting literature.

Mean Absolute Percentage Error (MAPE)

$$\text{MAPE} = \frac{1}{N}\sum_{i=1}^{N}\frac{|y_i - \hat{y}_i|}{|y_i|} \times 100 \tag{4.5}$$

This metric standardises accuracy assessments, allowing comparisons across markets and price regimes. Because electricity prices can approach zero or settle at negative values, the MAPE is restricted to observations satisfying $|y_i| > 5$ EUR/MWh, preventing numerical instability from near-zero denominators.

4.3.2 Bayesian-Specific Metrics

A core advantage of the BLR framework is its capacity to generate a full posterior predictive distribution for each observation via MCMC sampling. The 90% credible interval is defined as:

$$[P_5(\hat{y}|x), P_{95}(\hat{y}|x)] \tag{4.6}$$

where P_5 and P_{95} denote the 5th and 95th percentiles of the posterior predictive distribution conditional on the input vector x. This interval has a direct probabilistic interpretation: given the model and the data, there is a 90% posterior probability that the realised price falls within these bounds. This is conceptually distinct from a frequentist confidence interval, which refers to the long-run properties of an estimation procedure rather than to the probability of a specific outcome.

The distinction is particularly relevant for long-term scenarios where future observations cannot be repeatedly sampled.

Throughout the analysis, the median of the posterior predictive distribution is adopted as the measure of central tendency rather than the mean. The empirical distribution of MIBEL day-ahead prices exhibits moderate left-skewness (historical baseline mean of approximately 72.6 EUR/MWh versus a median of approximately 78.9 EUR/MWh), driven by roughly 20% of hours with depressed or negative prices coinciding with renewable surplus and low-demand periods. The posterior median offers greater robustness to this distributional asymmetry.

4.4 Neural Network Model

4.4.1 Architecture and Input Selection

The ANN was implemented in MATLAB using the Neural Network Toolbox. A feed-forward architecture with a single hidden layer was adopted, trained using the Levenberg–Marquardt backpropagation algorithm [43]. The final configuration follows a [15–60–1] structure: 15 input variables, a hidden layer with 60 neurons employing a hyperbolic tangent sigmoid activation function (*tansig*), and a single output neuron with a linear activation function (*purelin*). This configuration allows the network to model non-linear relationships while preserving an unrestricted output range, including negative prices.

Input selection was performed through a sequential model-building procedure. Six candidate specifications were evaluated, with each successive model incorporating an additional group of explanatory variables. To ensure comparability, all candidates were trained using the same architecture (10 hidden neurons) and evaluated over 10 independent initialisations.

Table 4.3: Sequential comparison of candidate input specifications

Model	**Additional inputs**	**Total inputs**	R^2_{med}	R^2_{max}	**MAPE**	**MAE (EUR/MWh)**
A	Wind, solar, hour, day-of-week	4	0.270	0.279	64.9%	26.97
B	+ Hydro, consumption, month, week	8	0.459	0.482	50.4%	22.39
C	+ Gas CC, gas cogeneration	10	0.576	0.608	43.1%	19.13
D	+ Other thermal	11	0.578	0.617	43.1%	18.98
E	+ Pumped storage, net balance	13	0.621	0.641	40.9%	18.35
F	+ TTF price, CO_2 price	15	0.698	0.728	36.5%	15.78

The progressive inclusion of variables resulted in systematic improvements across all metrics. The largest gains were obtained after incorporating thermal-generation variables and fuel-cost

indicators, highlighting their importance in price formation. Model F achieved the best overall performance ($R^2_{\max} = 0.728$, MAE = 15.78 EUR/MWh) and was retained for architecture selection.

Using Model F, a second selection stage determined the number of hidden neurons. Seven architectures (5, 10, 20, 30, 40, 50, and 60 neurons) were evaluated, each over 20 independent training runs.

Table 4.4: Comparison of alternative hidden-layer architectures

Neurons	R^2	MAPE	MAE (EUR/MWh)	Parameters
5	0.733	41.7%	18.36	86
10	0.792	36.3%	16.00	171
20	0.837	31.1%	13.96	341
30	0.849	30.1%	13.42	511
40	0.867	27.7%	12.58	681
50	0.873	27.2%	12.26	851
60	**0.882**	**26.4%**	**11.80**	**1,021**

The 60-neuron architecture achieved the highest predictive accuracy, with $R^2 = 0.882$ and MAE = 11.80 EUR/MWh, while preserving approximately 26 observations per trainable parameter. The final network, trained with a fixed random seed for reproducibility (Section 4.4.2), attains an all-data $R^2 = 0.883$ (MAE = 11.73 EUR/MWh), consistent with the architecture-selection result. The [15–60–1] configuration was therefore adopted as the final ANN architecture.

4.4.2 Training Process

The final architecture was trained using a fixed random seed (*rng(42)*) to ensure full reproducibility. The 26,304 hourly observations were randomly partitioned into training (70%), validation (15%), and test (15%) subsets. The primary reason for adopting a random partition, rather than a temporal block split (e.g., training on 2023–2024, testing on 2025), is that the objective of the model is to estimate structural relationships between generation shares and prices across the full range of market conditions, not to forecast sequentially. A temporal split would confound the assessment of model fit with changes in market regime between years, such as the transition from the elevated prices of 2023 to the more moderate conditions of 2024–2025, and would prevent the model from learning from the complete range of operating conditions during training. A recognised limitation of the random partition is that adjacent hours are autocorrelated, so that the train–test gap may understate the true generalisation error relative to genuinely unseen data. The reported fit metrics should therefore be interpreted as explanatory rather than predictive. The validation subset was used exclusively for early-stopping control, with training terminated after six consecutive validation checks without improvement in the loss function. The training, validation, and test R^2 of the final network are 0.890, 0.868, and 0.865 respectively (MAE = 11.36, 12.64, and 12.55 EUR/MWh). The small and consistent differences across subsets suggest that the degree of overfitting is limited, although the limitation noted above should be kept in mind.

4.4.3 Sensitivity Analysis

To evaluate the relative influence of each explanatory variable on the ANN predictions, a perturbation-based sensitivity analysis was performed. For each input variable (x_j), a small perturbation $\delta_j = \sigma_j/10$ was applied while all remaining variables were held unchanged. Because all inputs are z-score normalised, $\sigma_j = 1$ and $\delta_j = 0.1$ for all variables. The sensitivity index is:

$$S_j = \frac{1}{N}\sum_{i=1}^{N} \left| f(x_{1,i}, \ldots, x_{j,i} + \delta_j, \ldots, x_{15,i}) - f(x_{1,i}, \ldots, x_{j,i}, \ldots, x_{15,i}) \right| \tag{4.7}$$

expressed in EUR/MWh. The results are presented in Table 4.5.

Table 4.5: Perturbation-based sensitivity analysis – ANN Model F, 60 neurons

Variable	S_j **(EUR/MWh per** $\sigma/10$**)**
Net balance	8.85
Hydro	7.96
Week	7.02
Wind	6.48
Month	5.78
Solar	4.67
Hour	4.33
Pumped storage	3.99
Gas CC	3.90
TTF	2.89
CO_2	2.47
Consumption	1.17
Gas cogeneration	1.16
Day of week	1.14
Other thermal	0.93

Perturbation: $\delta_j = \sigma_j/10 = 0.1$. S_j is the average absolute price variation across all 26,304 observations.

The ranking of sensitivity indices may appear counter-intuitive: the net interconnection balance and hydroelectric generation exhibit higher sensitivities than wind or solar. This reflects the fact that a swing in net imports or hydroelectric availability changes which technology is marginal and can produce a large price movement, whereas the effect of wind and solar, although economically important, is more gradual and distributed across hours. The full interpretation of these results is presented in Section 5.2.

4.5 Bayesian Linear Regression

4.5.1 Model Formulation

The Bayesian linear regression specifies the following generative model for the price:

$$y_t = \alpha + \sum_{j=1}^{J} \beta_j x_{j,t} + \varepsilon_t, \qquad \varepsilon_t \sim \mathcal{N}(0, \sigma^2) \tag{4.8}$$

where y_t is the observed price at hour t (EUR/MWh, with inputs z-score normalised), α is the intercept, β_j are the regression coefficients, and ε_t is Gaussian noise with unknown variance σ^2. Because all continuous inputs are standardised, each β_j can be interpreted as the expected change in price (EUR/MWh) associated with a one-standard-deviation increase in input j, holding all other inputs constant. The intercept α represents the expected price when all standardised inputs are at their historical mean values.

Two versions of this model are estimated. The hourly model operates on 26,304 observations and includes 16 variables (14 base variables plus two Solar×Hour interaction terms; see Sections 4.5.2 and 4.5.4). The daily model operates on 1,096 observations (simple averages of all hourly values within each day) and includes 13 variables (the 14 base variables minus the hour-of-day variable, which has no meaning after daily aggregation).

In the Bayesian framework, inference requires specifying prior distributions $p(\beta, \sigma)$ before observing the data, then combining them with the likelihood $p(y \mid X, \beta, \sigma)$ via Bayes' theorem:

$$p(\beta, \sigma \mid y, X) \propto p(y \mid X, \beta, \sigma) \cdot p(\beta, \sigma) \tag{4.9}$$

Rather than point estimates, inference yields full posterior distributions for all parameters, encoding both the estimated effects and the uncertainty about those effects. The posterior predictive distribution for a new observation $\tilde{y}$ at input $\tilde{x}$ is:

$$p(\tilde{y} \mid \tilde{x}, y, X) = \int p(\tilde{y} \mid \tilde{x}, \beta, \sigma) \cdot p(\beta, \sigma \mid y, X)\, d\beta\, d\sigma \tag{4.10}$$

This integral is approximated using MCMC sampling. The estimated posterior coefficients (posterior medians and 90% highest-density intervals) are presented in Section 5.3.2, together with the comparison between the prior means and the posterior estimates.

4.5.2 Variable Selection and Prior Specification

Variable selection for the BLR was conducted using a Bayesian spike-and-slab prior, in which each coefficient is modelled as a mixture between a diffuse slab component (allowing a substantial effect) and a spike concentrated at zero (allowing the variable to be effectively excluded). The posterior inclusion probability (PIP) of each variable quantifies the posterior evidence that it belongs in the model. The median-probability threshold (PIP > 0.5) was adopted as the selection criterion. All variables exhibited posterior inclusion probabilities above this threshold except the day-of-week indicator, which was therefore excluded from the final BLR specification. The resulting posterior inclusion probabilities are presented in Figure 4.2.

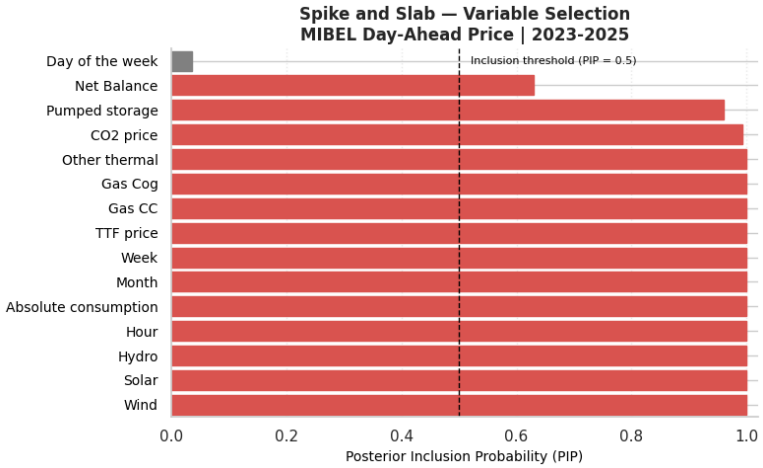


Figure 4.2: Posterior inclusion probabilities from the spike-and-slab variable selection, MIBEL day-ahead price, 2023–2025. The dashed line marks the median-probability inclusion threshold (PIP = 0.5).

A distinctive advantage of the Bayesian framework is its ability to incorporate domain knowledge directly into the estimation process through the prior distributions. In the context of electricity-price modelling, this means that the well-established economic relationships can be encoded as prior expectations, so that the model does not need to discover these relationships from the data alone. This is particularly valuable when the data is limited, when variables are correlated, or when the model must be extrapolated to conditions outside the estimation period (precisely the setting considered in this dissertation).

For the variables retained after the selection stage, informative priors were assigned whenever economic theory suggested both the expected direction and the approximate magnitude of an effect. In contrast, flat priors were reserved for the temporal controls, whose patterns are left entirely to the data. The prior means were anchored in the merit-order literature and deliberately kept conservative, with standard deviations broad enough to permit substantial posterior updating. The full specification is given in Table 4.6, the rationale is summarised by variable group below.

Table 4.6: Prior distributions adopted for the Bayesian model

Variable	Distribution	μ	σ
Renewable generation			
Wind generation share (sh_eolica)	Normal	-8	8
Solar generation share (sh_solar)	Normal	-8	8
Hydroelectric generation share (sh_hidrica)	Normal	-8	8
Demand			
Electricity consumption (consumo)	Normal	10	5
Thermal generation			
Combined-cycle gas share (sh_gas_cc)	Normal	8	4
Gas cogeneration share (sh_gas_cog)	Normal	5	3
Other thermal generation (sh_termica)	Normal	3	3
Storage and exchanges			
Pumped-storage share (sh_bombagem)	Normal	-3	3
Net interconnection balance (sh_saldo)	Normal	-6	4
Fuel and carbon prices			
TTF natural-gas price (preco_ttf)	Normal	10	3
EU ETS carbon price (preco_co2)	Normal	2	2
Temporal controls			
Hour effects (hora)	Flat	–	–
Month effects (mes)	Flat	–	–
Week effects (semana)	Flat	–	–
Interaction terms			
Solar $\times \sin(\text{hour})$	Normal	0	5
Solar $\times \cos(\text{hour})$	Normal	0	5
Model parameters			
Intercept (α)	Flat	–	–
Error scale (σ)	HalfNormal	–	20

Renewable generation (wind, solar, hydro) received negative prior means ($\mu = -8$, $\sigma = 8$). The negative sign follows from the merit-order mechanism (Section 2.3). The magnitude of -8 EUR/MWh per standard deviation is conservative relative to the empirical estimates in the literature [8, 9]. The wide standard deviation ($\sigma = 8$) was chosen to ensure that the data can move the posterior substantially away from the prior if the historical evidence warrants it.

Demand ($\mu = +10$, $\sigma = 5$) received a positive prior: higher load moves the system up the supply curve, dispatching progressively more expensive generation. The prior mean of $+10$ reflects the approximate slope of the supply curve in the relevant range of MIBEL demand levels, and the standard deviation allows the data to adjust this estimate.

Thermal generation received positive means scaled to each technology's typical position in the merit order: gas CC ($\mu = +8$, $\sigma = 4$), gas cogeneration ($\mu = +5$, $\sigma = 3$), and other thermal ($\mu = +3$, $\sigma = 3$). The gas CC prior is the most informative of this group because combined-cycle plants are the dominant price-setting technology in MIBEL. A higher gas CC share in a given hour

signals that more expensive generation is on the margin, which is directly associated with higher prices.

The TTF natural-gas price received a prior of $\mu = +10$, $\sigma = 3$, making it the tightest prior in the specification. This choice reflects the strong and well-documented gas-to-power pass-through: in a system where gas-fired plants frequently set the marginal price, a one-standard-deviation increase in the gas price translates almost directly into a higher electricity price, with the magnitude governed by the heat rate of the marginal plant and the normalisation of the input. The CO_2 prior ($\mu = +2$, $\sigma = 2$) is weaker, reflecting both the smaller share of the carbon cost in the SRMC of a gas plant (typically 20–30% of the total, versus 70–80% for the fuel cost) and the limited variability of the EU ETS price during the estimation period.

The storage and exchange terms received weak negative priors (pumped storage $\mu = -3$; net balance $\mu = -6$), as both are associated with periods of ample supply and downward price pressure, but with wider uncertainty given the complex operational logic of these variables.

The temporal controls (hour, month, week) were given flat priors, so that intraday, seasonal, and intra-annual structure is identified solely by the data. The Solar×Hour interaction terms were assigned zero-centred priors ($\sigma = 5$), since economic theory provides no clear directional expectation for the intraday modulation of the solar effect. The intercept received a flat prior, the error scale follows $\sigma \sim \text{HalfNormal}(20)$, consistent with price variability on the order of tens of EUR/MWh.

In all cases, the prior standard deviations were deliberately set wide enough to allow the data to dominate the posterior. The adequacy of this choice is assessed in Section 5.3.2, where the posterior coefficients are compared with the prior means. Cases in which the posterior departs substantially from the prior confirm that the data, rather than the prior, is driving the estimate.

4.5.3 Interaction Terms: Solar × Hour

The inclusion of Solar×Hour interaction terms is motivated by the empirical observation, well documented in the MIBEL context (Section 2.4.2), that the price effect of solar generation varies systematically with the hour of day. During solar peak hours (approximately 10h–16h), high solar generation is associated with a pronounced price trough. At night, solar generation is structurally zero and exerts no price effect regardless of installed capacity.

A linear model without interaction terms would estimate a single average coefficient for solar, implying that each additional unit of solar generation reduces prices equally at all hours, including hours when solar generation is zero by physical definition. This is both economically incorrect and statistically problematic, as it would force the intercept and other time-of-day variables to compensate for an incorrectly specified solar effect.

Rather than including 24 separate hour-specific coefficients, the interaction is parameterised

using trigonometric components:

$$\text{solar_x_hour_sin} = \text{sh_solar} \times \sin\left(\frac{2\pi\,\text{hour}}{24}\right) \tag{4.11}$$

$$\text{solar_x_hour_cos} = \text{sh_solar} \times \cos\left(\frac{2\pi\,\text{hour}}{24}\right) \tag{4.12}$$

This two-component specification captures the dominant periodic component of the intraday solar effect with only two additional parameters. Together, $\beta_{\sin}$ and $\beta_{\cos}$ determine both the amplitude and the phase of the intraday solar price modulation.

The interaction terms are included only in the hourly BLR model, as daily aggregation removes the intraday variation that motivates them. As with the remaining coefficients, their application to long-term scenarios assumes that the estimated historical relationships remain valid under future operating conditions.

4.5.4 Hourly vs. Daily Model

The hourly and daily specifications were estimated in parallel to assess the robustness of the projections to temporal aggregation.

Table 4.7: Differences between the hourly and daily BLR specifications

Dimension	**Hourly model**	**Daily model**
Sample size	26,304 observations	1,096 observations
Variables	16 (incl. hour, Solar×Hour)	13 (no hour, no interaction)
Constraint limits	Hourly caps	Daily caps
R^2	0.593	0.702
MAE	23.26 EUR/MWh	16.25 EUR/MWh

Metrics correspond to the final specification (Stage 2: informative priors, solar saturation, Solar×Hour interaction for the hourly model). The Stage 1 specification (flat priors, no saturation, no interaction) attains $R^2 = 0.565$ and MAE $= 24.07$ EUR/MWh for the hourly model; the daily model is unaffected by the stage refinements ($R^2 = 0.702$, MAE $= 16.24$–16.25 EUR/MWh across all stages).

The higher R^2 of the daily model is expected, as aggregation reduces short-term volatility and noise. Both BLR specifications exhibit lower in-sample R^2 than the ANN. This is an expected consequence of the linear functional form and is an accepted trade-off given the BLR's interpretable coefficients and explicit uncertainty quantification, whose value for long-term scenario analysis is assessed in Section 5.6. The hourly model provides the finer temporal resolution; the daily model serves as an independent robustness check.

4.5.5 MCMC Estimation and Convergence Diagnostics

The posterior distribution defined by the Bayesian model does not have a closed-form solution for the specification used here, and must therefore be approximated numerically. Markov Chain Monte Carlo sampling draws correlated samples from the posterior distribution, and convergence diagnostics verify that the samples adequately represent the target distribution.

Posterior distributions for both BLR specifications were estimated via the No-U-Turn Sampler (NUTS), implemented in PyMC (version 5.28.5). NUTS is an adaptive variant of Hamiltonian Monte Carlo (HMC) [44] that automatically tunes the step size and trajectory length, eliminating the manual tuning required by standard HMC and producing efficient sampling in correlated parameter spaces, which is relevant here because the generation-share variables are correlated through the energy-balance identity.

The sampling configuration was as follows:

- 4 independent chains, initialised from different starting points drawn from the prior;
- 2,000 posterior draws per chain after warm-up (8,000 total posterior samples);
- 3,000 warm-up (tuning) steps per chain, discarded before posterior sampling.

The four-chain configuration enables convergence to be diagnosed by comparing chains and increases the diversity of the posterior sample. The 2,000-draw specification was determined from pilot runs in which effective sample sizes exceeded 1,000 for all parameters, satisfying the minimum recommended for stable posterior summaries. The 3,000 warm-up steps exceed the typical minimum and were chosen to ensure that the NUTS adapter converges for the interaction terms, whose posterior geometry is less concentrated than that of the main coefficients.

Convergence was assessed using three diagnostics applied to all parameters. The potential scale reduction factor ($\hat{R}$), computed across the four chains, was required to satisfy $\hat{R} < 1.05$, more stringent than the traditional 1.1 threshold. Both bulk and tail effective sample sizes (ESS) were monitored, with a minimum of 1,000. Finally, the trace plots were visually inspected to confirm satisfactory mixing and the absence of systematic trends or divergences. All estimated models satisfied these convergence criteria.

4.6 RNC2050 Scenario Construction

Given the long-term horizon considered in this study, a scenario-based approach was adopted instead of direct price forecasting. Over horizons extending to 2050, uncertainty regarding technology deployment, electricity demand, regulatory developments, and fuel markets becomes sufficiently large that a single forecast trajectory would provide a misleading representation of future outcomes. Scenario analysis offers a more transparent framework by explicitly linking projected prices to a defined set of assumptions.

The RNC2050 establishes quantitative targets for installed generation capacity by technology and projections for final electricity consumption, from which the demand-growth factors used in

this study are derived. These targets provide externally defined reference points that can be translated into model inputs through a transparent scaling procedure. Two scenarios are considered, both incorporating the same generation-mix evolution and differing exclusively in the treatment of fuel and carbon prices.

Before describing the scenario-construction procedure, it is useful to recall the distinction between variable renewable energy (VRE), defined in Section 2.1.2, and synchronous generation (hydroelectric and gas-fired plants that provide inertia and frequency support through rotating machines).

4.6.1 Methodological Assumptions

The scenario construction relies on a number of simplifying assumptions intended to ensure methodological consistency and transparency.

1. **Demand profile preservation.** The temporal structure of the historical load profile is assumed to remain unchanged. Future demand is represented by applying annual scaling factors to the historical series. Structural changes in demand patterns arising from electric-vehicle charging, heat-pump deployment, demand-side flexibility, or sector coupling are not explicitly modelled. This assumption implies that the scenario projections capture the effect of demand *level* growth on prices but not the effect of demand *profile* changes. The response to RQ3 is therefore conditional on the historical demand profile and does not capture the additional price effects that a restructured load shape might produce.

2. **Stationary hydroelectric behaviour.** Hydroelectric generation is maintained at its historical share of demand and is not scaled according to installed capacity. This reflects the fact that hydroelectric output is primarily constrained by hydrological conditions and reservoir operation rather than by installed capacity alone.

3. **Stationary interconnection behaviour.** Net electricity exchanges with Spain are assumed to remain consistent with historical observations. The future evolution of the Spanish electricity system and wider European market interactions is not modelled explicitly.

4. **Limited representation of storage technologies.** System flexibility is represented exclusively through pumped-storage capacity. Battery storage and other flexibility technologies are not modelled separately.

5. **Exogenous capacity evolution.** Future generation capacities are taken directly from the RNC2050 targets rather than determined by the model. The analysis evaluates the price implications of the RNC2050 pathway, not the optimal generation portfolio.

6. **Exogenous fuel and carbon prices.** Natural-gas and EU ETS allowance prices are treated as external inputs whose trajectories are specified independently of developments in the Portuguese electricity sector.

7. **Stable price-formation relationships.** The statistical relationships estimated from the 2023–2025 dataset are assumed to remain applicable throughout the projection horizon. In particular, the coefficients relating fuel and carbon prices to the electricity price are estimated from a period in which gas generation averaged roughly 10% of demand and are applied unchanged to future horizons in which gas may represent as little as 0.6%. As discussed in Chapter 3, the transmission channel through which fuel and carbon prices affect the electricity price narrows as the gas share becomes residual. This extrapolation is therefore most uncertain for the 2050 horizon.

8. **No endogenous market redesign.** The fundamental structure of the electricity market is assumed to remain unchanged. Potential future changes in market design, ancillary-service arrangements, flexibility-remuneration mechanisms, capacity markets, or regulatory frameworks are not modelled.

The scenario projections are therefore conditional on these assumptions.

4.6.2 Scenario Inputs: Scaling Factors and Price Assumptions

Installed-capacity targets are obtained from the RNC2050 generation-capacity projections [4]. Demand-growth factors are derived from the projected evolution of electricity in final energy consumption presented in the same document (Table 2.1), using the 2020 reference value of 173.59 PJ as the base. The year 2020 is used because it is the reference year explicitly reported in the RNC2050 trajectory. Using the 2023–2025 average would require back-calculating an adjusted trajectory not available in the original document. This choice may slightly overestimate the demand-growth factors relative to the study period, since 2020 demand was depressed by the pandemic. Where the RNC2050 reports a range of values (reflecting alternative scenario variants), the lower bound is used throughout. This corresponds to the more conservative variant and avoids selecting different bounds across horizons, ensuring internal consistency:

$$\begin{aligned} f_{\text{demand},2030} &= \frac{193.41}{173.59} = 1.114, \\ f_{\text{demand},2040} &= \frac{264.74}{173.59} = 1.525, \\ f_{\text{demand},2050} &= \frac{307.58}{173.59} = 1.772 \end{aligned} \tag{4.13}$$

Table 4.8 presents the RNC2050 capacity and demand targets used for scenario construction.

Table 4.8: RNC2050 capacity and demand targets used for scenario construction

Variable	2023–2025	2030	2040	2050
Solar (GW)	1.9[a]	6.9	17.0	26.0
Wind, onshore (GW)	5.2	8.0	11.0	13.0
Gas (GW)	4.9	3.5	2.3	0.2
Pumped storage (GW)	2.5	3.4	3.4	3.4
Demand growth	–	+11.4%	+52.5%	+77.2%

[a] This value reflects the RNC2050 baseline, which was developed in 2017–2018 and approved in July 2019 [4]. At that time, Portugal's installed solar PV capacity stood below 2 GW. By the end of 2024, actual installed capacity had reached approximately 5.7 GW [17] (Section 4.2.1), substantially exceeding the RNC2050 trajectory. This acceleration reflects a combination of falling technology costs, successive capacity auction programmes, and a broader policy push to accelerate renewable deployment. Because the present study uses the RNC2050 as its primary source for scenario construction, the lower baseline value is retained.

For each technology, the effective scaling factor (expressed as a change in generation share relative to demand) is:

$$f_{\text{effective},j} = \frac{\text{Capacity}_{\text{target},j}}{\text{Capacity}_{\text{historical},j}} \cdot \frac{1}{f_{\text{demand}}} \tag{4.14}$$

The division by the demand-growth factor converts the installed-capacity increase into a change in generation share. As total electricity demand increases, a given capacity level supplies a smaller fraction of the overall load. For wind generation in 2030, for example:

$$f_{\text{wind},2030} = \frac{8.0}{5.2} \cdot \frac{1}{1.114} = 1.38 \tag{4.15}$$

For solar generation specifically, a hyperbolic tangent saturation function is applied to the effective scaling factor:

$$f^{\text{sat}}_{\text{effective}} = 6 \times \tanh\left(\frac{f_{\text{effective}}}{6}\right) \tag{4.16}$$

The saturation function was introduced to represent the diminishing ability of the system to physically absorb additional solar generation at very high penetration levels: at very high solar shares, curtailment, self-consumption, and grid-absorption limits constrain the effective output that reaches the market, so that the relationship between installed capacity and effective generation share becomes increasingly non-linear. This physical saturation is conceptually distinct from the price-cannibalization mechanism captured by the Solar×Hour interaction terms in the BLR: the saturation function limits *how much* solar generation enters the market (a pre-market, physical effect), whereas the interaction terms govern *how each unit of solar generation that does enter the market affects the price at different hours* (an intra-market, price effect). The two mechanisms are therefore complementary rather than redundant, although their joint application means that the

scenario results should be interpreted as reflecting both channels simultaneously. The function preserves approximately linear behaviour for moderate increases in solar capacity while progressively limiting growth at higher penetration levels. The parameter value of 6 was selected as a modelling assumption, it is not a calibrated physical quantity, but it ensures that saturation remains limited under moderate deployment while becoming progressively relevant under the highest solar penetrations of the RNC2050 scenarios. For 2050, the unsaturated factor is:

$$f_{\text{solar,2050}} = \frac{26.0}{1.9} \cdot \frac{1}{1.772} = 7.72 \tag{4.17}$$

which after saturation becomes:

$$f^{\text{sat}}_{\text{solar,2050}} = 6 \times \tanh\left(\frac{7.72}{6}\right) = 5.15 \tag{4.18}$$

The effective scaling factors for all technologies, after the application of the saturation function to solar, are summarised in Table 4.9.

Table 4.9: Effective scaling factors after saturation

Variable	**2030**	**2040**	**2050**
Solar (after tanh)	$\times 2.97$	$\times 4.51$	$\times 5.15$
Wind	$\times 1.38$	$\times 1.39$	$\times 1.41$
Gas CC (GAS_MAX)	10.4%	6.8%	0.6%
Consumption	+11.4%	+52.5%	+77.2%
Pumped storage	$\times 1.36$	$\times 1.36$	$\times 1.36$

The maximum gas combined-cycle share (GAS_MAX) is obtained by scaling the historical average gas share (approximately 14.5% of demand) by the ratio of projected to historical installed capacity:

$$\text{GAS_MAX} = 14.5\% \times \frac{\text{Capacity}_{\text{target}}}{\text{Capacity}_{\text{historical}}} \tag{4.19}$$

This yields $14.5\% \times [3.5/4.9,\ 2.3/4.9,\ 0.2/4.9] = [10.4\%,\ 6.8\%,\ 0.6\%]$ for 2030, 2040, and 2050 respectively.

For pumped-storage factor the scaling factor of $\times 1.36$ corresponds to the ratio between the RNC2050 target of 3.4 GW and the historical reference of 2.5 GW ($3.4/2.5 = 1.36$). No additional expansion is foreseen after 2030, so the same factor applies across all horizons.

The two scenarios differ exclusively in the treatment of natural-gas and carbon prices, summarised in Table 4.10. This is the area of the scenario construction in which the author's assumptions play the largest role, and the resulting projections should be interpreted with this in mind. For the 2030 horizon, the Scenario A values are anchored in published projections: the TTF trajectory is informed by the IEA World Energy Outlook 2025 Net-Zero Emissions scenario [45], and the EU ETS trajectory by Bloomberg/ABN AMRO consensus forecasts [46]. For the 2040 and 2050 horizons, however, published long-term projections for both variables are scarce and subject

to considerable uncertainty. The values adopted for these horizons were obtained by interpolation and extrapolation from the available sources and therefore represent modelling assumptions by the author rather than consensus forecasts. In particular, the assumed decline of the TTF to approximately 17 EUR/MWh by 2050 ($\times$0.46 relative to the historical average) and the rise of the EU ETS allowance price to approximately 300 EUR/t ($\times$4.00) are plausible under a net-zero pathway but carry substantial uncertainty. Scenario B avoids this uncertainty entirely by maintaining both variables at their 2023–2025 average levels, which is precisely the reason it serves as the reference for providing a conditional estimate of the structural effect of the modelled demand and generation-mix changes, with fuel and carbon prices held constant.

Table 4.10: Fuel and carbon-price assumptions by scenario

	2023–25	**2030**	**Factor**	**2040**	**Factor**	**2050**	**Factor**
Sc. A – TTF (EUR/MWh)	$\sim$37	$\sim$28	$\times$0.76	$\sim$22	$\times$0.59	$\sim$17	$\times$0.46
Sc. B – TTF (EUR/MWh)	$\sim$37	$\sim$37	$\times$1.00	$\sim$37	$\times$1.00	$\sim$37	$\times$1.00
Sc. A – EU ETS (EUR/t)	$\sim$75	$\sim$145	$\times$1.93	$\sim$260	$\times$3.47	$\sim$300	$\times$4.00
Sc. B – EU ETS (EUR/t)	$\sim$75	$\sim$75	$\times$1.00	$\sim$75	$\times$1.00	$\sim$75	$\times$1.00

Factors are relative to the 2023–2025 historical average.

4.6.3 Conceptual Dispatch Logic

The scenario-construction procedure transforms the historical generation mix into future configurations consistent with the RNC2050 targets while preserving physical feasibility. The procedure approximates the economic logic of merit-order dispatch, in which variable renewable energy is dispatched first at near-zero marginal cost, followed by hydroelectric generation and, last, gas-fired generation in ascending order of cost. The net interconnection balance and pumped storage operate alongside this sequence: pumped storage absorbs surplus renewable generation (adding to demand) and releases it during higher-price hours, while the net cross-border balance reflects imports and exports with Spain that smooth the domestic supply–demand gap. The procedure follows five sequential steps:

1. Historical solar and wind shares are scaled according to the corresponding effective factors. Solar scaling is subject to the saturation function and the renewable-share limits.

2. Hydroelectric and interconnection shares are held at their historical values (Assumptions 3–4).

3. Pumped-storage activity is scaled by $\times$1.36 and treated as net additional demand[1], thereby increasing the room available for renewable absorption.

4. Gas-fired generation supplies the residual demand not met by the remaining technologies, subject to the GAS_MAX ceiling and the SINC_MIN synchronous-generation floor.

[1] In practice, pumped storage operates in both directions: it adds to demand when charging and contributes to hydroelectric generation when turbining. The BLR's negative posterior coefficient for this variable (-3.99 EUR/MWh per σ) suggests that the net historical effect is to smooth price peaks rather than to increase system load.

5. The resulting generation mix is adjusted to satisfy the energy-balance constraint, with solar and wind reduced proportionally whenever total generation exceeds 100% of load.

The resulting shares represent approximate generation outcomes rather than direct translations of installed-capacity ratios. The procedure does not represent chronological unit commitment, minimum technical constraints, ramping limits, reserve requirements, or network congestion. It should be interpreted as a simplified dispatch approximation.

4.6.4 Operational Constraints

To prevent unrealistic generation configurations, a set of operational constraints is applied sequentially to every scenario–year combination. The constraints are applied in a fixed order because each one modifies the generation shares available to subsequent steps.

The renewable caps SOLAR_MAX, EOLICA_MAX, and RENOV_MAX take different numerical values in the hourly and daily models. Each model's caps are anchored to the historical maxima and 95th-percentile values observed at its own temporal resolution: a daily-average generation share is structurally lower than an individual hourly peak, so calibrating both models with the same caps would render the constraints effectively inert in the daily model. SINC_MIN is identical across both models, as the same physical grid-stability requirement applies regardless of temporal aggregation.

Table 4.11: Operational constraints, values by model and horizon

#	Constraint	Purpose	Model	2030	2040	2050
1	tanh saturation	Saturates solar scaling factor	both	$\times$2.97	$\times$4.51	$\times$5.15
2	SOLAR_MAX	Maximum solar share	hourly	60%	75%	90%
			daily	25%	35%	45%
3	EOLICA_MAX	Maximum wind share	hourly	90%	110%	130%
			daily	80%	90%	100%
4	RENOV_MAX	Maximum wind + solar	hourly	90%	95%	100%
			daily	85%	90%	95%
5	GAS_MAX	Maximum gas CC share	both	10.4%	6.8%	0.6%
6	Energy balance	Total generation $\leq$ 100% of load	both	$\leq$100%	$\leq$100%	$\leq$100%
7	SINC_MIN	Minimum synchronous generation	both	$\geq$30%	$\geq$20%	$\geq$10%
(8)	GAS_MIN	Minimum gas at 50%$\times$GAS_MAX	BLR only	$\geq$5.2%	$\geq$3.4%	$\geq$0.3%

It should be noted that the wind and solar caps exceeding 100% in some horizons do not imply that these technologies alone supply all demand. Rather, they allow for hours in which the individual technology share exceeds load before the energy-balance constraint and the SINC_MIN floor redistribute the surplus.

The minimum synchronous-generation thresholds of 30%, 20%, and 10% are modelling assumptions introduced to avoid unrealistically low levels of synchronous generation. The thresholds decrease over time to reflect the expected expansion of grid-forming technologies, advanced

inverter controls, and storage resources. As no explicit inertia or system-stability model is included, these values should be interpreted as illustrative assumptions rather than engineering limits.

The optional GAS_MIN constraint imposes a minimum gas generation level equal to 50% of GAS_MAX, yielding values of 5.2%, 3.4%, and 0.3% for 2030, 2040, and 2050 respectively. This constraint represents the operational reality that combined-cycle gas turbines cannot always be reduced to zero output under high-renewable conditions, due to capacity-availability contracts and their contribution to inertia and primary frequency regulation. The 50% factor is a modelling assumption and is not derived from the RNC2050.

The GAS_MIN constraint was applied only within the BLR scenario framework. Since it constitutes an additional assumption not directly supported by the RNC2050, ANN projections were generated using the seven-constraint configuration only. This preserves consistency with the objective of minimising the assumptions imposed on the ANN framework while allowing the sensitivity of the BLR projections to the constraint to be assessed explicitly.

The scenario-construction procedure described above produces the future explanatory-variable datasets used as inputs to the ANN and BLR models. Because the scenario projections depend jointly on the estimated price-formation relationships and on the constraint parameters imposed during scenario construction, there is a risk that the projected prices are driven as much by the construction assumptions as by the estimated coefficients. To assess the sensitivity of the results to the most consequential constraint, Section 5.5 reports BLR projections both with and without the GAS_MIN constraint. The remaining constraints (SINC_MIN, SOLAR_MAX, RENOV_MAX, and the saturation parameter) are treated as fixed modelling assumptions. Their individual influence on the results is not separately quantified, which should be borne in mind when interpreting the projections.

Chapter 5

Results and Discussion

5.1 Descriptive Analysis of Historical Prices

This section characterises the historical dataset (2023–2025) that underpins the model estimation and the scenario projections. The analysis covers the price distribution, the composition of the generation mix, and the intraday and seasonal patterns of renewable output, establishing the empirical baseline against which the scenario results are compared. All generation variables are expressed as percentages of hourly demand.

5.1.1 Price Distribution

The dataset comprises 26 304 hourly observations of the Portuguese day-ahead price. Figure 5.1 shows the distribution, which is visibly left-skewed: the mean (72.6 EUR/MWh) lies below the median (78.9 EUR/MWh), pulled down by a mass of low-price and negative-price hours. Approximately 20% of hours record prices below 25 EUR/MWh, corresponding to periods of high renewable generation and low demand in which near-zero-marginal-cost technologies dominate the dispatch. At the other extreme, a thin right tail extends above 150 EUR/MWh, driven by hours in which gas-fired generation sets the price under elevated fuel-cost conditions. Negative prices account for 396 hours (1.5% of the sample), a proportion that, while modest, has been increasing year on year as variable renewable capacity, particularly solar, expands, foreshadowing the more frequent occurrence of such episodes under the decarbonised scenarios.

The concentration of the distribution around 50–120 EUR/MWh, combined with the heavy left tail, means that the mean is pulled below the median by the low-price tail and is therefore a less representative measure of the typical price level. For this reason, the posterior median is adopted as the central-tendency measure throughout the scenario analysis, as discussed in Section 4.3.2.

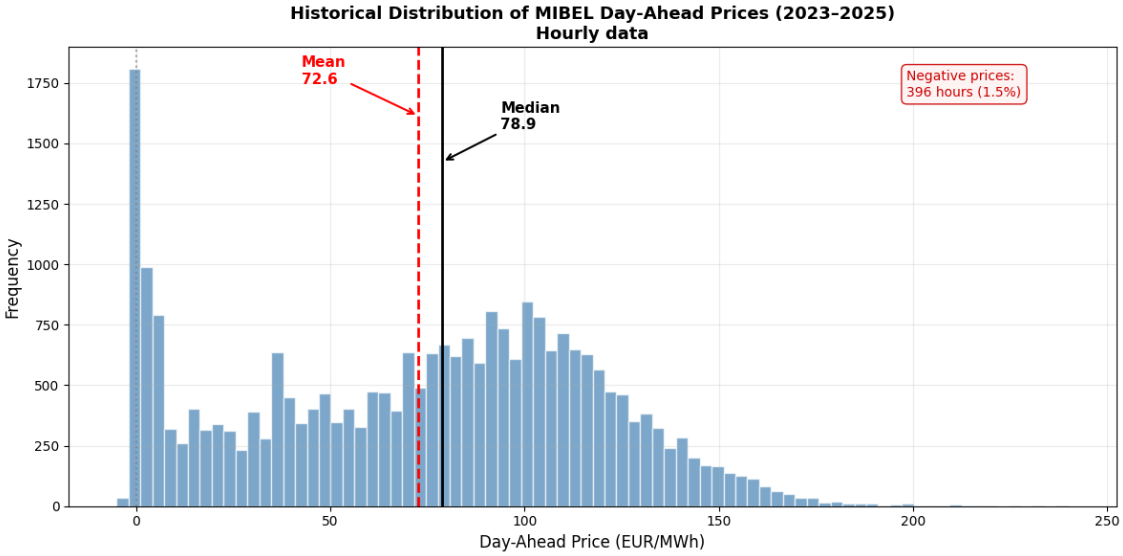


Figure 5.1: Distribution of hourly day-ahead prices in the Portuguese zone of MIBEL, 2023–2025. Vertical lines: mean (72.6 EUR/MWh) and median (78.9 EUR/MWh).

5.1.2 Generation Shares and System Composition

Table 5.1 summarises the generation-share statistics. The P95 column reports the 95th percentile, i.e. the value below which 95% of the observations lie (or equivalently, exceeded in only 5% of the hours). It therefore characterises the upper tail of the distribution without being overly influenced by extreme values.

Table 5.1: Descriptive statistics of generation shares (% of load) and system aggregates, 2023–2025 ($N = 26\,304$).

Variable	**Mean**	**Median**	**P95**	**Max**	**Min**
Wind	26.7	22.3	65.9	111.8	0.0
Solar	9.2	0.3	38.0	62.7	0.0
Hydro	32.5	27.3	78.9	130.5	0.0
Gas CC	11.5	10.7	32.1	60.9	0.0
Gas cogeneration	3.0	2.9	4.8	16.6	0.2
Pumped storage	9.2	3.6	33.3	68.2	0.0
Net balance	20.1	23.2	59.3	95.1	−86.6
Synchronous	47.4	42.7	95.1	147.7	4.2
VRE	35.9	33.7	73.2	126.0	0.1

Synchronous = hydro + gas CC + gas cogeneration + other thermal. VRE = wind + solar.

Hydroelectric generation is the single largest contributor (mean 32.5% of load), but with very

high variability (maximum 130.5%, reflecting hours in which hydro alone exceeds domestic demand, with the surplus exported). Wind contributes a mean of 26.7%, with a 95th percentile of 65.9% and a maximum of 111.8%, confirming that wind output can on its own exceed total demand in extreme hours. Solar, by contrast, has a mean of only 9.2% but a maximum of 62.7%, reflecting the concentrated nature of its production profile: the median of 0.3% shows that solar contributes nothing or almost nothing in more than half of the hours (all night-time and most dawn/dusk hours). Gas combined-cycle generation averages 11.5% of demand, with a maximum of 60.9%, consistent with its role as the dominant dispatchable thermal technology. The net interconnection balance averages 20.1% (Portugal is a net importer on average), but swings between -86.6% (strong export) and $+95.1\%$ (strong import), reflecting the variable nature of cross-border flows with Spain.

The aggregate variables at the bottom of the table provide an additional perspective. Variable renewable energy (wind + solar) averages 35.9% of demand, but reaches a maximum of 126.0%, demonstrating that the system already experiences hours in which VRE alone could theoretically supply all demand and more. Synchronous generation averages 47.4% but falls to a minimum of 4.2%, with 214 hours (0.8% of the sample) below 10% and 3 543 hours (13.5%) below 20%. These figures confirm that the SINC_MIN thresholds adopted for the scenarios (30%/20%/10% for 2030/2040/2050) are conservative relative to the operating conditions already observed in the Portuguese system. It should be noted that these hours of very low synchronous generation occurred without reported stability incidents during the historical period, but the extrapolation to future horizons with substantially higher VRE shares does not guarantee that the same levels can be sustained without additional grid-forming capacity. The operational implications of very low synchronous levels (reduced inertia and frequency stability) fall outside the scope of this work.

5.1.3 Intraday Renewable Generation Profiles

Figure 5.2 presents the mean, 75th-percentile and 95th-percentile envelopes of the combined VRE share by hour of day.

The profile exhibits two distinct regimes. During the night (hours 0–6), VRE is driven entirely by wind, with a mean of approximately 31–36% and a 95th percentile reaching 82%. During the day (hours 8–16), solar generation adds to the wind base, pushing the mean VRE share to a peak of approximately 48% at hour 13 and the 95th percentile to approximately 79%. The transition between regimes is abrupt: between hours 6 and 10, the mean VRE share rises from 34% to 44% as solar generation ramps up, and between hours 16 and 19 it falls from 42% to 25% as solar output collapses. This rapid transition is the origin of the intraday price profile documented in the literature and is the empirical basis for the Solar$\times$Hour interaction term in the BLR specification.

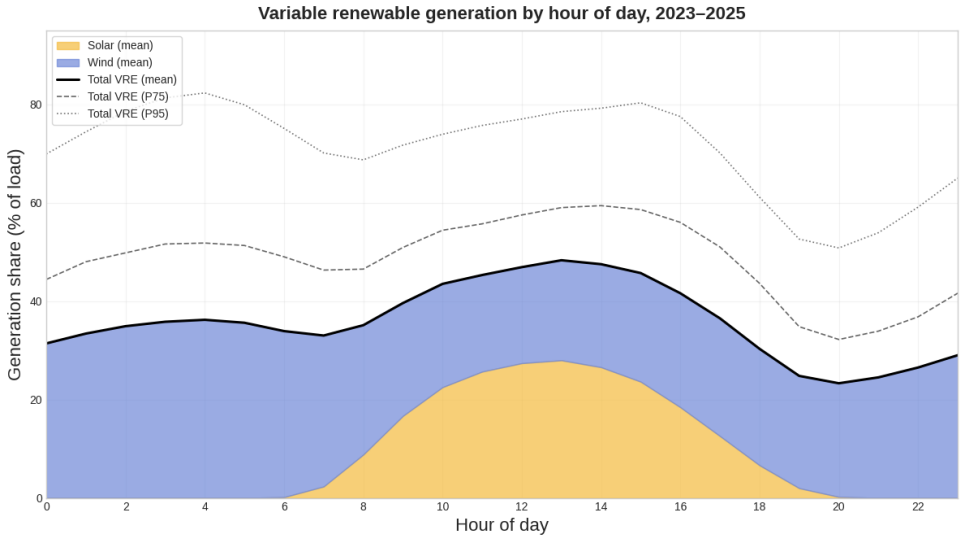


Figure 5.2: Combined VRE share (% of load) by hour of day, 2023–2025. Shaded bands: P75 and P95 envelopes.

5.1.4 Solar Generation: Hour-by-Month Structure

Figure 5.3 maps the mean solar share by hour and month, revealing the two-dimensional structure that governs the solar price effect.

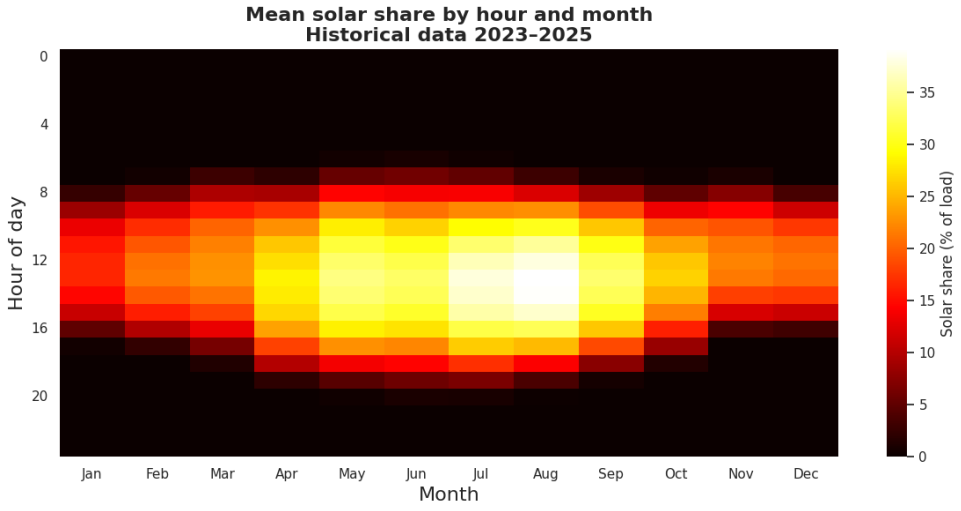


Figure 5.3: Mean solar generation share (% of load) by hour and month, 2023–2025. The colour scale ranges from 0% (night-time) to approximately 39% (summer midday).

The solar window spans roughly hours 7–18 in summer but narrows to hours 8–16 in winter. Within this window, the peak solar share ranges from approximately 16–21% in winter months (December–February, around hours 12–13) to approximately 37–39% in summer (July–August, at hours 13–14). The most extreme value in the dataset is 39.2% (August, hour 13), meaning that in an average August early-afternoon hour, solar alone supplies nearly 40% of national demand.

This high share reflects not only August's strong solar irradiance but also the fact that electricity demand is lower in August than in winter months. The same absolute solar output would represent a smaller share of demand in December or January. By contrast, in December at hour 16, the solar share has already fallen to 3.1%, illustrating the sharp seasonal asymmetry. This structure confirms that a model without Solar×Hour interaction would be severely misspecified, as the solar effect varies by a factor of more than ten between summer midday and winter morning. It also provides the empirical envelope within which the scenario projections extrapolate the solar share to higher penetration levels.

5.1.5 Wind Generation: Seasonal Profile

Figure 5.4 presents the wind generation share by month.

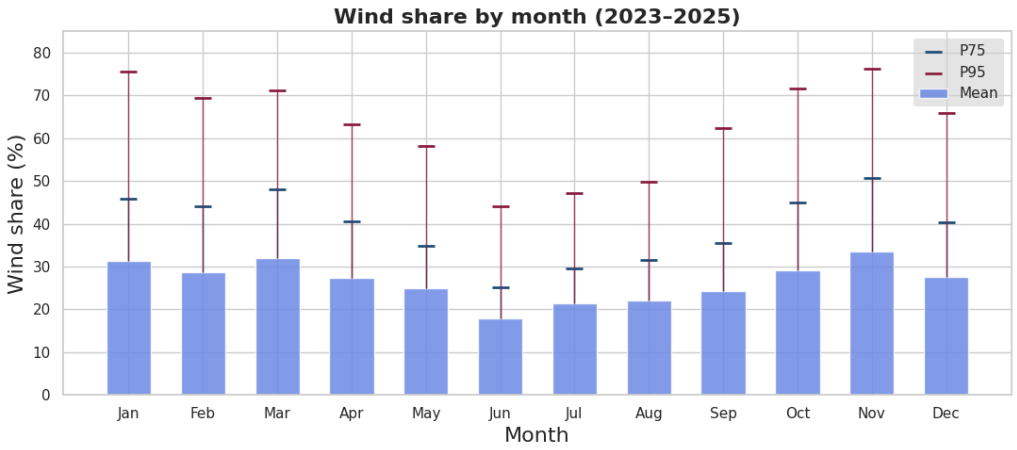


Figure 5.4: Wind generation share (% of load) by month, 2023–2025. Bars: mean; error bars: P75 and P95.

Wind output exhibits a clear seasonal pattern that is complementary to solar: the highest monthly means occur in November (33.6%) and January (31.4%), while the lowest occurs in June (18.0%). The seasonal swing in the mean is approximately 15 percentage points, but the variability within each month is substantial: the 95th percentile reaches 76% in November and does not fall below 44% even in June, indicating that high-wind episodes occur year-round. This complementarity between wind and solar is observed at the level of monthly averages and is relevant for the scenario projections, because it means that, on a seasonal basis, the system benefits from alternating VRE sources. However, the complementarity does not hold at every individual hour: solar is absent at night, and there are night-time periods with simultaneously low wind availability, during which the system depends entirely on dispatchable and imported generation. It also implies that the seasonal price pattern is shaped by the interaction of two opposing forces: summer months have high solar but low wind, while winter months have the reverse.

5.1.6 Empirical Validation of Operational Constraints

Table 5.2 relates the key historical statistics to the constraint values adopted for the scenario construction. The P95 of the hourly solar share (38.0%) and its historical maximum (62.7%) provide the empirical anchor for the SOLAR_MAX caps (60%/75%/90% for 2030/2040/2050), which allow solar shares progressively beyond the historical record in the later horizons. The wind P95 (65.9%) and maximum (111.8%) similarly anchor the EOLICA_MAX values. The combined VRE P95 (73.2%) and maximum (126.0%) anchor the RENOV_MAX caps. The minimum synchronous share of 4.2%, with 214 hours below 10%, confirms that the SINC_MIN thresholds are conservative: even the 10% floor (2050) has already been breached in the historical record, while the 30% floor (2030) is well above the observed extreme. These observations provide empirical support for the constraint values and ensure that the scenario projections extend the historical operating envelope gradually rather than imposing discontinuous breaks. The cap values were selected to extend the historical envelope progressively, using the P95 and maximum as anchoring references and allowing increasingly aggressive penetration at the longer horizons. For example, the 2030 SOLAR_MAX of 60% lies just below the historical maximum of 62.7%, while the 2050 value of 90% permits shares well beyond the historical record, reflecting the expectation of a five-fold increase in installed solar capacity. No formal optimisation of these values was performed, their individual sensitivity is not quantified in this work, which should be borne in mind when interpreting the projections.

Table 5.2: Empirical validation of the operational constraints: historical statistics versus scenario limits.

Variable	**Mean hist.**	**P95 hist.**	**Max hist.**	**2030 (cap)**	**2040 (cap)**	**2050 (cap)**
Solar (hourly)	9.2%	38.0%	62.7%	60%	75%	90%
Wind (hourly)	26.7%	65.9%	111.8%	90%	110%	130%
VRE (hourly)	35.9%	73.2%	126.0%	90%	95%	100%
Synchronous (min.)	47.4%	—	4.2%	$\geq$30%	$\geq$20%	$\geq$10%

5.2 Artificial Neural Network

5.2.1 In-Sample Performance

The in-sample performance metrics and the perturbation-based sensitivity analysis of the final ANN were reported in Section 4.4. This section presents two additional diagnostics: the predicted-versus-observed scatter plot and the disaggregation of prediction errors by price regime, season, and period of the day.

Figure 5.5 plots predicted against observed prices for a random subsample of 3 000 observations. The cloud follows the 45° line closely over the central region of the price distribution,

indicating good predictive accuracy for the range where most observations are concentrated. Dispersion increases towards both tails: the model tends to overestimate very low prices and underestimate the highest prices, consistent with a regression-to-the-mean effect. This behaviour is typical of feed-forward neural networks trained on heavy-tailed distributions, where most observations lie in the central region of the distribution, causing the optimisation process to prioritise reducing errors for common price levels rather than the comparatively rare extreme events.

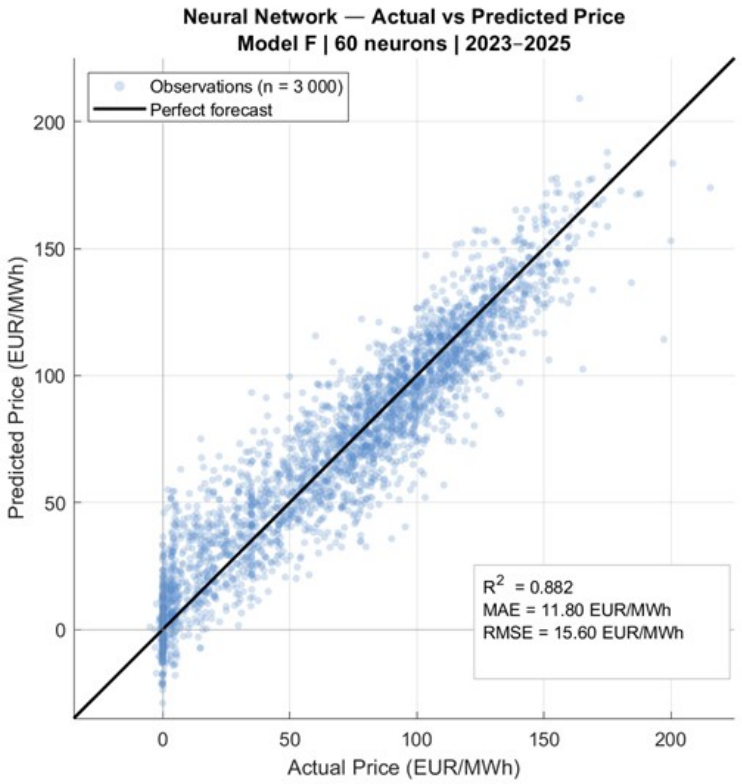


Figure 5.5: ANN predicted versus observed prices (3 000 randomly sampled observations). The diagonal represents perfect prediction.

Table 5.3 confirms this pattern quantitatively. The bias (mean signed error) measures the systematic tendency of the model to over- or underestimate prices in a given regime. A positive bias indicates overestimation, a negative bias indicates underestimation. The model performs best in the medium-price range (50–100 EUR/MWh, MAE = 11.48) and worst at the extremes. In the very-low-price regime (0–25 EUR/MWh), the average bias is +8.46 EUR/MWh. In the very-high-price regime (>150 EUR/MWh), the bias is −10.14 EUR/MWh, indicating that the most extreme price spikes are systematically under-captured. This asymmetric error profile is relevant for the scenario analysis: under deeply decarbonised conditions, the frequency of very-low-price hours is expected to increase, and the model's tendency to overestimate in this range means that the projected mean prices may be slightly higher than they would be under a model with better tail performance.

The disaggregation by price regime serves as a diagnostic proxy, confirming that the residual structure is dominated by regression-to-the-mean effects at the tails rather than by systematic misspecification in the central range.

Table 5.3: ANN prediction error by price regime, 2023–2025.

Regime (EUR/MWh)	**N (%)**	**MAE**	**RMSE**	**Bias**
Negative (< 0)	1.5%	9.01	11.52	-1.52
Very low (0–25)	19.2%	12.56	16.94	$+8.46$
Low (25–50)	12.2%	12.24	16.05	$+5.32$
Medium (50–100)	35.2%	11.48	14.78	-1.91
High (100–150)	28.8%	10.98	14.55	-4.78
Very high (> 150)	3.1%	15.78	22.50	-10.14
Overall	100%	11.73	15.56	-0.12

Table 5.4 disaggregates the error by season and by period of the day. Seasonal variation is modest (MAE from 11.38 in winter to 12.11 in autumn), indicating good generalisation across the year. The intraday pattern shows slightly higher errors in the evening hours (MAE = 13.15), consistent with the higher price volatility during peak demand.

Table 5.4: ANN prediction error by season and by period of the day.

Season	**MAE**	**RMSE**	**Bias**	**Period**	**MAE**	**RMSE**	**Bias**
Winter	11.38	15.15	-0.08	Night (0–6 h)	10.57	14.07	-0.13
Spring	11.77	15.75	$+0.19$	Morning (7–11 h)	11.97	15.86	$+0.02$
Summer	11.67	15.34	-0.53	Solar (12–16 h)	11.14	14.61	-0.54
Autumn	12.11	15.99	-0.04	Evening (17–23 h)	13.15	17.33	$+0.10$

5.2.2 Scenario Projections

The ANN was applied to both scenarios using the seven-constraint configuration (without GAS_MIN). Table 5.5 presents the results.

Table 5.5: ANN scenario projections (EUR/MWh).

	Baseline	**Scenario A**			**Scenario B**		
		2030	**2040**	**2050**	**2030**	**2040**	**2050**
EUR/MWh	83.25	96.01	-63.69^{*}	-90.61^{*}	82.85	93.52	91.62
Δ		+15.3%	-176.5%	-208.8%	-0.5%	+12.3%	+10.1%

* Economically meaningless – extrapolation failure (see text).

Under Scenario B (constant fuel and carbon prices), the ANN produces plausible results across all horizons: a negligible decrease in 2030 (-0.5%) followed by moderate increases at 2040 ($+12.3\%$) and 2050 ($+10.1\%$). This suggests that, within the non-linear mapping learned by the network, the upward pressure from demand growth slightly dominates the downward pressure from renewable expansion when fuel prices are held constant.

Under Scenario A, the 2030 projection ($+15.3\%$) remains plausible, as the fuel and carbon price scaling factors are still moderate. The 2040 and 2050 projections, however, produce median prices of -63.7 and -90.6 EUR/MWh, which are economically meaningless. This catastrophic failure arises because the Scenario A inputs lie far outside the historical training domain. The TTF natural-gas price at the 2050 horizon is scaled to approximately 17 EUR/MWh, which in z-score terms represents $z = (17 - 37.24)/6.15 \approx -3.3$ standard deviations below the training mean (outside the range but not extreme). The EU ETS allowance price at approximately 300 EUR/t, however, lies at $z = (300 - 75.13)/9.44 \approx +23.8$ standard deviations above the training mean. No observation remotely close to this value was seen during training. The non-linear activation functions of the hidden layer, which perform well within the training envelope, produce cascading distortions when driven this far outside it, resulting in outputs that have no economic meaning.

Based on the historical data and the direct application of the trained network to the scenario inputs, the ANN was unable to produce credible projections under conditions that deviate substantially from the training domain. This finding does not imply that neural networks are inherently unsuitable for long-term scenario analysis. Rather, it demonstrates that a standard feedforward network, applied without explicit mechanisms to handle extrapolation, may produce physically implausible projections under structurally different conditions. The implications of this result are discussed in Section 5.6.

5.2.3 Intraday Price Profiles

Figure 5.6 presents the ANN intraday profiles under Scenario B. The profiles are qualitatively consistent with the historical pattern, confirming that the ANN produces plausible intraday structure when the inputs remain within the training domain. Under the baseline, the daily price range (evening peak minus midday trough) is approximately 70.6 EUR/MWh (minimum 40.2 at h15, maximum 110.8 at h22). In 2030, the range narrows to 55.6 EUR/MWh as the expanding renewable capacity compresses prices without yet fundamentally altering the profile shape. By 2040–2050, however, the maximum shifts from the evening (h22) to the morning (h8), and the range widens to approximately 79–81 EUR/MWh, indicating that the ANN captures a structural change in the intraday pattern even under constant fuel prices. The midday minimum remains at h15 across all horizons.

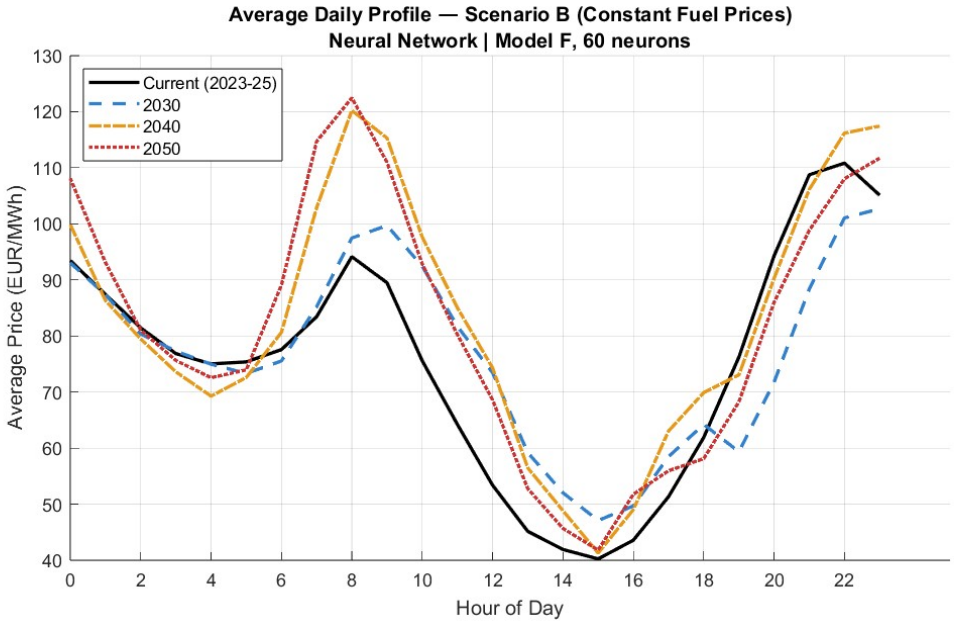


Figure 5.6: ANN intraday price profiles under Scenario B (constant fuel prices): baseline versus 2030, 2040, and 2050.

Under Scenario A (Figure 5.7), distortions are already visible at the 2030 horizon: the minimum drops to −14.8 EUR/MWh at h19 and the maximum jumps to 166.0 EUR/MWh at h11, producing an implausible daily range of 180.8 EUR/MWh that is more than double the historical range. The intraday shape is inverted relative to the baseline, with the peak in the morning rather than the evening. The 2040 and 2050 profiles collapse entirely, with median prices negative across most hours (2050: minimum −173.4 at h18, maximum +5.6 at h14). This provides a visual confirmation of the extrapolation failure documented in Section 5.2.2.

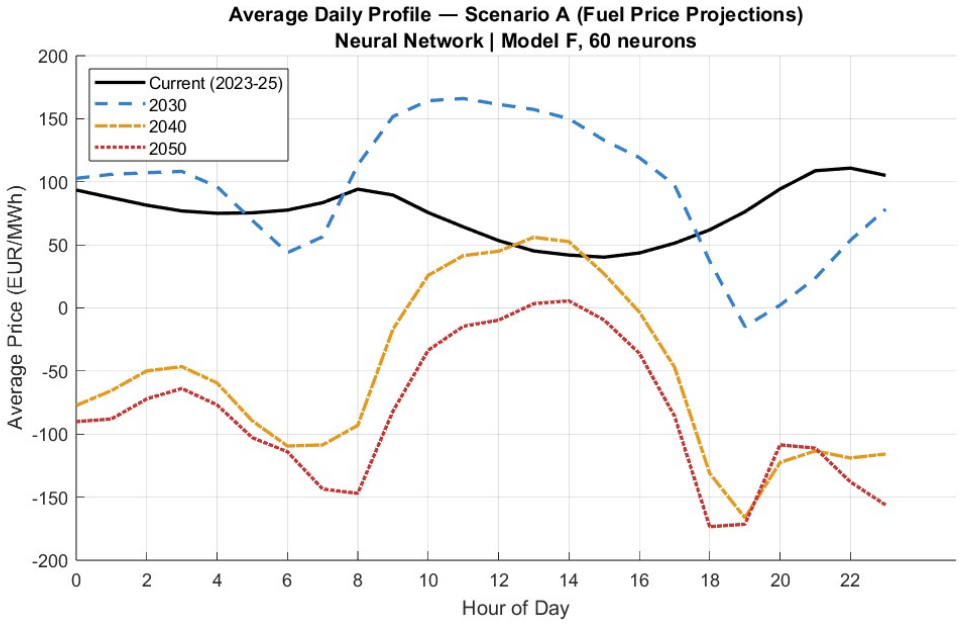


Figure 5.7: ANN intraday price profiles under Scenario A (projected fuel prices): baseline versus 2030, 2040, and 2050.

5.2.4 Assessment

Table 5.6 summarises the ANN's suitability across the scenario space.

Table 5.6: ANN suitability by scenario and horizon.

	In-sample	**2030**	**2040**	**2050**
Scenario B	$R^2 = 0.883$	Plausible (-0.5%)	Plausible ($+12.3\%$)	Plausible ($+10.1\%$)
Scenario A	$R^2 = 0.883$	Plausible ($+15.3\%$)	**Fails** (-176.5%)	**Fails** (-208.8%)

The ANN is suitable for characterising historical price-formation dynamics and for scenario analysis in which the inputs remain within or close to the training domain. The extrapolation failure extends beyond the price level to the volatility metrics: under Scenario A at 2040, the projected standard deviation rises to 144.6 EUR/MWh and the frequency of negative prices reaches 61%, confirming that the distortion is pervasive rather than confined to the central tendency. It is not suitable for Scenario A at the 2040 and 2050 horizons, where the fuel and carbon price inputs lie far outside the historical range. This limitation motivates the development of the Bayesian linear regression, presented in the following sections.

5.3 Bayesian Linear Regression: Estimation

5.3.1 Development Stages

The BLR was developed through three iterative stages, described in detail in Section 4.5.2. Stage 1 (flat priors, no saturation, no interaction) attains $R^2 = 0.565$ and MAE = 24.07 EUR/MWh. Stage 2 introduces informative priors, the solar saturation function, and the Solar×Hour interaction ($R^2 = 0.593$, MAE = 23.26). Stage 3 adds the GAS_MIN constraint, which affects only the scenario inputs. Stage 2 is adopted as the primary specification; Stage 3 is assessed as a sensitivity extension in Section 5.5. The empirical comparison of the three stages' scenario projections is presented in Section 5.4.1.

5.3.2 Posterior Coefficients

The prior distributions were specified in Section 4.5.2. This section presents the posterior coefficients that result from updating those priors with the 2023–2025 historical data. Table 5.7 presents the full posterior coefficient table of the final hourly BLR, including the temporal controls and the Solar×Hour interaction terms.

Table 5.7: Posterior coefficients of the final hourly BLR (EUR/MWh per standard deviation of input). HDI: 95% highest-density interval.

Variable	**PIP**	**Post. med.**	**Post. std**	**95% HDI**	
				Lower	Upper
Generation shares					
Wind	1.000	−16.54	4.25	−23.45	−12.25
Solar	1.000	−18.82	2.73	−23.09	−15.73
Hydro	1.000	−14.74	5.28	−23.34	−9.38
Gas CC	1.000	+8.76	2.11	+5.46	+11.14
Gas cog.	1.000	+4.47	0.31	+3.95	+4.98
Other thermal	1.000	+3.54	0.24	+3.15	+3.95
Pumped storage	0.961	−6.59	2.44	−9.34	−2.76
Net balance	0.630	−4.90	5.84	−14.49	+0.90
Demand and fuel prices					
Consumption	1.000	+11.25	0.33	+10.70	+11.78
TTF	1.000	+11.74	0.21	+11.40	+12.08
CO_2	0.993	+0.89	0.25	+0.51	+1.30
Temporal controls					
Hour	1.000	−2.25	0.24	−2.64	−1.85
Month	1.000	+10.52	0.75	+9.31	+11.75
Week	1.000	−5.08	0.74	−6.28	−3.84
Solar×Hour interaction					
Solar × sin(hour)	1.000	+4.31	0.18	+4.00	+4.62
Solar × cos(hour)	1.000	−8.51	0.18	−8.82	−8.19

The renewable coefficients are substantially more negative than the prior mean of -8, consistent with the merit-order effect (Section 3.1) and indicating that the effect in the 2023–2025 MIBEL data is stronger than the conservative prior. Solar exhibits the largest absolute coefficient (-18.82), consistent with the concentrated production profile documented in Section 5.1.4: because solar output is compressed into a narrow band of hours, each percentage point of solar share produces a sharper price depression than the more evenly distributed wind (-16.54) or hydro (-14.74). The consumption coefficient ($+11.25$) is close to the prior ($+10$), confirming the expected demand-driven upward pressure. The gas CC coefficient ($+8.76$) is close to the prior ($+8$), consistent with its frequent role as the price-setting technology.

The TTF coefficient ($+11.74$) is estimated with very high precision (posterior standard deviation 0.21, 95% HDI $[11.40, 12.08]$), reflecting the strong and well-documented gas-to-power pass-through. The CO_2 coefficient ($+0.89$) is well below the prior of $+2$: the data pulled the posterior substantially towards zero, reflecting the limited variability of the EU ETS price during the estimation period. This asymmetry between the TTF and CO_2 coefficients (the gas price exerts more than thirteen times the effect of the carbon price) has direct consequences for the scenario projections, because it means that the declining TTF trajectory in Scenario A dominates the rising EU ETS trajectory.

The net balance coefficient (-4.90) has the widest posterior uncertainty (standard deviation 5.84, 95% HDI including zero), and its PIP of 0.630 is the lowest among the retained variables, consistent with the complex and bilateral nature of cross-border flows.

Among the temporal controls, the Month coefficient ($+10.52$) is the second largest in absolute value after Solar. This magnitude captures residual seasonal effects not fully explained by the generation shares alone, principally the seasonal covariation of gas prices, hydrological conditions, and demand patterns that affect the price level beyond what the individual technology shares represent. The Hour coefficient (-2.25) appears modest in isolation, but the hour variable is coded as 0–23 and z-normalised, so the full intraday effect is captured by the combination of this linear term with the Solar$\times$Hour interaction terms (solar_x_sin: $+4.31$, solar_x_cos: -8.51). Together, these three coefficients determine the amplitude ($\sim$9.3 EUR/MWh) and phase ($\sim -37^{\circ}$) of the intraday modulation of the solar effect, whose role in the scenario projections is analysed in Section 5.4.5. Table 5.8 and Figure 5.8 summarise the prior-to-posterior updating for all economically motivated variables.

Table 5.8: Prior-to-posterior updating for the economically motivated variables (EUR/MWh per standard deviation of input).

Variable	**Prior μ**	**Post. med.**	**Interpretation**
Solar	-8	-18.82	Merit-order effect stronger than prior
Wind	-8	-16.54	Same direction, substantially stronger
Hydro	-8	-14.74	Same direction, substantially stronger
Consumption	$+10$	$+11.25$	Close to prior; demand effect confirmed
Gas CC	$+8$	$+8.76$	Close to prior; marginal role confirmed
Gas cog.	$+5$	$+4.47$	Close to prior
Net balance	-6	-4.90	Data suggests weaker effect than prior
TTF	$+10$	$+11.74$	Close to prior; gas pass-through confirmed
CO_2	$+2$	$+0.89$	Data pulled towards zero

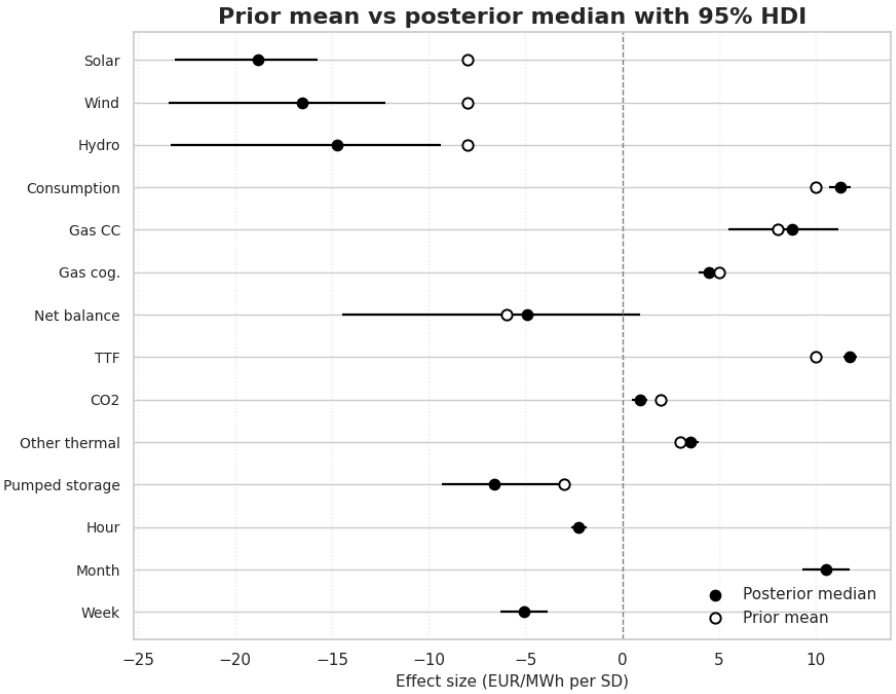


Figure 5.8: Prior-to-posterior updating: prior mean (open circle) and posterior median with 95% HDI (solid circle and bar) for each economically motivated variable. The Solar×Hour interaction terms are omitted from this figure.

The energy-balance caveat discussed in Section 4.5 applies: individual coefficients are partial effects within the linear model, not isolated causal impacts. The scenario-construction procedure mitigates this by varying the shares jointly.

5.3.3 Baseline Profiles

5.3.3.1 Intraday Profile

Table 5.9 presents the posterior predictive intraday profile for the historical baseline and Figure 5.9 illustrates the corresponding profile. Median prices fall from approximately 79 EUR/MWh at midnight to a minimum of approximately 46 EUR/MWh at hour 15 (the trailing edge of the solar window), before rising to approximately 91 EUR/MWh at hours 20–21 (the evening peak). Therefore, the daily price range is approximately 45 EUR/MWh, substantially narrower than the 70.6 EUR/MWh range produced by the ANN for the same baseline (Section 5.2.3), reflecting the BLR's linear specification, which compresses the tails of the price distribution. The BLR baseline range serves as the reference against which the scenario projections are compared in Section 5.4.4. The 90% credible interval widens during the afternoon hours, reaching 141 EUR/MWh at hour 16, reflecting the greater conditional uncertainty associated with solar-driven price depression.

The width of the 90% credible interval (79.0–140.6 EUR/MWh depending on the hour) reflects the natural dispersion of individual hourly prices rather than imprecision of the model's central estimate. Within any given hour of the day, the actual price varies substantially across the 1 096 days in the sample depending on the specific combination of wind, solar, hydro availability, demand level, and fuel prices. The interval is widest during the afternoon hours (h15–16, width $\approx$ 135–141 EUR/MWh), where the solar share is most variable, and narrowest during the evening peak (h20–21, width $\approx$ 79–83 EUR/MWh), where demand is consistently high and the generation mix is more predictable.

Table 5.9: BLR hourly: baseline intraday price profile (posterior predictive distribution, EUR/MWh).

Hour	Median	P5	P95	90% CI width
0	78.6	28.4	129.2	100.8
4	72.7	16.5	132.4	115.9
8	81.1	29.9	131.4	101.5
12	60.7	13.0	117.0	104.0
15	45.8	−20.6	114.2	134.8
16	52.4	−19.5	121.1	140.6
20	91.0	51.1	130.1	79.0
21	91.4	49.8	132.9	83.1

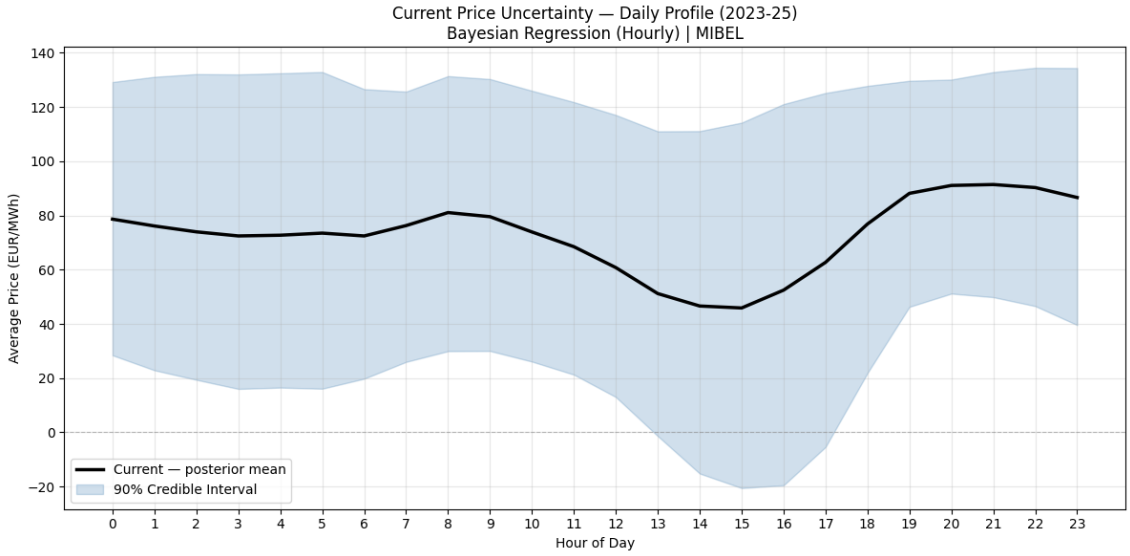


Figure 5.9: BLR hourly baseline intraday price profile: posterior predictive median (solid line) with 90% credible interval (shaded band), 2023–2025.

5.3.3.2 Monthly Profile

Table 5.10 presents the posterior predictive monthly profile and Figure 5.10 illustrates the corresponding profile.

The seasonal pattern is characterised by a spring trough and a winter peak, but the contrast is less sharp than a simple two-season summary would suggest. The lowest median prices occur in spring: March and May share the minimum at approximately 55—58 EUR/MWh, with April even lower at 47.5 EUR/MWh. April stands out as the single cheapest month because it combines above-average wind (Section 5.1.5) with rising solar output and moderate demand, creating conditions that frequently push the system into the low-cost segment of the supply curve. The highest median prices are spread across a broad autumn–winter plateau: August (76.7), October (79.8), November (81.1), January (80.2) and February (81.3) all cluster between 77 and 81 EUR/MWh, with December (86.5) standing above them as the annual peak. The December peak reflects the combination of the highest winter demand with the lowest solar contribution (Section 5.1.4), which maximises the frequency of gas-fired marginal dispatch. The relative flatness of the July—February plateau (74—87 EUR/MWh) indicates that the price-moderating effect of summer solar is approximately offset by the lower wind availability in those months, producing a seasonal equilibrium that is broken only in spring.

The 90% credible intervals span the full range of hourly prices observed within each month, including both low-price solar-surplus hours and high-price evening hours. The narrowest intervals occur in November (85.2 EUR/MWh width) and December (92.7), months in which the generation mix is relatively stable. The widest intervals occur in February (135.6) and March (124.9), reflecting the greater hydrological and wind uncertainty characteristic of late winter and early spring: in these months, the generation mix can vary substantially from one year to the next

depending on rainfall and wind patterns, and this input uncertainty propagates directly into the price predictions. This seasonal uncertainty structure is relevant for the scenario projections: the months with the widest historical uncertainty are precisely those where the most extreme price outcomes occur under the decarbonised scenarios.

Table 5.10: BLR hourly: baseline monthly price profile (posterior predictive distribution, EUR/MWh).

Month	Median	P5	P95	90% CI width
Jan	80.2	25.5	131.7	106.2
Feb	81.3	8.7	144.3	135.6
Mar	58.4	-0.4	124.5	124.9
Apr	47.5	-6.8	113.6	120.4
May	55.2	1.3	110.1	108.8
Jun	73.5	11.0	127.2	116.2
Jul	74.4	9.4	123.7	114.4
Aug	76.7	10.2	131.3	121.1
Sep	77.4	20.0	128.9	108.8
Oct	79.8	28.3	127.5	99.2
Nov	81.1	33.6	118.8	85.2
Dec	86.5	39.0	131.7	92.7

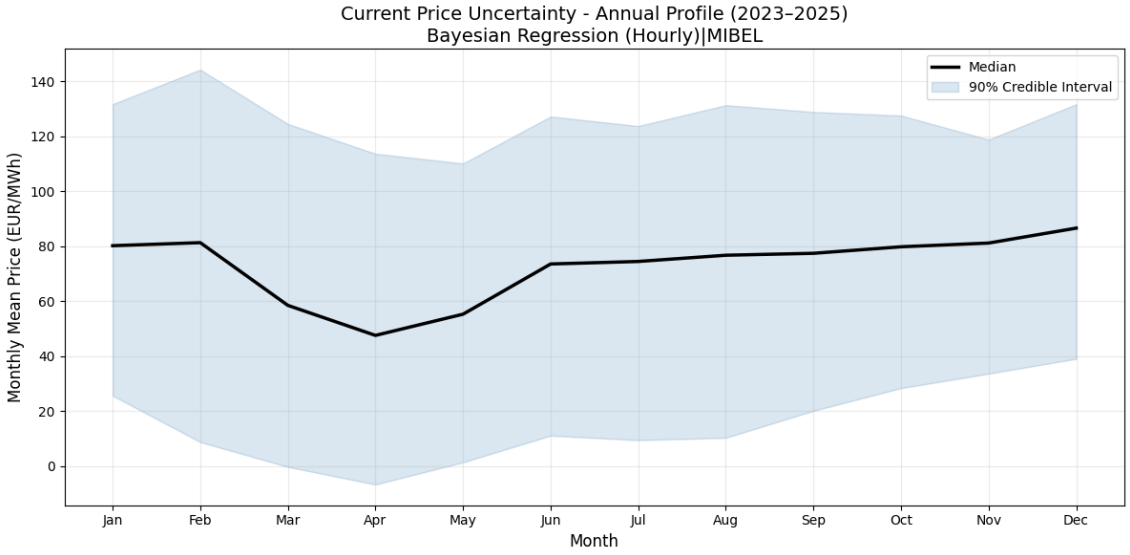


Figure 5.10: BLR hourly baseline monthly price profile: posterior predictive median with 90% credible interval, 2023–2025.

5.4 BLR Scenario Projections

5.4.1 Constraint Diagnostics and Stage Comparison

Before analysing the projections, Table 5.11 summarises the frequency with which each operational constraint binds across the scenario horizons. Because the constraints are applied during the scenario construction, before the generation shares are fed to either model, the seven-constraint diagnostics reported here apply identically to the ANN and to the BLR Stage 2 (the two models compared in Section 5.4.3). The generation shares are also identical in Scenarios A and B, since the two scenarios differ only in fuel and carbon prices. The GAS_MIN constraint, which applies exclusively to BLR Stage 3, is discussed separately in Section 5.5.

Table 5.11: Frequency with which each operational constraint binds (% of 26 304 scenario hours). These diagnostics apply to both the ANN and BLR Stage 2 (seven-constraint configuration, without GAS_MIN).

Constraint	**2030**	**2040**	**2050**
tanh solar saturation	8.8%	23.1%	33.3%
SOLAR_MAX	20.9%	25.4%	24.2%
EOLICA_MAX	5.3%	1.6%	0.4%
RENOV_MAX	14.3%	20.9%	27.0%
GAS_MAX	24.4%	27.8%	35.2%
Energy balance (>100%)	61.3%	63.6%	64.1%
SINC_MIN	49.2%	37.5%	22.5%

The tanh saturation row reports the percentage reduction in the solar scaling factor relative to the unsaturated value. All other rows report the percentage of the 26 304 scenario hours in which the constraint binds at its upper or lower limit.

Several patterns are noteworthy. The energy-balance constraint binds in over 60% of hours across all horizons, confirming that the combination of scaled renewable shares and demand growth frequently produces generation totals that exceed 100% of load before the balancing step clips them. This high binding frequency means that the constraint is not merely a safety check but an active shaper of the scenario generation mixes, a point that should be borne in mind when interpreting the projections.

The solar saturation function becomes progressively more consequential as the horizon advances. At the 2030 horizon, the tanh function compresses the raw scaling factor from $\times 3.26$ to $\times 2.97$ (an 8.8% reduction), affecting a relatively modest number of hours. By 2050, the compression is from $\times 7.72$ to $\times 5.15$ (a 33% reduction), affecting every solar hour and preventing the solar share from reaching physically implausible levels. Without this saturation, the 2050 solar shares would extend far beyond any plausible grid-absorption capacity.

The SINC_MIN constraint exhibits a declining trend: it binds in 49.2% of hours in 2030 (where the 30% floor is most demanding) but drops to 22.5% by 2050 as the floor is progressively relaxed to 10%. This decline reflects the modelling assumption that grid-forming technologies and advanced inverter controls will reduce the minimum synchronous requirement over the horizon.

The GAS_MAX constraint, by contrast, tightens across horizons (from 24.4% to 35.2%), reflecting the progressive reduction of installed gas capacity under the RNC2050: by 2050, over a third of hours see gas capped at the residual 0.6% of demand.

The RENOV_MAX constraint (combined wind + solar ceiling) binds increasingly across horizons, from 14.3% in 2030 to 27.0% in 2050, reflecting the growing frequency of hours in which the combined VRE share approaches or exceeds the scenario-specific cap.

The EOLICA_MAX constraint is rarely binding, especially by 2050 (0.4%), because the wind scaling factors are moderate ($\times 1.38$–$\times 1.41$) and the wind caps are set well above the scaled historical maxima.

5.4.2 Effect of BLR Specification Stages on Scenario Projections

Table 5.12 compares the median projected prices across the three BLR development stages for the hourly model. Figure 5.11 illustrates the same comparison graphically. The stage comparison is presented for the hourly model only, because the refinements that distinguish the stages are either specific to the hourly specification or have their most consequential effects at hourly resolution.

Table 5.12: BLR hourly: median projected prices (EUR/MWh) under Scenarios A and B by development stage.

		Scenario A			**Scenario B**		
Stage	**Baseline**	**2030**	**2040**	**2050**	**2030**	**2040**	**2050**
Stage 1 (flat priors)	72.62	67.98	80.30	78.61	71.60	78.52	78.57
Stage 2 (informative, no GAS_MIN)	72.63	70.07	77.84	74.59	75.05	79.61	78.86
Stage 3 (informative, GAS_MIN)	72.63	74.79	82.06	75.07	79.77	83.84	79.35

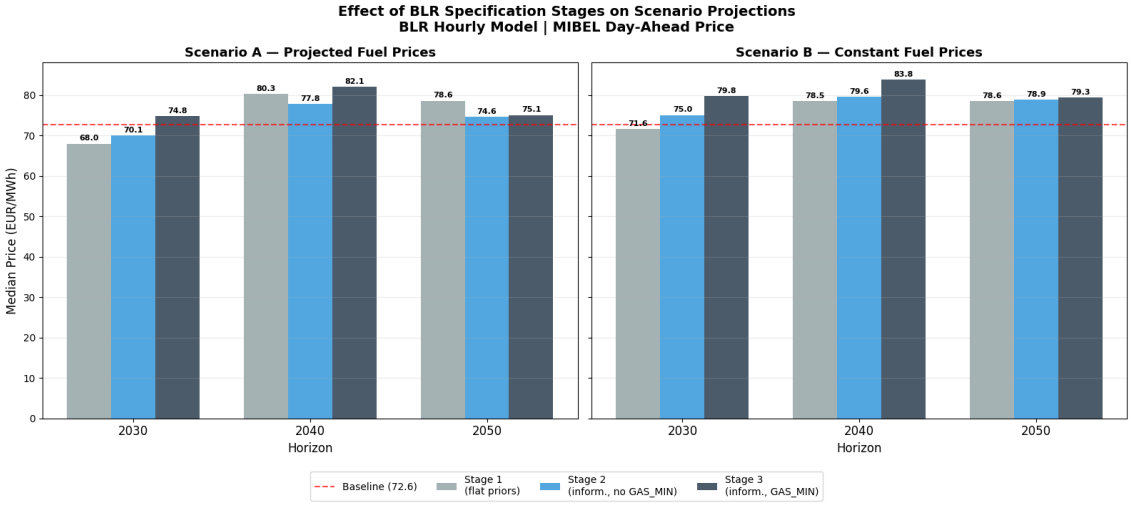


Figure 5.11: BLR hourly: median projected prices under Scenarios A and B by development stage.

The three stages produce broadly similar price-level projections, despite moderate differences in the projected price levels, confirming that the qualitative conclusions are robust to the specification choices. The choice of Stage 2 as the primary specification is therefore motivated not by superior aggregate projections but by the quality of the underlying model specification, namely the use of economically grounded priors, physical solar saturation, and hour-dependent solar effects. The importance of these refinements, however, only becomes apparent when the intraday profiles are examined.

Figure 5.12 presents the projected profiles under Stage 1.

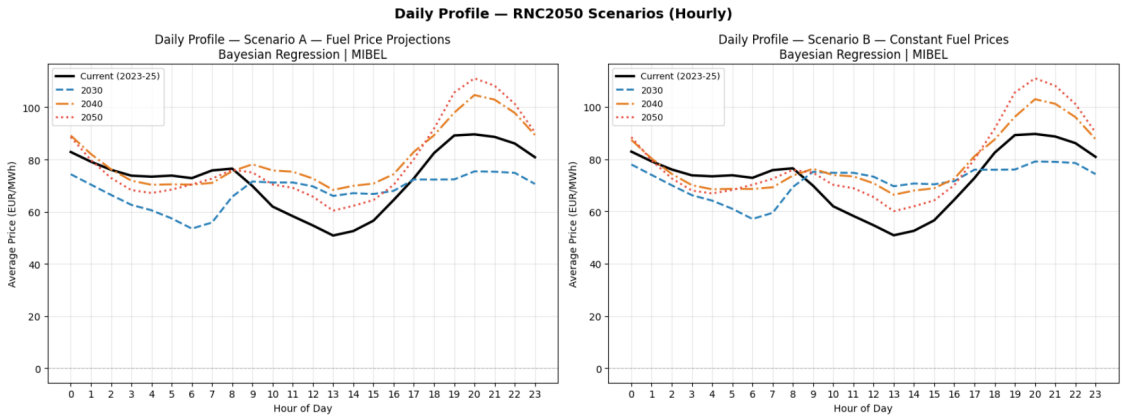


Figure 5.12: Projected intraday price profiles under Stage 1 (flat priors, without Solar×Hour interaction) for baseline, 2030, 2040, and 2050 under Scenarios A (left) and B (right).

The critical feature is the behaviour between hours 10 and 16. In the baseline, a clear midday trough is visible. As the projection horizon advances, the solar share increases and this trough should deepen, yet under Stage 1 it progressively flattens instead. The distortion is already apparent at 2030, where the afternoon depression weakens noticeably relative to the baseline, and becomes qualitatively incorrect by 2040, where the midday hours show prices comparable to the

morning level. This occurs because Stage 1 applies a single average solar coefficient to all hours: estimated as a compromise between the strong midday effect and the zero night-time effect, it underestimates the price-depressing power of solar during peak hours and overestimates it during non-solar hours. Without the Solar×Hour interaction, the model cannot differentiate the solar effect across hours, and the misspecification compounds as the solar share grows. The Stage 2 profiles, presented in the sections that follow, recover the empirically observed pattern of a deep midday trough and a persistent evening peak, providing the most direct empirical justification for the Solar×Hour interaction. Having established the rationale for adopting Stage 2 as the primary specification, the remainder of Section 5.4 presents its scenario projections in detail.

5.4.3 Projected Price Levels

To ensure a fair comparison across modelling approaches, the BLR results reported in this section correspond to Stage 2 (informative priors, solar saturation, and Solar×Hour interaction, without GAS_MIN), the same seven-constraint configuration used for the ANN in Section 5.2.2.

Table 5.13: Scenario projections: median prices (EUR/MWh) and percentage change versus baseline. BLR intervals are 90% posterior predictive [P5–P95].

		Scenario A			**Scenario B**		
Model	**Baseline**	**2030**	**2040**	**2050**	**2030**	**2040**	**2050**
BLR Hourly (Stage 2)	72.63	70.07	77.84	74.59	75.05	79.61	78.86
		(−3.5%)	(+7.2%)	(+2.7%)	(+3.3%)	(+9.6%)	(+8.6%)
		[66.8–73.3]	[69.5–86.0]	[64.3–84.9]	[73.5–76.5]	[77.3–82.0]	[75.7–82.0]
BLR Daily (Stage 2)	72.61	62.49	58.97	54.30	78.57	89.93	94.06
		(−13.9%)	(−18.8%)	(−25.2%)	(+8.2%)	(+23.8%)	(+29.5%)
		[52.5–72.9]	[32.4–96.9]	[20.9–89.1]	[75.2–82.1]	[82.4–97.6]	[83.3–105.1]

Scenario B: structural effect. Under Scenario B, where fuel and carbon prices are held constant, all BLR specifications project prices above the baseline across all horizons. The central finding is that demand growth dominates the merit-order effect: electricity demand under the RNC2050 increases by +11.4%, +52.5%, and +77.2% relative to the 2020 baseline, and this load growth pushes the system up the supply curve more frequently than the expanding renewable capacity can offset. The BLR hourly model projects a non-monotone pattern: prices peak at 2040 (+9.6%) and ease slightly by 2050 (+8.6%), suggesting that the massive solar expansion projected for 2050 partially compensates the continued demand growth but does not reverse the upward trend. The BLR daily model projects a monotonic increase reaching +29.5% by 2050.

Scenario A: the combined effect. Under Scenario A, the declining TTF and rising EU ETS have partially offsetting effects. As documented in Section 5.3.2, the TTF coefficient dominates the CO_2 coefficient, so the decline in gas prices exerts a stronger downward pressure than the rise in carbon prices exerts upward. In the hourly model, these two opposing forces nearly cancel,

resulting in modest net changes: −3.5% in 2030, +7.2% in 2040, and +2.7% in 2050. In the daily model, the downward pressure from fuel prices dominates, producing progressive declines (−13.9%, −18.8%, −25.2%).

The widening of the credible intervals across horizons reflects the compounding of uncertainty as the inputs diverge from the historical domain. The 2050 projections are best understood as directional assessments rather than precise estimates.

Contribution of fuel and carbon prices. The difference between Scenarios A and B, conditional on the same generation mix, isolates the contribution of the fuel and carbon price trajectories.

Table 5.14: Difference A−B in median projected prices (EUR/MWh). Negative values indicate that the Scenario A fuel and carbon trajectories reduce prices relative to constant-fuel Scenario B.

Model	**2030**	**2040**	**2050**
BLR Hourly (Stage 2)	−4.98	−1.77	−4.27
BLR Daily (Stage 2)	−16.08	−30.96	−39.76

The negative A−B differences confirm that the projected TTF decline exerts a net downward effect that exceeds the upward effect of the rising CO_2. A fundamental qualification applies to the 2050 results: the gas-price transmission channel narrows substantially when gas represents only 0.6% of demand (Assumption 7, Section 4.6.1). Scenario B provides the more robust reference. The implications of this qualification are discussed in Section 6.4.

It should be noted that the linearity of the BLR ensures numerical stability under extrapolation but does not resolve the question of whether the estimated CO_2 coefficient (+0.89, estimated from a range of 65–90 EUR/t) remains economically meaningful when applied to 300 EUR/t. At such extreme values, the true relationship between the carbon price and the electricity price may be non-linear or may operate through different channels than those captured by the historical data.

5.4.4 Intraday Price Profiles Under Scenarios

Figure 5.13 presents the intraday price profiles projected by the BLR hourly model (Stage 2) for both scenarios across all horizons. The contrast with the Stage 1 profiles (Section 5.4.1) is immediate: the interaction term recovers the deep midday trough and persistent evening peak that Stage 1 failed to reproduce.

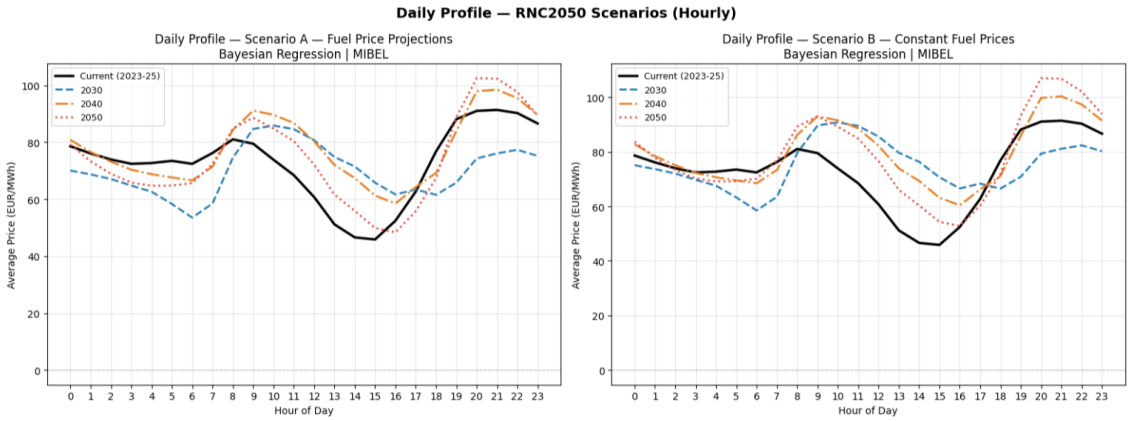


Figure 5.13: Intraday price profiles under Scenarios A (left) and B (right): posterior predictive median by hour for baseline, 2030, 2040, and 2050 (BLR hourly, Stage 2).

Under both scenarios, the intraday price profiles evolve progressively towards a duck-curve-like pattern as the projection horizon advances. Relative to the historical profile, the period of lower daytime prices becomes more extended, while the evening peak remains the dominant daily maximum. This evolution reflects the increasing influence of photovoltaic generation during daylight hours, which depresses prices through the merit-order effect, whereas prices recover rapidly after sunset as solar production declines and demand remains comparatively high.

The evolution is, however, non-monotonic. In 2030, the daily price range narrows substantially (from 46.7 to approximately 34 EUR/MWh in both scenarios), with the minimum shifting from the historical afternoon trough (h15) to the early morning (h6) and the maximum moving from the evening peak (h21) to mid-morning (h9–10). This behaviour suggests that, at moderate solar penetration, the increase in photovoltaic generation is sufficient to weaken the historical afternoon trough but not yet to establish the characteristic daytime pattern observed at longer horizons. At the same time, the projected increase in electricity demand offsets part of the downward pressure exerted by renewable generation during the afternoon. The 2030 profile thus represents a transitional regime: moderate solar scaling ($\times 2.97$) is sufficient to erode the historical afternoon-trough/evening-peak pattern but insufficient to establish the deep duck curve that emerges at 2040–2050. This transition has practical implications for flexibility scheduling, as the hours of greatest price spread shift from evening to morning at 2030 before returning to evening at the longer horizons.

From 2040 onwards, the historical pattern progressively re-emerges in a modified form. The minimum returns to the afternoon (approximately h15–16), while the evening peak again becomes the highest-priced period of the day (h20–21). Compared with the historical profile, the daytime period of relatively low prices extends over a wider interval, although the minimum price itself changes only modestly. By 2050, the daily price range increases to approximately 54–55 EUR/MWh, exceeding the historical range of 46.7 EUR/MWh. These results indicate that increasing photovoltaic penetration alters primarily the temporal distribution of prices throughout the day rather than simply reducing their overall level.

Although gas-fired combined-cycle generation becomes almost negligible in the RNC2050 pathway, the projected evening peak persists. Within the model, this behaviour is explained by the combined effect of demand growth and the estimated temporal structure rather than by the marginal cost of a specific generation technology. In a real system with near-zero gas generation, the evening price would be set by whichever technology fills the residual gap (storage, imports, demand response, or a yet-to-be-deployed flexibility resource) none of which are explicitly represented in the model. The projected evening peak should therefore be interpreted as indicating that evening scarcity conditions persist under the RNC2050 trajectory, rather than as a prediction of the specific price level that would be observed.

The two scenarios exhibit almost identical intraday shapes because they assume the same evolution of the generation mix. The principal difference lies in the overall price level: Scenario A produces consistently lower prices across the day owing to the projected decline in fuel prices, whereas Scenario B isolates the effect of the renewable transition by holding fuel prices constant. This nearly uniform downward shift is consistent with the additive structure of the BLR model, whereby the fuel-price variables modify the overall price level without materially changing the hourly profile.

5.4.5 Rightward Shift of the Price Minimum

A salient feature of the projected profiles is the progressive rightward shift of the entire intraday price curve across the horizons. Figure 5.14 illustrates this shift by comparing the solar share, net load and price profiles between the historical baseline and 2050 Scenario B.

In the baseline, the price minimum occurs at approximately hour 15 and the steepest afternoon-to-evening ramp begins at hour 17. By 2050, the low-price window extends further into the late afternoon, with the minimum shifting to approximately hour 16 and the evening ramp beginning later. This shift affects not only the position of the minimum but the entire afternoon and evening structure of the price profile.

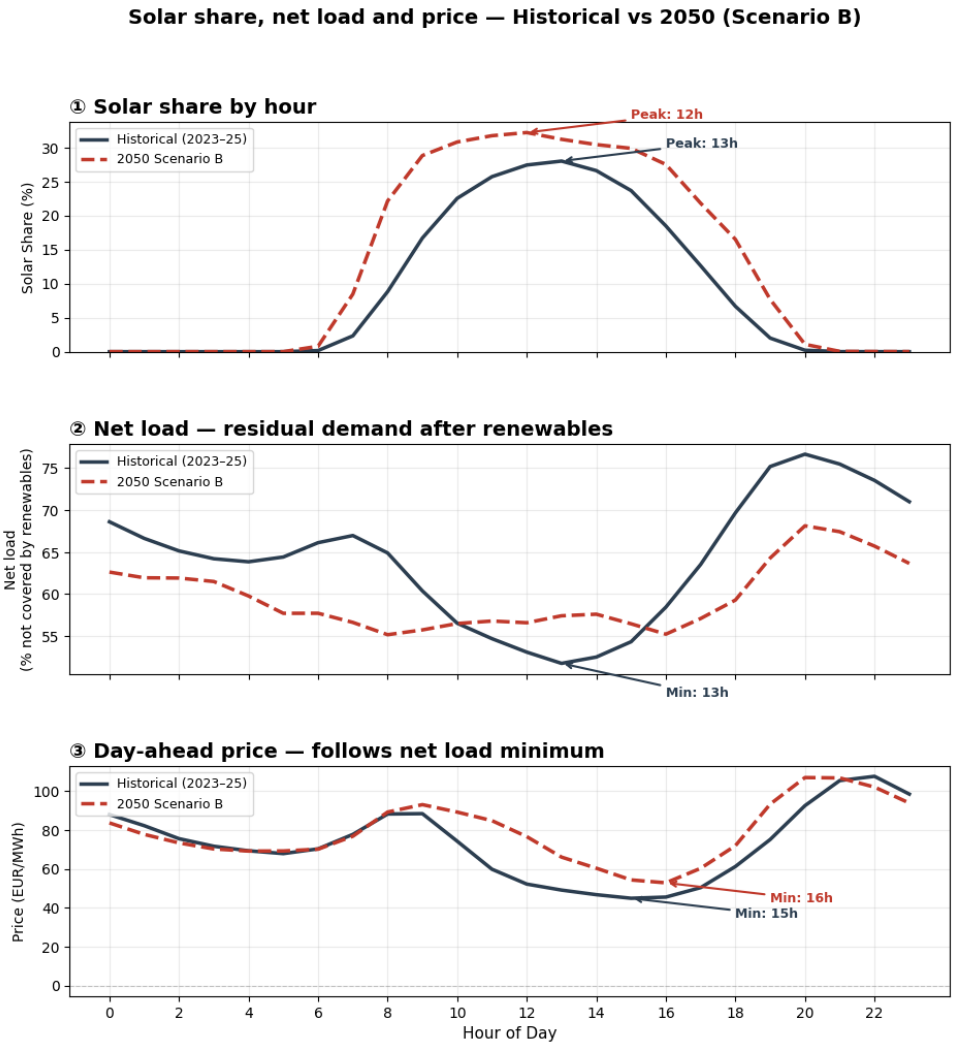


Figure 5.14: Solar share, net load and price profiles: historical baseline versus 2050 Scenario B (BLR hourly, Stage 2).

In the historical data, the solar peak and the net-load minimum both occur at approximately hour 13, but the price minimum occurs two hours later, at hour 15. In a real electricity market, this lag reflects start-up costs, minimum operating times and ramping constraints of thermal plants. The BLR does not represent these mechanisms explicitly but absorbs the lag pattern implicitly from the historical data.

In 2050, the solar peak shifts earlier (to approximately hour 12) and the window of high solar generation broadens substantially, producing a wide and flat net-load valley between approximately hours 8 and 16. The factor-group decomposition (Figure 5.15) identifies the Solar×Hour interaction term as the mechanism responsible for the rightward displacement. In 2050, its influence is visibly amplified because it is multiplied by a much higher solar share: during morning hours of rising solar output, the positive interaction coefficient pushes prices upward, partially offsetting the downward pressure. During the afternoon, the coefficient reverses sign and aligns with the negative renewable-share coefficients, so that the two effects reinforce each other rather than

opposing, amplifying the solar-driven depression and extending the low-price window towards the late edge of the solar period. The net effect is that the rightward displacement arises not because the solar peak moves later (it actually moves earlier, to approximately hour 12) but because the broadened solar window interacts with the trigonometric structure of the interaction term: the $\cos(2\pi h/24)$ component is more negative in the late afternoon than at midday, so that the price-depressing contribution of each unit of solar generation increases as the hour advances through the afternoon. When multiplied by the substantially higher solar shares projected for 2050, this asymmetry shifts the price minimum from hour 15 to hour 16.

The same mechanism, operating at different intensities, explains the contrasting behaviour at the earlier horizons described in Section 5.4.4. In 2030, the solar scaling factor ($\times$2.97) is insufficient for the Solar$\times$Hour interaction to dominate the profile: its amplitude is too small to overcome the combined effect of demand growth (+11.4%) and the baseline temporal coefficients, so the afternoon depression weakens without being replaced by a new, deeper trough, and the price minimum defaults to the hour of lowest absolute demand (h6). In 2040, the solar scaling factor ($\times$4.51) crosses the threshold at which the interaction term regains dominance: the cos component depresses afternoon prices enough to re-establish the duck-curve pattern and pull the minimum back to the afternoon (h15–16), though the rightward displacement is less pronounced than in 2050 because the solar shares are lower and the trigonometric asymmetry is less amplified.

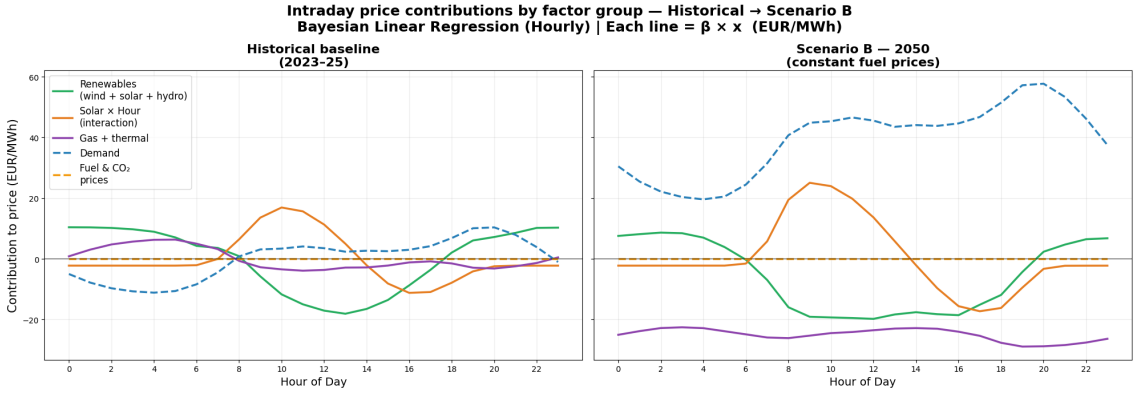


Figure 5.15: Decomposition of the intraday price profile by factor group: baseline versus Scenario B 2050 (BLR hourly, Stage 2).

This shift should be interpreted with caution. The Solar$\times$Hour interaction was estimated from historical data in which the solar share reached at most approximately 28% of demand during the relevant hours. In the 2050 scenario, the solar share is extrapolated to substantially higher levels. The broad pattern (that prices are low throughout the afternoon and high in the evening) is robust, because it is driven by the net-load structure. The precise magnitude of the rightward displacement, however, is a consequence of applying a historically fitted coefficient to inputs outside the estimation domain, and should be treated as a declared limitation of the linear extrapolation.

5.4.6 Seasonal Price Profiles

Figure 5.16 and Table 5.15 present the monthly price profiles projected by the BLR hourly model (Stage 2) for both scenarios across all horizons.

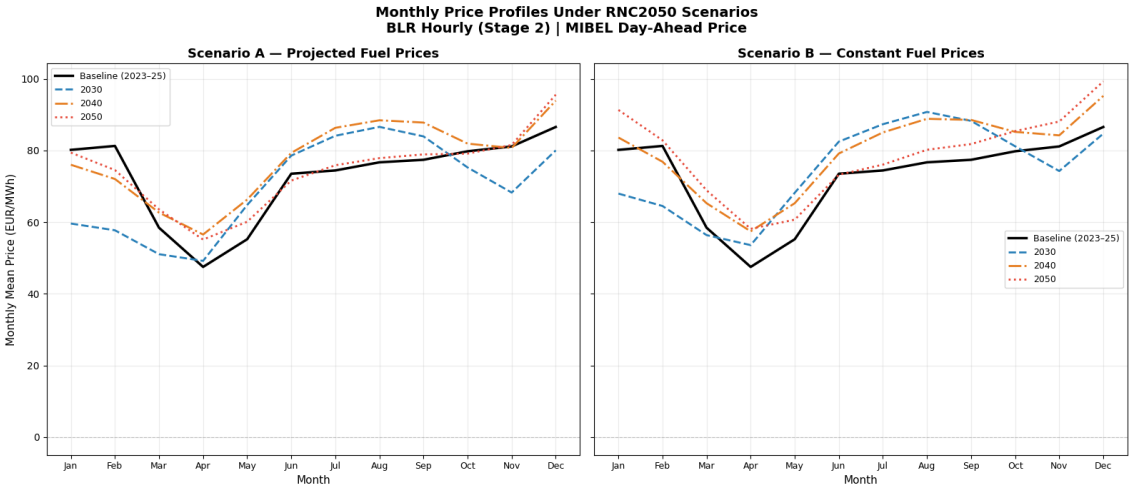


Figure 5.16: Monthly price profiles under Scenarios A (left) and B (right): posterior predictive median by month for baseline, 2030, 2040, and 2050 (BLR hourly, Stage 2).

Table 5.15: Monthly price profiles for BLR Hourly Stage 2.

		Scenario A			Scenario B		
Month	**Baseline**	**2030**	**2040**	**2050**	**2030**	**2040**	**2050**
Jan	80.2	59.6	76.0	79.4	68.0	83.6	91.3
Feb	81.3	57.7	72.0	74.5	64.5	76.8	82.8
Mar	58.4	51.0	62.7	63.5	56.4	65.3	68.9
Apr	47.5	49.2	56.5	55.1	53.6	57.4	58.1
May	55.2	64.8	66.3	60.1	68.2	65.3	60.7
Jun	73.5	78.6	79.3	71.6	82.5	79.1	73.2
Jul	74.4	84.1	86.3	75.9	87.3	85.0	76.0
Aug	76.7	86.6	88.4	77.9	90.7	88.8	80.2
Sep	77.4	83.9	87.8	78.9	88.2	88.5	81.8
Oct	79.8	75.2	81.9	79.1	81.2	85.2	85.4
Nov	81.1	68.2	80.7	81.5	74.3	84.2	88.1
Dec	86.5	80.0	93.9	95.5	84.7	95.2	99.3

The baseline seasonal pattern is characterised by a pronounced spring trough (March–April), a summer–autumn plateau, and a winter peak centred on December. This pattern is preserved across all horizons and both scenarios, confirming that the underlying seasonal drivers (the complementarity between wind (winter-dominant) and solar (summer-dominant) and the seasonal demand cycle) remain structurally intact under the RNC2050 trajectories. What changes is the level around

which the pattern oscillates and, to a lesser extent, its amplitude.

Under Scenario B, the entire seasonal profile shifts upward across the horizons, consistent with the demand-driven price increase documented in Section 5.4.3. The spring trough is elevated but preserved: March–April remains the cheapest period of the year, but at substantially higher price levels. The December peak rises markedly, reaching approximately 95 EUR/MWh by 2040 and continuing upward to nearly 100 EUR/MWh by 2050. The seasonal range (December minus April) widens relative to the baseline, because the demand-growth effect is strongest in winter months, when solar generation is scarce and the system must rely on dispatchable thermal capacity to meet load. The 2040 and 2050 profiles cross: winter months (October–February) continue to rise from 2040 to 2050, driven by demand growth in the period of lowest solar availability, while summer months (May–September) decline, as the massive solar expansion projected for 2050 depresses prices during the months of highest solar output. This seasonal divergence is consistent with the non-monotone annual trajectory: the easing from +9.6% at 2040 to +8.6% at 2050 is not a uniform decline but the net result of rising winter prices partially offset by falling summer prices.

Under Scenario A, the declining TTF price partially offsets the demand-driven increase, but the effect is not uniform across the year. In the winter months, where gas-fired generation remains more frequently price-setting, the fuel-price decline produces the largest reductions relative to Scenario B: for example, January 2050 falls from 91.3 (Scenario B) to 79.4 EUR/MWh (Scenario A), a difference of nearly 12 EUR/MWh. In the summer months, where solar expansion already moderates prices, the fuel-price effect is smaller: July 2050 differs by only 0.1 EUR/MWh between the two scenarios (75.9 versus 76.0).

Relative to the baseline, Scenario A produces a mixed pattern by 2050. Among the winter months, only November and December remain at or above the baseline level (December rises from 86.5 to 95.5 EUR/MWh), whereas January and especially February fall below it (February drops from 81.3 to 74.5 EUR/MWh), indicating that the fuel-price decline more than offsets demand growth in these months. The spring months rise above the baseline (April from 47.5 to 55.1 EUR/MWh, March from 58.4 to 63.5), though they remain the cheapest period of the year. The summer months stay close to or slightly above baseline levels. The net result is that the seasonal amplitude under Scenario A (December minus April $= 95.5 - 55.1 = 40.4$ EUR/MWh in 2050) is comparable to that under Scenario B ($99.3 - 58.1 = 41.2$ EUR/MWh), confirming that the fuel-price trajectory primarily affects the overall price level rather than the relative seasonal structure.

5.4.7 Projected Volatility and Frequency of Negative Prices

The preceding sections analysed the level and the temporal structure of projected prices. This section addresses a third dimension: the volatility of prices and the frequency of extreme low-price events, both of which have direct implications for market participants and for the viability of renewable investment.

It is important to distinguish two different uses of the [P5–P95] notation in this chapter. In Table 5.13, the intervals refer to the uncertainty about the *median price level* across MCMC draws. In

Table 5.16 below, the P5–P95 width refers to the spread of the *individual hourly price predictions*. The former quantifies parameter uncertainty, the latter quantifies price dispersion.

The first two rows of Table 5.16 distinguish two references. "Historical (actual)" reports the statistics of the observed prices. "Baseline (model)" reports the statistics of the model's predictions when fed with the historical inputs. The difference measures the model's inability to capture the full variability of observed prices: the BLR's linear specification systematically compresses the tails, producing lower σ (35.0 versus 45.5 EUR/MWh) and a narrower P5–P95 width (116.6 versus 141.5) than the observed data. This compression means the projected volatility figures likely underestimate the true volatility that would be observed in a real decarbonised system.

Table 5.16: Projected price volatility and frequency of negative prices by scenario and horizon (BLR hourly, Stage 2). Brackets denote the [P5–P95] interval of each statistic computed across the 8 000 MCMC posterior draws, reflecting the posterior uncertainty about that statistic.

Scenario	**Horizon**	σ EUR/MWh	**P5–P95 width** EUR/MWh	**% neg.**
Historical (actual)		45.5	141.5	1.5%
Baseline (model)		35.0 [34.7–35.3]	116.6 [115.6–117.6]	2.6% [2.5–2.7]
A	2030	35.9 [34.9–36.8]	119.1 [115.5–122.5]	3.5% [2.7–4.4]
A	2040	31.5 [30.9–32.2]	102.7 [100.8–104.9]	1.4% [0.8–2.4]
A	2050	30.1 [29.4–30.8]	97.6 [95.3–100.0]	1.3% [0.7–2.5]
B	2030	36.1 [35.1–37.1]	120.4 [116.8–123.8]	2.7% [2.3–3.2]
B	2040	31.9 [31.5–32.5]	104.4 [102.7–106.2]	1.3% [1.0–1.7]
B	2050	31.2 [30.6–31.8]	101.6 [99.7–103.8]	1.1% [0.8–1.5]

The projected volatility metrics reveal a non-monotone pattern. At the 2030 horizon, all three metrics increase slightly relative to the baseline: σ rises from 35.0 to approximately 36 EUR/MWh, and the frequency of negative prices increases from 2.6% to 3.5% under Scenario A. This increase is consistent with the moderate scaling factors applied at 2030, which expand the range of VRE shares without yet triggering the constraining effect of the renewable caps. At the 2040 and 2050 horizons, however, all three metrics *decrease*: σ falls to approximately 30–32 EUR/MWh, and the frequency of negative prices drops to 1.1–1.4%.

This reversal requires careful interpretation. The decrease does not mean that future prices will be less volatile than present prices. It reflects a property of the linear model interacting with the scenario-construction procedure: the operational constraints bind increasingly at the longer horizons (Table 5.11), compressing the variability of the generation-share inputs, and a linear model translates reduced input variability directly into reduced output variability. In practice, a deeply decarbonised system is likely to exhibit *greater* price volatility, driven by scarcity pricing, start-up cost recovery, and flexibility mechanisms not represented in the model. The moderate increase at 2030, where the constraints are less binding and the inputs remain closer to the historical domain, is more likely to reflect a genuine directional tendency.

5.4.8 Hourly Versus Daily Model Divergence

The BLR hourly and daily models diverge progressively across the horizons. Table 5.17 quantifies the difference for the Stage 2 specification.

Table 5.17: Divergence between hourly and daily BLR median projections (EUR/MWh): hourly minus daily (Stage 2).

Scenario	**Baseline**	**2030**	**2040**	**2050**
A: Hourly − Daily	+0.0	+7.6	+18.9	+20.3
B: Hourly − Daily	+0.0	−3.5	−10.3	−15.2

The baseline agreement (both models recover a median of approximately 72.6 EUR/MWh) confirms that the divergence is driven by the scenario extrapolation, not by a systematic estimation difference. Under Scenario B, the hourly model projects consistently lower prices than the daily model, and the gap widens from −3.5 in 2030 to −15.2 EUR/MWh in 2050. Under Scenario A, the direction reverses: the hourly model projects higher prices, with the gap reaching +20.3 EUR/MWh by 2050.

This divergence reflects two structural differences. First, the daily model lacks the Solar×Hour interaction, which in the hourly model redistributes the solar price-depressing effect across the day rather than applying a single average coefficient. Second, daily aggregation removes the within-day variance of the generation shares. The hourly model responds differently to the same average conditions because the relationship between extreme hourly shares and price is non-trivially different from the relationship between daily-average shares and price. The divergence demonstrates that the temporal resolution at which the model operates is not a neutral choice but a substantive modelling decision that affects the projected price trajectory. It is not possible to isolate which of these two mechanisms is dominant, since the daily model cannot accommodate the Solar×Hour interaction (hour-of-day has no meaning after daily aggregation), and the two effects are therefore structurally confounded. Given this confounding, the daily model's projections are best used as a consistency check on the direction of change rather than as an independent estimate of price levels, and the hourly model is preferred wherever intraday resolution is available.

The value of this comparison lies not in quantifying the individual mechanisms but in demonstrating that the temporal resolution at which the model operates is a consequential modelling decision: the hourly model, which captures intraday structure, produces systematically different projections from the daily model, which does not. This result informs the choice of the hourly model as the primary specification.

The divergence pattern described above is reported for Stage 2. The same pattern is preserved under Stage 3 (with GAS_MIN), because GAS_MIN shifts both models upward by a similar amount without altering the structural differences between them (Section 5.5).

5.5 Sensitivity to the GAS_MIN Constraint

The preceding sections presented results under a common seven-constraint configuration (without GAS_MIN). This section introduces the GAS_MIN constraint (Stage 3) and assesses its effect on the projected price levels and profiles. Because GAS_MIN was not applied to the ANN, the Stage 3 results are presented as a sensitivity extension of the BLR projections. The rationale for the constraint, representing capacity-availability contracts and the contribution of gas turbines to system inertia, was established in Section 4.6.2.

5.5.1 Effect on Price Levels

Table 5.18 presents the median projected prices under Stage 3, which adds the GAS_MIN constraint to the Stage 2 specification. The Stage 3 projections follow the same qualitative pattern as Stage 2: under Scenario B, prices rise at all horizons, peaking at 2040 (+15.4%) before easing at 2050 (+9.3%). The absolute levels are uniformly higher than Stage 2, reflecting the GAS_MIN floor.

Table 5.18: BLR scenario projections with GAS_MIN (Stage 3). Median prices (EUR/MWh) and percentage change versus baseline. Intervals are 90% posterior predictive [P5–P95].

			Scenario A			Scenario B		
Model		**Baseline**	**2030**	**2040**	**2050**	**2030**	**2040**	**2050**
BLR Hourly	EUR/MWh	72.63	74.79	82.06	75.07	79.77	83.84	79.35
	Δ		+3.0%	+13.0%	+3.4%	+9.8%	+15.4%	+9.3%
	[P5–P95]		[71.5–78.0]	[73.8–90.2]	[64.8–85.3]	[78.2–81.3]	[81.5–86.1]	[76.2–82.5]
BLR Daily	EUR/MWh	72.61	66.16	62.43	54.70	82.31	93.40	94.44
	Δ		−8.9%	−14.0%	−24.7%	+13.3%	+28.6%	+30.0%
	[P5–P95]		[56.2–76.6]	[35.9–90.1]	[21.3–89.4]	[78.6–86.2]	[85.9–101.2]	[83.8–105.5]

Table 5.19 quantifies the effect of GAS_MIN by comparing Stage 3 to Stage 2 for each scenario, horizon, and resolution.

Table 5.19: Effect of the GAS_MIN constraint on median projected prices (EUR/MWh): Stage 3 minus Stage 2.

Scenario	**Model**	**2030**	**2040**	**2050**
A	Hourly	+4.72	+4.22	+0.48
A	Daily	+3.67	+3.46	+0.40
B	Hourly	+4.72	+4.23	+0.49
B	Daily	+3.74	+3.47	+0.38

The constraint raises prices at all horizons in both scenarios, because enforcing a minimum gas share increases the frequency with which gas-fired generation, the most expensive technology, is dispatched. The effect is largest in 2030 (approximately +4.7 EUR/MWh in the hourly model), where GAS_MIN = 5.2% is binding in a meaningful number of hours. By 2050, where GAS_MIN = 0.3%, the effect is negligible (< 0.5 EUR/MWh). The effect is virtually identical across Scenarios A and B (within ± 0.02 EUR/MWh) and consistent across temporal resolutions, confirming the mechanical nature of the constraint. The qualitative conclusions of the scenario analysis are not altered by the presence or absence of GAS_MIN.

The introduction of GAS_MIN also affects the binding frequency of the other constraints. Because gas is synchronous generation, enforcing a minimum gas share reduces the frequency with which SINC_MIN binds (from 49.2% to 44.8% in 2030, from 22.5% to 22.1% in 2050). At the same time, the additional gas generation raises total supply, which increases the frequency with which the energy-balance constraint binds (from 61.3% to 68.7% in 2030, from 64.1% to 64.5% in 2050). The remaining constraints (solar, wind, and renewable caps) are unaffected, as they are applied earlier in the sequential procedure.

5.5.2 Effect on Profiles

Figure 5.17 presents the intraday profiles under Stage 3 for both scenarios across all horizons.

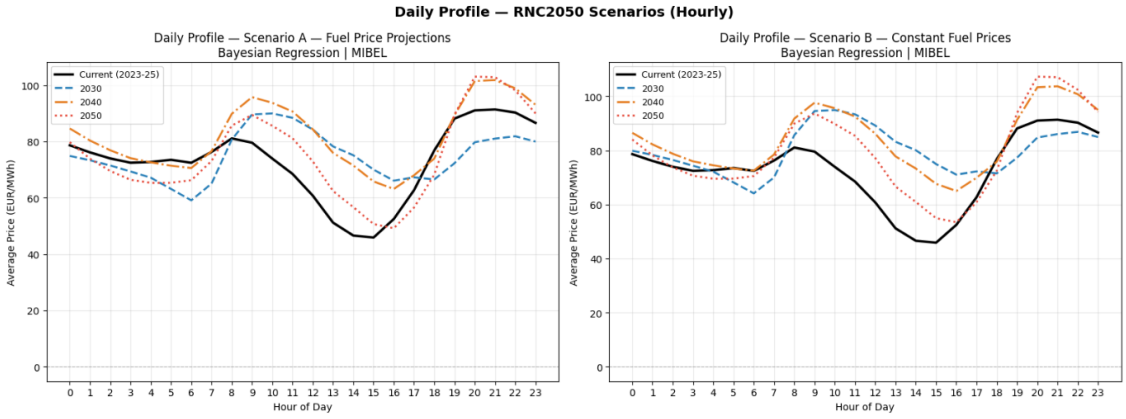


Figure 5.17: Intraday price profiles under Scenarios A (left) and B (right): posterior predictive median by hour for baseline, 2030, 2040, and 2050 (BLR hourly, Stage 3).

The intraday profiles under Stage 3 are qualitatively identical to those of Stage 2 (Figure 5.13), with only a slight upward vertical shift reflecting the higher price levels reported in Table 5.19. The shape of the profile (the midday trough, the evening peak, and the rightward shift across horizons) is preserved, because GAS_MIN affects the absolute level at which gas-fired generation enters the dispatch but does not alter the relative contribution of solar, wind, or the Solar×Hour interaction to the intraday price structure. Therefore, the rightward shift of the price minimum documented in Section 5.4.5 persists under Stage 3.

Table 5.20 and Figure 5.18 present the seasonal profiles under Stage 3.

Table 5.20: Monthly median projected prices (EUR/MWh) under Scenarios A and B, BLR hourly Stage 3.

		Scenario A			Scenario B		
Month	**Baseline**	**2030**	**2040**	**2050**	**2030**	**2040**	**2050**
Jan	80.2	68.7	82.9	80.1	77.0	90.4	91.9
Feb	81.3	63.3	77.1	75.0	70.1	82.0	83.3
Mar	58.4	59.5	69.4	64.3	64.9	72.0	69.6
Apr	47.5	58.1	64.2	55.9	62.6	65.1	58.9
May	55.2	69.9	71.3	60.8	73.3	70.3	61.3
Jun	73.5	80.8	82.1	72.1	84.8	81.9	73.7
Jul	74.4	85.4	87.7	76.1	88.6	86.4	76.3
Aug	76.7	87.4	89.5	78.0	91.6	89.9	80.4
Sep	77.4	84.9	88.9	79.1	89.2	89.7	81.9
Oct	79.8	79.1	85.7	79.6	85.0	89.0	85.9
Nov	81.1	73.6	85.2	82.0	79.6	88.7	88.6
Dec	86.5	85.0	98.5	96.0	89.6	99.8	99.8

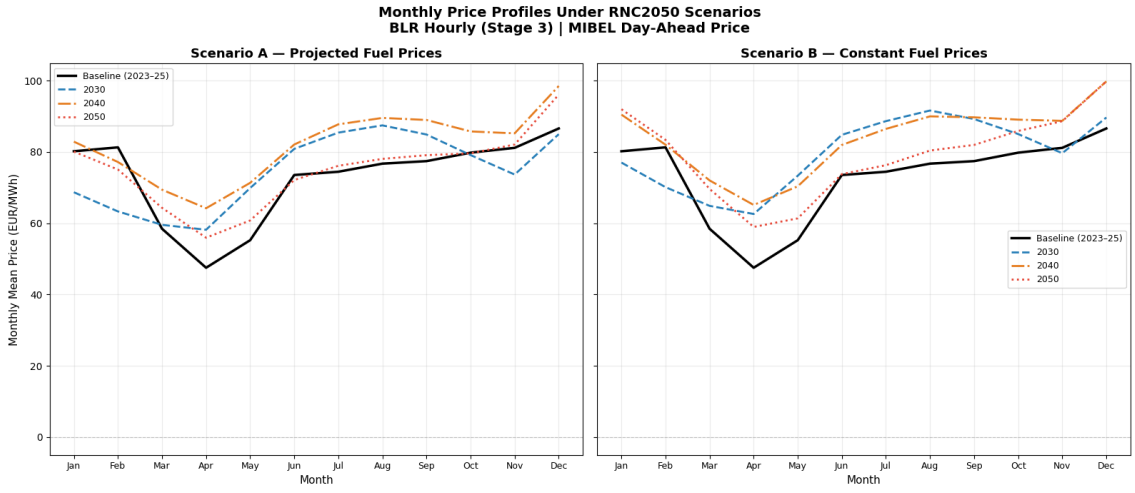


Figure 5.18: Monthly price profiles under Scenarios A (left) and B (right): posterior predictive median by month for baseline, 2030, 2040, and 2050 (BLR hourly, Stage 3).

The broad seasonal structure under Stage 3 mirrors that of Stage 2: the spring trough and winter peak are preserved, the seasonal range widens marginally under Scenario B (from 39 to approximately 41 EUR/MWh by 2050), and late-spring and summer prices converge as photovoltaic capacity expands.

A notable feature is the relative depression of November prices, which is more pronounced in Scenario A, where November (73.6 EUR/MWh in 2030; 85.2 in 2040) falls below the adjacent months of October and December. This behaviour is consistent with the wind generation profile documented in Section 5.1.5: November exhibits the highest mean wind share (33.6% of load), and the strong merit-order effect of wind (-16.54 EUR/MWh per σ; Table 5.7) contributes to

lower prices in this month than in October or December, when wind availability is lower. Under Scenario B the same pattern is also visible but less pronounced because, in the absence of the projected TTF decline, the higher overall price level reduces the prominence of the local November trough.

Under Scenario A, the seasonal profile shifts downward relative to Scenario B while preserving an almost identical monthly pattern. Although projected prices are consistently lower across the year, the seasonal amplitude changes only marginally (40.1 versus 40.9 EUR/MWh in 2050), indicating that declining fuel prices primarily affect the overall price level rather than the relative seasonal structure. However, the downward shift is not perfectly uniform across the year. The difference between the two scenarios is largest during the winter months (e.g. 11.8 EUR/MWh in January 2050) and smallest during late spring and summer (less than 3 EUR/MWh from May to September). This seasonal variation is consistent with a greater role of gas-fired generation during winter, when lower solar availability increases the frequency with which gas plants remain price-setting.

5.6 Model Comparison and Suitability

Table 5.21 summarises the comparative assessment of the three model configurations.

Table 5.21: Comparative assessment of the three model configurations.

Criterion	**ANN**	**BLR Hourly**	**BLR Daily**
Baseline (EUR/MWh)	83.25 (median)	72.63 (median)	72.61 (median)
In-sample R^2	0.883	0.593	0.702
MAE (EUR/MWh)	11.73	23.26	16.25
Interpretable coefficients	No	Yes	Yes
Uncertainty quantification	No	Yes (posterior)	Yes (posterior)
Intraday profile capability	Yes (implicit)	Yes (Solar×Hour)	No
Sc. B: all horizons	Plausible	Plausible	Plausible
Sc. A: 2030	Plausible	Plausible	Plausible
Sc. A: 2040	**Fails**	Plausible	Plausible
Sc. A: 2050	**Fails**	Plausible	Plausible

The ANN and BLR baselines differ by approximately 10 EUR/MWh (83.25 versus 72.63). Both are medians of each model's predictions applied to the same historical inputs, so the difference reflects the models' distinct functional forms rather than a difference in the data or in the summary statistic. The ANN, with its non-linear hidden layer and higher in-sample R^2 (0.883), fits the central mass of the price distribution more tightly and produces a median prediction that is closer to the median of the observed prices (78.9 EUR/MWh). The BLR, with its linear specification and lower R^2 (0.593), compresses the tails of the distribution, pulling the median of its predictions downward. The relevant comparison is therefore between each model's scenario projections and its own baseline, expressed as percentage changes in the preceding tables, rather than

between the absolute price levels of the two models. In particular, the BLR's systematic underestimation of the baseline level (72.63 versus 78.9 EUR/MWh observed) means that the absolute price levels reported in the scenario projections should not be interpreted as forecasts of the actual price. The percentage changes relative to the model's own baseline provide the more reliable signal.

The ANN achieves the highest in-sample accuracy by a substantial margin, but as demonstrated in Section 5.2.2, this advantage does not transfer to the scenario projections: the non-linear mapping that gives the network its flexibility within the training domain produces substantially unstable outputs when the fuel and carbon price inputs lie far outside the historical range. The intraday profiles (Section 5.2.3) confirm that the failure is pervasive, affecting the entire daily cycle rather than individual hours. The BLR, by contrast, responds linearly and proportionately to out-of-domain inputs, producing projections that remain bounded and interpretable. Under Scenario B, both models agree on the direction of change (prices rise above the baseline) but differ in magnitude: the ANN projects +10–12% at 2040–2050, while the BLR hourly projects +9–10% over the same horizons. This convergence is reassuring, as it suggests that the structural conclusion (demand growth dominates the merit-order effect under constant fuel prices) is robust to the choice of functional form. The modest quantitative difference reflects the ANN's ability to capture non-linear interactions that the BLR's additive specification cannot represent, an advantage that is confined to Scenario B, where the inputs remain within the training domain.

The BLR hourly model (Stage 2) is therefore adopted as the primary model for the scenario projections. Its lower in-sample R^2 is an accepted trade-off: the linearity that limits its explanatory power within the historical sample is the same property that ensures stable, interpretable, and probabilistically quantified behaviour under extrapolation. The daily BLR serves as a robustness check, with the caveat that its projections diverge progressively from the hourly model due to the loss of intraday information (Section 5.4.8). The ANN is retained as a benchmark for Scenario B and for the 2030 horizon, and its extrapolation failure under Scenario A constitutes an independent methodological finding.

A methodological caveat is warranted regarding the fairness of the model comparison. The BLR benefits from several specification choices that were not applied to the ANN: informative priors grounded in economic theory, an externally imposed solar saturation function, and the operational constraints applied during scenario construction. Although the ANN can, in principle, capture interactions such as Solar$\times$Hour implicitly through its non-linear hidden layer, it does so without the structural guarantees that the BLR's explicit parameterisation provides, and it receives the scenario inputs directly without equivalent conditioning mechanisms. This asymmetry means that the ANN's extrapolation failure reflects not only an inherent limitation of feedforward networks but also the absence of domain-specific safeguards that could, in principle, be implemented (e.g., input clipping, constrained output layers, or hybrid architectures). Conversely, the BLR's natural acceptance of prior information (including plausible coefficient ranges, sign constraints, and uncertainty quantification) makes it structurally better suited to scenario analysis in which expert knowledge about the direction and magnitude of effects is available. The comparison, therefore, illustrates a broader methodological point: that for policy-oriented extrapolation exer-

cises, a model's ability to incorporate external knowledge may be more valuable than its capacity to fit historical patterns.

The interpretation of these findings in light of the research questions, limitations, and policy implications is developed in Chapter 6.

Chapter 6

Conclusions

This chapter synthesises the findings of the dissertation in light of the research questions, compares them with the existing literature, derives recommendations for policymakers and market participants, identifies the principal limitations of the analysis, and outlines directions for future work.

6.1 Answers to Research Questions

RQ1: How does electrification-driven electricity demand growth influence price formation in the day-ahead wholesale market, and in particular how does rising demand affect the frequency with which higher-cost marginal technologies are required to meet load?

Under Scenario B, which isolates the structural effect by holding fuel prices constant, the BLR hourly model (Stage 2) projects prices above the baseline at all horizons: $+3.3\%$, $+9.6\%$, and $+8.6\%$ (Table 5.13). The ANN confirms the direction under the same scenario (-0.5%, $+12.3\%$, $+10.1\%$ for 2030, 2040, 2050), strengthening confidence that the result is robust to the choice of functional form. Demand growth under the RNC2050 ($+11.4\%$ to $+77.2\%$) thus dominates the merit-order effect of renewable expansion at the annual level.

The effect is not uniform across the year: winter prices rise more sharply than spring prices because solar generation is scarce and the system must rely on higher-cost dispatchable capacity. December median prices reach approximately 100 EUR/MWh by 2050 under Scenario B, while April remains below 60 EUR/MWh (Table 5.15). This seasonal asymmetry confirms that rising demand increases the frequency of marginal thermal dispatch most sharply in the months with the lowest renewable availability. The constraint diagnostics (Table 5.11) provide indirect quantification: the GAS_MAX ceiling binds in 24.4% of hours at the 2030 horizon and in 35.2% at 2050, indicating that even under a generation mix in which gas capacity is reduced to 0.2 GW, demand growth pushes the system to its thermal-dispatch limit with increasing frequency.

RQ2: To what extent does increasing renewable penetration alter wholesale price levels and their temporal distribution through the displacement of higher-cost generation?

The posterior coefficients (Table 5.7) confirm a strong merit-order effect, with solar exhibiting the largest impact (-18.82 EUR/MWh per σ). Despite this large per-unit effect, the scenario projections show that renewable expansion does not reduce annual average prices, because demand growth offsets the displacement effect in aggregate. The modest price increase under Scenario B (+8.6% by 2050 despite a +77.2% increase in demand) implies that renewable expansion absorbs the bulk of the demand-driven upward pressure on an annual basis, even though it does not reverse it. The merit-order effect manifests instead in the temporal distribution: the intraday profiles evolve progressively towards a duck-curve pattern, with the daily price range widening from 46.7 EUR/MWh in the baseline to 54–55 EUR/MWh by 2050 and the midday minimum shifting from hour 15 to hour 16 (Section 5.4.4). The seasonal structure is preserved across all horizons (April remains the cheapest month, December the most expensive) but at progressively higher levels (Section 5.4.6). Renewable penetration thus reshapes the *temporal distribution* of prices without reducing the *annual average level*.

RQ3: How does the interaction between demand growth and renewable deployment jointly shape wholesale price outcomes under carbon neutrality scenarios in MIBEL, including the level, the intraday profile, and the volatility of prices?

The dual-scenario structure separates the joint effect into its components. The difference between Scenarios A and B isolates the contribution of fuel and carbon prices (Table 5.14). Under Scenario A, the declining TTF and rising EU ETS have partially offsetting effects. Because the gas-price coefficient is substantially larger than the carbon-price coefficient (Section 5.3.2), the net fuel-price effect is deflationary and nearly cancels the demand-driven upward pressure, producing modest net changes (-3.5% to $+7.2\%$). The interaction between the two drivers produces a non-monotonic trajectory: demand growth dominates up to 2040, but the massive solar expansion projected for 2050 begins to offset it, causing the Scenario B price increase to ease from +9.6% at 2040 to +8.6% at 2050. The overall conclusion is that the RNC2050 pathway does not, by itself, produce a substantial reduction in average electricity prices: the structural effect is upward (Scenario B), and only the projected decline in gas prices can counterbalance this trend, and even then, only partially.

The intraday profiles evolve non-monotonically: a transitional regime at 2030, where the historical afternoon-trough/evening-peak pattern is temporarily disrupted, gives way to a pronounced duck curve at 2040–2050 (Section 5.4.4). The evening peak persists despite near-zero gas generation, indicating a structural scarcity condition. Projected volatility increases slightly at 2030 but decreases at 2040–2050. This counter-intuitive result does not indicate that a deeply decarbonised system would exhibit less volatile prices, it reflects the compressing effect of the operational constraints, which bind in over 60% of scenario hours (Table 5.11) and reduce the variability of the generation-share inputs that drive the linear model's output dispersion (Section 5.4.7). In a real system with scarcity pricing, start-up costs and flexibility mechanisms not represented in the model, price volatility at the 2050 horizon would likely exceed the projected values. A cross-cutting methodological finding is the demonstrated unsuitability of neural networks for this type

of analysis: the ANN produces substantially unstable outputs under Scenario A at 2040–2050 (Section 5.2.2), confirming that in-sample accuracy does not guarantee extrapolation reliability.

6.2 Interpretation in Light of the Literature

The finding that demand growth can offset the merit-order effect complements the existing literature, which has predominantly analysed the merit-order effect in isolation from demand-side structural change. The seminal quantifications by Sensfuß et al. [8] and Würzburg et al. [9] for the German market, the projected intensification of the merit-order effect by Cludius et al. [38], Ketterer's [37] finding that wind depresses prices but increases volatility, and López Prol et al.'s [14] documentation of solar cannibalization in California all describe a context in which electricity demand remained broadly stable. This is precisely the respect in which the present work differs: by embedding the merit-order analysis within the electrification-driven demand growth prescribed by the RNC2050 (+11.4% to +77.2%), the dissertation captures a regime that the earlier studies did not address, and the central result (that demand growth dominates the renewable displacement effect at the annual level) is a direct consequence of this difference in scope. The finding suggests that the wholesale-price decline documented in the European literature may not persist once electrification becomes the dominant driver of demand growth.

For the Iberian context, Figueiredo and Pereira da Silva [32] confirmed the merit-order mechanism in MIBEL. The posterior coefficients estimated here are consistent with or larger than the magnitudes reported in the earlier European literature, which may reflect the higher solar penetration levels reached in Portugal by 2023–2025 and the consequent intensification of the cannibalization effect documented by Hirth [13] and López Prol et al. [14].

The emergence of the duck-curve pattern in the projected intraday profiles is consistent with the literature on high-solar systems. The projected daily price range of 54–55 EUR/MWh by 2050 aligns with the expectation that solar penetration widens the intraday price spread, though direct quantitative comparison is complicated by differences in scenario assumptions and base years. The dominance of the gas-price coefficient over the carbon-price coefficient is consistent with Ciarreta and Zarraga [35], who documented the strong role of gas prices in Iberian price formation.

The ANN's extrapolation failure aligns with the comparative assessments by Weron [20] and Lago et al. [21], who noted that machine-learning models may not generalise to structurally different conditions. The present work illustrates the failure mechanism concretely: the instability arises from out-of-domain carbon-price inputs ($z \approx +23.8$) interacting with non-linear activation functions. The Bayesian approach with informative priors, consistent with the framework advocated in recent electricity-price modelling literature [39, 40, 41], demonstrates the value of economic priors as a regularisation mechanism. The projected increase in negative-price frequency at 2030 is consistent with the evidence on negative-price episodes in high-renewable markets [11, 12], while the subsequent decrease at 2040–2050 reflects a model artefact rather than a genuine tendency, as discussed in Section 5.4.7.

6.3 Recommendations

The results support several recommendations for policymakers and market participants.

For policymakers and regulators. The finding that demand growth dominates the renewable merit-order effect under constant fuel prices implies that the RNC2050 pathway does not guarantee lower electricity prices despite the massive expansion of near-zero-marginal-cost generation. Under Scenario B, December prices reach approximately 100 EUR/MWh by 2050 while April remains below 60 EUR/MWh, widening the seasonal spread to roughly 41 EUR/MWh. This implies that policies focusing exclusively on renewable capacity deployment, without complementary demand-side management and energy-efficiency measures, risk producing a system in which prices remain elevated and seasonally unequal. Consumer-protection mechanisms designed for the current seasonal profile will need to accommodate a wider winter–spring differential than they do today.

The persistence of the evening peak despite near-zero gas generation indicates a structural need for flexibility resources (storage, demand response, and interconnection capacity) that is not met by renewable expansion alone. The projected daily price range of 54–55 EUR/MWh by 2050 creates price signals that favour storage deployment, though the adequacy of these signals for attracting sufficient investment requires further analysis.

More broadly, the comparison between Scenarios A and B demonstrates that the trajectory of fossil-fuel prices remains the primary determinant of wholesale electricity price levels, even under a generation mix in which gas supplies less than 1% of demand. Because Portugal has limited influence over international gas and carbon prices, the effectiveness of domestic decarbonisation policy in reducing electricity costs depends critically on external commodity-market conditions. This finding underscores the importance of hedging mechanisms (long-term power-purchase agreements, contracts for difference, and strategic interconnection investments) that can insulate domestic consumers from commodity-price volatility during the transition.

For market participants. The deepening midday trough and the persistent evening peak indicate that the value of load-shifting from evening to midday hours will increase over the projection horizon. For solar generators, the cannibalization effect implies that the capture price of solar energy will decline relative to the wholesale average, reinforcing the case for co-location with storage. The transitional regime at 2030, where the intraday pattern temporarily loses its clear structure, suggests that flexibility assets designed around the current price pattern may face a period of reduced arbitrage value before the duck curve re-emerges at 2040–2050.

For modellers and researchers. The extrapolation instability observed with the neural network in this study cautions against the uncritical application of standard feedforward networks to scenario analysis involving out-of-domain inputs. This does not imply that neural networks should be discarded: techniques such as input clipping, domain-aware regularisation, ensemble methods, or

hybrid architectures that combine a neural network with a linear extrapolation layer could potentially mitigate the instability observed here. However, when the objective is to project prices under structurally different conditions, the results suggest that complementing any non-linear model with explicit extrapolation safeguards and uncertainty quantification is essential. The Bayesian linear approach adopted in this dissertation offers one such framework, trading in-sample accuracy for interpretability and stable out-of-domain behaviour.

6.4 Limitations of the Analysis

Several limitations should be borne in mind when interpreting the results.

Model limitations. The BLR's linear specification compresses the tails of the price distribution, producing a baseline median of 72.63 EUR/MWh versus the observed 78.9 EUR/MWh. Percentage changes relative to the model's own baseline are therefore more reliable than absolute price levels (Section 5.6). The linear form also translates reduced input variability directly into reduced output variability, which explains the counter-intuitive decrease in projected volatility at 2040–2050 (Section 5.4.7). The model does not represent storage, demand response, or other flexibility mechanisms: the persistent evening peak (Section 5.4.4) indicates a structural scarcity condition, but in a real system with adequate flexibility the peak would be moderated, so the projected daily price range likely overstates what would be observed. Similarly, the rightward shift of the price minimum (Section 5.4.5) is driven by extrapolating the Solar×Hour interaction coefficient beyond the estimation domain (historical solar shares up to ∼28%). The broad pattern is robust but its precise magnitude should be treated as a declared limitation. The analysis also assumes that the day-ahead marginal-pricing market structure remains unchanged through 2050. Potential reforms (capacity markets, pay-as-bid, locational pricing) are not modelled.

Data and estimation limitations. The TTF and CO_2 coefficients were estimated from a period in which gas-fired generation averaged ∼10% of demand and are applied to 2050 where gas represents only 0.6%. The transmission channel through which gas prices affect electricity prices narrows substantially, and the coefficients may overstate gas-price influence at the longest horizon. The CO_2 coefficient (+0.89), estimated from a range of 65–90 EUR/t, is applied to 300 EUR/t in Scenario A 2050, an extrapolation beyond the estimation domain where the true relationship may be non-linear. Scenario B, which holds fuel prices constant, is less sensitive to these limitations. The 2023–2025 estimation period partially overlaps with the Iberian exception mechanism (Section 2.4.2), which may attenuate the estimated gas-price coefficient, though the effect is mitigated by ∼18 months of post-exception data. Hydroelectric generation and cross-border interconnection flows are held at their historical values across all horizons (Assumptions 3–4), an assumption that does not capture the potential effects of climate change on river flows or the expected expansion of interconnection capacity.

Scenario-construction limitations. The operational constraint values (SOLAR_MAX, EOLICA _MAX, RENOV_MAX, SINC_MIN, GAS_MAX) were selected based on empirical analysis and engineering judgment, not derived from formal optimisation (Section 5.1.6). Their individual sensitivity is not quantified. In particular, the solar saturation parameter ($c = 6$ in the tanh function) was selected as a modelling assumption and not subjected to a formal sensitivity analysis. Alternative values would change the 2050 solar scaling factor and therefore the magnitude, though not the direction, of the projected price effects. The energy-balance constraint binds in over 60% of scenario hours (Table 5.11), actively shaping the generation mixes and compressing input variability, which contributes to the artificial decrease in projected volatility at the longer horizons. Alternative constraint specifications could produce materially different projections, particularly at 2050. A related concern is the progressive divergence between the hourly and daily BLR projections (Section 5.4.8), which reaches 15–20 EUR/MWh by 2050. Because the two structural differences between the models (the Solar×Hour interaction and the within-day variance of generation shares) cannot be isolated, this divergence represents an irreducible modelling uncertainty that bounds the precision of the hourly projections at the longest horizons.

6.5 Future Work

Several directions for future work emerge from the limitations identified in this dissertation.

At the methodological level, the cyclical temporal variables (hour, month, week) should be re-encoded using sine/cosine transformations to enforce the natural periodicity that the current integer coding does not capture. This refinement would be straightforward to implement within the BLR framework. Non-linear Bayesian models such as BART [47] or Gaussian processes with informative priors could offer intermediate positions between the linear BLR and the neural network, combining greater flexibility with extrapolation stability.

At the scenario-construction level, incorporating storage and demand-response mechanisms would address the most significant gap in the current framework. A hybrid approach using the BLR's scenario projections as boundary conditions for a unit-commitment model could capture both long-term structural trends and short-term flexibility dynamics. A systematic sensitivity analysis of the operational constraint values would quantify the dependence of the projections on the author's modelling assumptions.

At the data level, as post-2025 data accumulate, re-estimating the model on a longer sample would improve the reliability of the fuel-price coefficients and reduce the influence of the Iberian exception period. Relaxing the stationarity assumption for hydroelectric generation by incorporating climate-change projections of precipitation would capture an important source of uncertainty, given the large posterior coefficient for hydro and the wide credible intervals in winter months.

Finally, extending the framework to the Spanish zone of MIBEL, or to other European markets with different generation mixes, would test the generalisability of the findings.

In summary, this dissertation has demonstrated that the RNC2050 decarbonisation pathway reshapes Iberian wholesale electricity prices in ways that are conditional on the interplay between demand growth, renewable deployment, and fuel-price trajectories. The Bayesian framework developed here provides a transparent, interpretable, and probabilistically grounded tool for assessing these interactions, and the empirical comparison with a neural network benchmark underscores the importance of model selection in policy-oriented scenario analysis.

References

[1] European Commission. *The European Green Deal*. 2019. URL: https://eur-lex.europa.eu/legal-content/EN/TXT/?uri=COM:2019:640:FIN.

[2] Katherine Calvin et al. *IPCC, 2023: Climate Change 2023: Synthesis Report. Contribution of Working Groups I, II and III to the Sixth Assessment Report of the Intergovernmental Panel on Climate Change [Core Writing Team, H. Lee and J. Romero (eds.)]. IPCC, Geneva, Switzerland.* Edition: First. Intergovernmental Panel on Climate Change (IPCC), July 25, 2023. DOI: 10.59327/IPCC/AR6-9789291691647. URL: https://www.ipcc.ch/report/ar6/syr/ (visited on 07/06/2026).

[3] IEA. *Net Zero by 2050: A Roadmap for the Global Energy Sector*. International Energy Agency, 2021. URL: https://www.iea.org/reports/net-zero-by-2050.

[4] Government of Portugal. *ROADMAP FOR CARBON NEUTRALITY 2050 (RNC2050)*. 2019, p. 102. URL: https://www.portugal.gov.pt/download-ficheiros/ficheiro.aspx?v=%3D%3DBAAAAB%2BLCAAAAAAABACzMDexBAC4h9DRBAAAAA%3D%3D (visited on 10/17/2025).

[5] Joana Monjardino et al. "Carbon Neutrality Pathways Effects on Air Pollutant Emissions: The Portuguese Case". In: *Atmosphere* 12.3 (Mar. 2, 2021), p. 324. ISSN: 2073-4433. DOI: 10.3390/atmos12030324. URL: https://www.mdpi.com/2073-4433/12/3/324 (visited on 07/06/2026).

[6] República Portuguesa. *Plano Nacional de Energia e Clima 2021–2030 (PNEC 2030)*. Governo de Portugal, 2024. URL: https://www.portugal.gov.pt/pt/gc23/governo/comunicado-de-conselho-de-ministros?i=631.

[7] REN — Redes Energéticas Nacionais. *Dados Técnicos Eletricidade 2024*. 2024. URL: https://datahub.ren.pt/ (visited on 10/15/2025).

[8] Frank Sensfuß, Mario Ragwitz, and Massimo Genoese. "The merit-order effect: A detailed analysis of the price effect of renewable electricity generation on spot market prices in Germany". In: *Energy Policy* 36.8 (2008), pp. 3076–3084. DOI: 10.1016/j.enpol.2008.03.035.

[9] Klaas Würzburg, Xavier Labandeira, and Pedro Linares. "Renewable generation and electricity prices: Taking stock and new evidence for Germany and Austria". In: *Energy Economics* 40 (2013), S159–S171. DOI: 10.1016/j.eneco.2013.09.011.

[10] Richard Green and Nicholas Vasilakos. "Market behaviour with large amounts of intermittent generation". In: *Energy Policy* 38.7 (2010), pp. 3211–3220. DOI: 10.1016/j.enpol.2009.07.038.

[11] Marco Nicolosi. "Wind power integration and power system flexibility – An empirical analysis of extreme events in Germany under the new negative price regime". In: *Energy Policy* 38.11 (2010), pp. 7257–7268. DOI: 10.1016/j.enpol.2010.08.002.

[12] Enzo Fanone, Andrea Gamba, and Marcel Prokopczuk. "The case of negative day-ahead electricity prices". In: *Energy Economics* 35 (2013), pp. 22–34. DOI: 10.1016/j.eneco.2011.12.006.

[13] Lion Hirth. "The market value of variable renewables: The effect of solar wind power variability on their relative price". In: *Energy Economics* 38 (2013), pp. 218–236. DOI: 10.1016/j.eneco.2013.02.004.

[14] Javier López Prol, Karl W. Steininger, and David Zilberman. "The cannibalization effect of wind and solar in the California wholesale electricity market". In: *Energy Economics* 85 (2020), p. 104552. DOI: 10.1016/j.eneco.2019.104552.

[15] OMIE. *Annual reports and market data*. 2025. URL: https://www.omie.es/en/market-results (visited on 12/15/2025).

[16] Jorge Borges. "MIBEL and the Market Splitting - 5th International Conference on the European electricity market". In: *2008 5th International Conference on the European Electricity Market*. 2008 5th International Conference on the European Electricity Market. May 2008, pp. 1–5. DOI: 10.1109/EEM.2008.4579105. URL: https://ieeexplore.ieee.org/document/4579105 (visited on 12/26/2025).

[17] DGEG. *MIBEL*. 2025. URL: https://www.dgeg.gov.pt/pt/areas-transversais/mercados-e-mecanismos-de-capacidade/mibel/ (visited on 10/21/2025).

[18] Carlos Ruiz, Ákos Horváth, and Ignacio Solera. "Evaluating the Iberian electricity market mechanism: A synthetic control approach". In: *Energy Policy* 185 (2024), p. 113953. DOI: 10.1016/j.enpol.2023.113953.

[19] Richard Loulou et al. *Documentation for the TIMES Model*. IEA-ETSAP, 2021. URL: https://iea-etsap.org/docs/Documentation_for_the_TIMES_Model-Part-I.pdf.

[20] Rafał Weron. "Electricity price forecasting: A review of the state-of-the-art with a look into the future". In: *International Journal of Forecasting* 30.4 (2014), pp. 1030–1081. DOI: 10.1016/j.ijforecast.2014.08.008.

[21] Jesús Lago et al. "Forecasting day-ahead electricity prices: A review of state-of-the-art algorithms, best practices and an open-access benchmark". In: *Applied Energy* 293 (2021), p. 116983. DOI: 10.1016/j.apenergy.2021.116983.

[22] European Parliament and Council. *Directive (EU) 2023/959 amending Directive 2003/87/EC (EU ETS)*. 2023. URL: https://eur-lex.europa.eu/eli/dir/2023/959/oj.

[23] IRENA. *Renewable Power Generation Costs in 2023*. International Renewable Energy Agency, 2024. URL: https://www.irena.org/Publications/2024/Sep/Renewable-Power-Generation-Costs-in-2023.

[24] ERSE. *Mercado de eletricidade*. 2025. URL: https://www.erse.pt/eletricidade/mercado-de-eletricidade/ (visited on 12/15/2025).

[25] Conselho de Reguladores do MIBEL. *DESCRIÇÃO DO FUNCIONAMENTO DO MIBEL*. 2009, p. 249. URL: https://www.mibel.com/wp-content/uploads/2018/08/Descricao_Funcionamento_MIBEL_Marco_2009.pdf (visited on 10/21/2025).

[26] Jose María Ballester, Francisco Climent, and Dolores Furió. "Market efficiency and price discovery relationships between spot, futures and forward prices: the case of the Iberian Electricity Market (MIBEL)". In: *Spanish Journal of Finance and Accounting / Revista Española de Financiación y Contabilidad* 45.2 (Apr. 2, 2016), pp. 135–153. ISSN: 0210-2412, 2332-0753. DOI: 10.1080/02102412.2016.1144441. URL: http://www.tandfonline.com/doi/full/10.1080/02102412.2016.1144441 (visited on 07/06/2026).

[27] OMIP. *OMIP — Iberian Energy Derivatives Exchange*. 2025. URL: https://www.omip.pt/ (visited on 12/15/2025).

[28] Daniel Kirschen and Goran Strbac. *Fundamentals of Power System Economics*. 1st ed. Wiley, Mar. 26, 2004. ISBN: 978-0-470-84572-1 978-0-470-02059-3. DOI: 10.1002/0470020598. URL: https://onlinelibrary.wiley.com/doi/book/10.1002/0470020598 (visited on 03/22/2026).

[29] *Commission Regulation (EU) 2015/1222 establishing a guideline on capacity allocation and congestion management (CACM)*. 2015. URL: https://eur-lex.europa.eu/legal-content/EN/TXT/?uri=CELEX:32015R1222 (visited on 12/15/2025).

[30] República Portuguesa. *Decreto-Lei n.º 33/2022 de 14 de maio*. Diário da República, 1.ª série, N.º 94. 2022. URL: https://diariodarepublica.pt/dr/detalhe/decreto-lei/33-2022-183771373.

[31] Lion Hirth. "What caused the drop in European electricity prices? A factor decomposition analysis". In: *The Energy Journal* 39.1 (2018), pp. 143–158. DOI: 10.5547/01956574.39.1.lhir.

[32] Nuno Carvalho Figueiredo and Patrícia Pereira da Silva. "The "Merit Order Effect" of wind and solar power: Volatility and determinants". In: *Renewable and Sustainable Energy Reviews* 102 (2019), pp. 54–62. DOI: 10.1016/j.rser.2018.11.042.

[33] Stefano Clò, Alessandra Cataldi, and Pietro Zoppoli. "The merit-order effect in the Italian power market: The impact of solar and wind generation on national wholesale electricity prices". In: *Energy Policy* 77 (2015), pp. 79–88. DOI: 10.1016/j.enpol.2014.11.038.

[34] ENTSO-E and ENTSOG. *Ten-Year Network Development Plan 2022 (TYNDP 2022)*. European Network of Transmission System Operators, 2022. URL: https://tyndp.entsoe.eu/.

[35] Aitor Ciarreta and Ainhoa Zarraga. "Analysis of Mean and Volatility Price Transmissions in the MIBEL and EPEX Electricity Spot Markets". In: *The Energy Journal* 36.4 (Oct. 2015), pp. 41–60. ISSN: 0195-6574, 1944-9089. DOI: 10.5547/01956574.36.4.acia. URL: https://journals.sagepub.com/doi/10.5547/01956574.36.4.acia (visited on 07/06/2026).

[36] Paulo Pereira da Silva and Paulo Horta. "The effect of variable renewable energy sources on electricity price volatility: The case of the Iberian market". In: *International Journal of Sustainable Energy* 38.8 (2019), pp. 794–813. DOI: 10.1080/14786451.2019.1602126.

[37] Janina C. Ketterer. "The impact of wind power generation on the electricity price in Germany". In: *Energy Economics* 44 (2014), pp. 270–280. DOI: 10.1016/j.eneco.2014.04.003.

[38] Johanna Cludius et al. “The merit order effect of wind and photovoltaic electricity generation in Germany 2008–2016: Estimation and distributional implications”. In: *Energy Economics* 44 (2014), pp. 302–313. DOI: 10.1016/j.eneco.2014.04.020.

[39] Jakub Nowotarski and Rafał Weron. “Recent advances in electricity price forecasting: A review of probabilistic forecasting”. In: *Renewable and Sustainable Energy Reviews* 81 (2018), pp. 1548–1568. DOI: 10.1016/j.rser.2017.05.234.

[40] Christian Nickelsen and Jaroslav Knapek. “Bayesian approach to electricity price forecasting with emphasis on prior selection”. In: *Energy Reports* 11 (2024), pp. 5345–5359. DOI: 10.1016/j.egyr.2024.05.003.

[41] Angelica Gianfreda, Francesco Ravazzolo, and Luca Rossini. “Comparing the forecasting performances of linear models for electricity prices with high RES penetration”. In: *International Journal of Forecasting* 36.3 (2020), pp. 974–986. DOI: 10.1016/j.ijforecast.2019.11.002.

[42] Richard Loulou et al. *Documentation for the TIMES Model – Part I*. Tech. rep. Last update February 2021. International Energy Agency – Energy Technology Systems Analysis Programme (IEA-ETSAP), Feb. 2021. URL: https://iea-etsap.org/index.php/documentation.

[43] Donald W. Marquardt. “An algorithm for least-squares estimation of nonlinear parameters”. In: *Journal of the Society for Industrial and Applied Mathematics* 11.2 (1963), pp. 431–441.

[44] Matthew D. Hoffman and Andrew Gelman. “The No-U-Turn Sampler”. In: *Journal of Machine Learning Research* 15 (2014), pp. 1593–1623.

[45] International Energy Agency. *World Energy Outlook 2025*. Tech. rep. Paris: International Energy Agency, 2025. URL: https://www.iea.org/reports/world-energy-outlook-2025.

[46] Moutaz Altaghlibi and Giovanni Gentile. *Scenarios Shaping EU ETS Prices*. Sustainability Research – ESG Economist. ABN AMRO Group Economics, Sept. 2025.

[47] Hugh A. Chipman, Edward I. George, and Robert E. McCulloch. “BART: Bayesian Additive Regression Trees”. In: *The Annals of Applied Statistics* 4.1 (2010), pp. 266–298. DOI: 10.1214/09-AOAS285.